Photochemistry and Photobiology, 2023, 99: 356–419

Special Issue Invited Review

The Photosensitizer Temoporfin (*m*THPC) – Chemical, Pre-clinical and Clinical Developments in the Last Decade†‡

Arno Wiehe*[1,2] and Mathias O. Senge*[3,4]

[1]biolitec research GmbH, Jena, Germany
[2]Institut für Chemie und Biochemie, Freie Universität Berlin, Berlin, Germany
[3]Medicinal Chemistry, Trinity Translational Medicine Institute, Trinity Centre for Health Sciences, Trinity College Dublin, The University of Dublin, St. James's Hospital, Dublin, Ireland
[4]Institute for Advanced Study (TUM-IAS), Technical University of Munich, Garching, Germany

Received 4 August 2022, accepted 21 September 2022, DOI: 10.1111/php.13730

ABSTRACT

This review follows the research, development and clinical applications of the photosensitizer 5,10,15,20-tetra(*m*-hydroxyphenyl)chlorin (*m*THPC, temoporfin) in photodynamic (cancer) therapy (PDT) and other medical applications. Temoporfin is the active substance in the medicinal product Foscan® authorized in the EU for the palliative treatment of head and neck cancer. Chemistry, biochemistry and pharmacology, as well as clinical and other applications of temoporfin are addressed, including the extensive work that has been done on formulation development including liposomal formulations. The literature has been covered from 2009 to early 2022, thereby connecting it to the previous extensive review on this photosensitizer published in this journal [Senge, M. O. and J. C. Brandt (2011) *Photochem. Photobiol.* 87, 1240–1296] which followed its way from initial development to approval and clinical application.

INTRODUCTION

Slowly but surely photodynamic therapy (PDT) is becoming a standard treatment modality in clinical practice. The basic principle of PDT was established over a century ago by O. Raab, H. v. Tappeiner *et al*. (1–3), later H. Kautsky, D. R. Snelling, C. S. Foote *et al*. contributed to the understanding of the underlying mechanism (4). Fundamentally, the light of a suitable wavelength is used to photoexcite a dye molecule (the photosensitizer). After intersystem crossing, a longer-lived triplet state of the dye molecule is formed allowing diffusion-controlled interaction with neighboring molecules. The triplet photosensitizer can then facilitate either an electron transfer (Type I) or energy transfer to oxygen (Type II) generating reactive oxygen species (5,6). These result in various biological effects, such as destruction of biomolecules, cell death, vascular damage or vascular destruction and promotion of immune responses (7–9). In a clinical setting, the ultimate goal of PDT is to eradicate malignant cells and tissue (10), the promotion of wound healing (11), use in cosmetics and dermatology (12,13) and the treatment or prevention of bacterial and viral infections (14–16). Emerging efforts are also targeted at using photosensitizers in a more 'materials oriented' setting, e.g. for degradation of pollutants and remediation (17).

All these interests and efforts have resulted in an almost exponential growth in the available literature. Certainly, more than an individual researcher can follow. If we take a simple look at the occurrence of the term 'photodynamic therapy' in Clarivate's Web of Science database, the first mention in 1972 (18) was followed by 100 publications in 1987, crossed the 1000 papers per year in 2004, and, since 2020, now exceeds 4000 publications per year. In part, this is driven by contemporary prolific publication practices but is also a result of continuous advances (19,20) in developing new clinical photosensitizers (21–23), advances in nanomedicine (24,25), new developments such as sonodynamic therapy and other deep tissue activation methods (26–28), increased awareness of PDT by clinical practitioners, and global issues. Here we note the worsening situation regarding antibacterial resistance (29), and the recent Covid-19 pandemic (30), both with a resultant focus on new antimicrobials. In a sense, the latter brought the PDT community back to its roots; after all, the very first large-scale clinical success of phototherapy by Finsen (31) is probably due to antimicrobial PDT (32).

One way of making sense of the advances in the field is to focus on a specific photosensitizer or 'success story' in PDT. Despite all the developments, the number of photosensitizers in clinical practice or trials is still limited (33,34). Historically, haematoporphyrin derivative (Porfimer sodium, Photofrin®), the first clinically approved PDT agent (5), δ-aminolevulinic acid (ALA, *e.g.* Levulan®) as the biosynthetic precursor of protoporphyrin (35), Verteporfin ('benzoporphyrin derivative', Visudyne®) and its success in treating age-related macular degeneration (36), and the established photochemotherapeutic

*Corresponding authors email: arno.wiehe@biolitec.com (Arno Wiehe), email: mathias.senge@tum.de (Mathias O. Senge)
†This publication is dedicated to Prof. Silvia E. Braslavsky, a pioneer in photobiology and photobiophysics, on the occasion of her 80th birthday.
‡This article is part of a Special Issue celebrating the 50th Anniversary of the American Society for Photobiology.

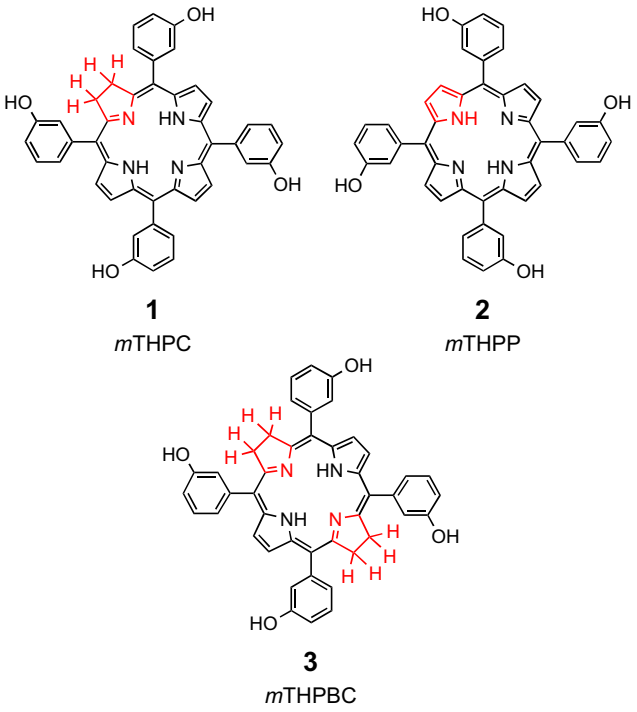

Figure 1. Chemical formulae of 5,10,15,20-tetra(*m*-hydroxyphenyl)porphyrins related to *m*THPC: 1, the chlorin, a dihydroporphyrin, *m*THPC; 2, the parent porphyrin, *m*THPP; 3, the bacteriochlorin, a tetrahydroporphyrin, *m*THPBC.

PUVA therapy (37) are noted success stories. In terms of resulting from a more logical drug design development leading to clinical use, temoporfin (Fig. 1, *m*THPC, 5,10,15,20-tetrakis(3-hydroxyphenylchlorin, **1**)) still takes a unique position (38) and thus can serve as an example of the state-of-the-art, ongoing developments and limitations of PDT (39).

Developed by Bonnett almost 40 years ago (40) to create a second-generation photosensitizer, this compound has the advantage of being a well-characterized single molecule. Temoporfin is the active pharmaceutical ingredient in the medicinal product Foscan® which is on the market in the EU for the palliative treatment of head and neck cancer and since then is in continuous clinical use. In the intervening years, it has served as a test bed for many advances in third-generation photosensitizer design. This is reflected in – again using Web of Science (with the key words *m*THPC, *m*-THPC, temoporfin, Foscan) as a benchmark – about 900 publications since the early 1990s (41). The number of annual publications is about 40 per year, a more manageable body of work than of PDT as a whole.

The historical development of temoporfin and the related literature on its uses, developments and clinical applications up to 2010 was covered in a review by Senge and Brandt in this journal (42). In addition, a brief review covering the literature on developments in formulation, chemical modifications and targeting strategies was published at the same time (43). The main purpose of the present treatise is to survey the primary literature since 2010 and close the gap with these earlier reviews. For ease of access, we have maintained the structure and topical breakdown of the earlier paper (42).

CHEMISTRY

The synthesis (40,44), standard modifications of the macrocycle and the 3-hydroxyphenyl groups, and degradation reactions of temoporfin were reviewed earlier (42,43). Here we focus on recent developments in the chemical modification of *m*THPC, synthesis of related structures, and methodological advances with related porphyrins. In chemical terms *m*THPC **1** is derived by the reduction of *m*THPP **2** and can be further reduced to the bacteriochlorin *m*THPBC **3** (Fig. 1). Overall, its synthesis involves the condensation of pyrrole with (protected) 3-hydroxybenzaldehyde to the respective porphyrinogen, oxidation to *m*THPP and then reduction.

In a new development, the use of MnO_2 under microwave conditions for the oxidation step gave a **2** in 30% yield (45). The same authors also prepared the bacteriochlorin **3** from **1** via Whitlock reduction using microwave conditions. This could then be oxidized with MnO_2 to the chlorin **1** in ~90% yield. This approach uses less solvents and is more facile; however, both the reduction and oxidation steps yielded the respective chlorin and porphyrin as by-products (10%). Mechanochemistry has also been applied to the diimide reduction of porphyrins giving *m*THPC in 55% of *m*THPP (46).

Chemical modifications of *m*THPP and *m*THPC

Next to the central core for metallation, only the β-pyrrole positions and 3-hydroxyphenyl groups lend themselves to functionalization reactions. With regard to the former, Wiehe and coworkers presented an alternative approach towards 5,10,15,20-tetrakis(3-hydroxyphenyl)chlorins, albeit requiring a total synthesis approach (Fig. 2) (47). Using a method established by Crossley's group (48) they prepared the 3-methoxyphenyl diketone **4**. This compound could be disubstituted to the *vic*-dihydroxy chlorin **5** using Grignard reagents. Demethylation with BBr_3 then yielded the respective meso-3-hydroxyphenyl chlorin **6** (47). The compounds exhibited absorption and photophysical properties similar to *m*THPC. While the compound with 3,5-di(trifluoromethyl)phenyl residues exhibited a 50% higher singlet oxygen quantum yield compared to temoporfin, its PDT activity against HT29 cells was lower than the other compounds.

Naturally, there is more scope for functionalization of the hydroxyphenyl groups. They can be used to attach targeting groups, link the chromophore to carrier systems, or create covalently linked nanomaterials. However, one has the problem of having four reactive groups in the molecule, which, in the case of monofunctionalization, gives rise to regioisomeric mixtures.

To give only some examples for using standard substitution reactions, Capobianco and coworkers reacted *m*THPC with 4-(bromomethyl)benzoic acid in the presence of NaH to yield a mixture with 1 to 3 linkers units attached to temoporfin, most likely via O-CH_2-linkages (49). The modified chromophore was then used to functionalize $LiYF_4$:Tm^{3+}/Yb^{3+} upconverting nanoparticles (UCNPs) via reaction with the carboxylic acid groups to yield nanoparticles capable of inducing cell death with 980 nm irradiation. In another study, temoporfin mono-anhydride conjugates, which additionally contained a disulfide linker, were prepared to generate folate-conjugates (50).

In terms of synthetic methods, Rogers *et al.* (51) used Steglich conditions to prepare mono- and tetrafunctionalized

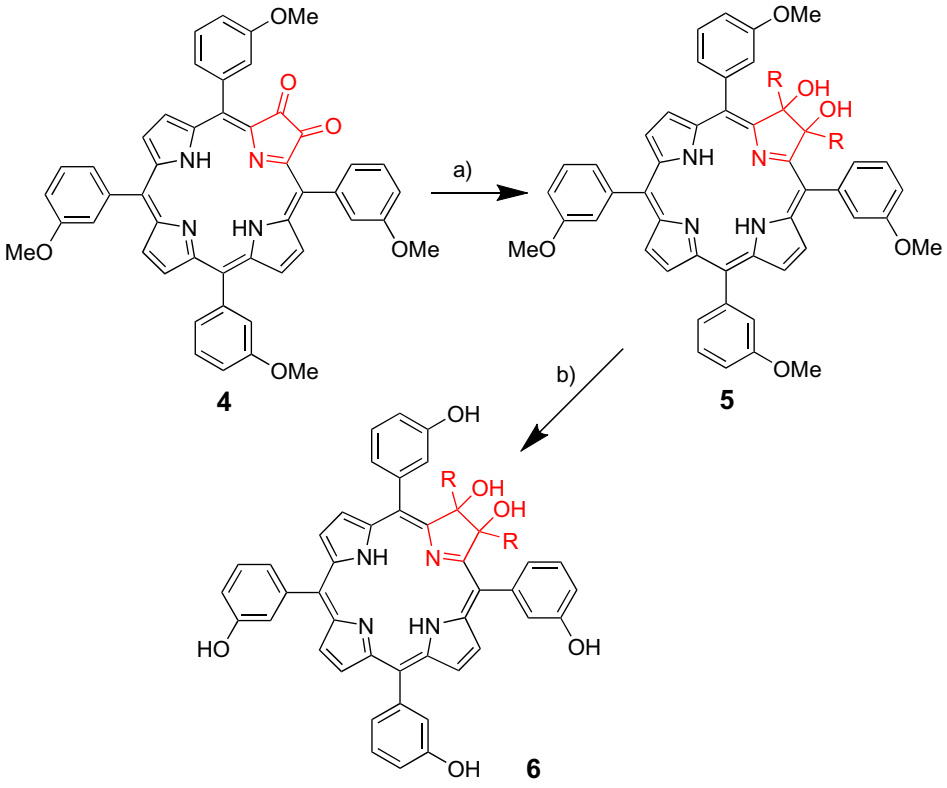

Figure 2. Synthesis of *vic*-dihydroxychlorins related to Temoporfin (46). Reagents and conditions: (a) RMgBr or Me_3SiCF_3/TBAF, THF, -45°C, 44–53%; (b) BBr_3, CH_2Cl_2, −50°C, 57–87%. R = hexyl, 3,5.bis(trifluoromethyl) phenyl, CF_3.

*m*THPC derivatives. The reaction of *m*THPC **1** with a range of non-steroidal anti-inflammatory drugs (NSAIDs) using 1-ethyl-3-(3-dimethylaminopropyl)carbodiimide (EDC) and hydroxybenzotriazole (HOBt) gave the respective ester conjugates as shown in Fig. 3. Depending on the number of equivalents used for the NSAIDs, either the mono- (2-4 equiv.) (**7**) or tetrafunctionalized (**8**) derivatives (10–20 equiv.) were obtained in 36–43% and 61–70% yield, respectively. While the compounds were all taken up by OE33 or SKGT-4 cells, no phototoxicity was observed at short illumination times (2 min). Similar reactions were used to link *m*THPC to nanodiamonds (52). Esterifications were also used in the generation of *m*THPC-Au-nanoparticles (AuNPs) (53). The reaction of the AuNPs with mercaptopropionic acid then allowed reaction of the carboxylic acid on the NPs with the hydroxy groups of temoporfin.

Rogers *et al*. (54) also developed methods for the selective mono- and tetrafunctionalization of *m*THPC and *m*THPP. The reaction of **1** or **2** with propargyl bromide in the presence of K_2CO_3 could be controlled to yield, e.g. **10** in 48% (with 2 equiv.) or **11** in 98% (with 10 equiv.) yield (Fig. 4). Similar reactions of broad substrate scope were implemented for reaction with 1-iodopropane, benzyl chloride, 4-bromobenzyl bromide, 4-nitrobenzyl bromide, 2-bromobenzoic acid and benzoic anhydride. Using NaH as base reaction with 1 equiv. yielded the monosubstituted *m*THPP derivatives in 35–44% yield, while 10 equiv. gave the tetrasubstituted products often in quantitative yield (59–96%). The reaction also allowed the preparation of the respective triflate and tosylate derivatives. Related reactions were used for the preparation of picket-fence and cofacial bisporphyrin derivatives. The Zn(II) complexes of *m*THPP also underwent Chan-Lam couplings with boronic acids yielding the respective monosubstituted derivatives in 35–39% yield.

Direct substitution of the hydroxyl groups can also be used to generate amphiphilic porphyrins. For example, the reaction of **2** with hexyl bromide gave the monofunctionalized compound in 30% yield. In turn, this could then be reacted with 2,3,4,6-tetra-O-acetyl-1-O-(3-chloropropyl)-α-D-mannopyranoside to yield compound **13** in 33% after deprotection of the carbohydrate units (Fig. 5) (55).

The propargylic group, e.g. in **9** or **10** is a useful synthetic handle for Cu(I) mediated 1,3-dipolar cycloaddition (‘click’) reactions. This allows for the facile preparation of bioconjugate derivatives of photosensitizers. For example, the reaction of the zinc(II) complex of **9** with an azido functionalized bile acid gave the bile acid conjugate **14** in 61% under microwave conditions (55). Such compounds were readily taken up in esophageal cancer cells, localized in the ER and Golgi apparatus, but showed no phototoxicity. In related works click reactions between ethynylphenyl residues on porphyrins with azido-functionalized carbohydrates generate amphiphilic photosensitizers (56). Similarly, *p*-azidophenylporphyrins can be reacted with propargylic derivatives of carbohydrates to generate water soluble and amphiphilic porphyrins (57–59). Click reactions are also a facile method for linking photosensitizers to nanomaterials. One such example was given by Chen *et al*. (60) who linked aliphatic azido residues with the hydroxyphenyl groups in *p*THPP and then performed click reactions with alkynyl residues on polyhedral oligomeric silsesquioxanes to yield nanoscale photosensitizing materials.

The propargylic groups in **9**–**12** can also be used in Pd-catalyzed coupling reactions. For example, a reaction of **12** with

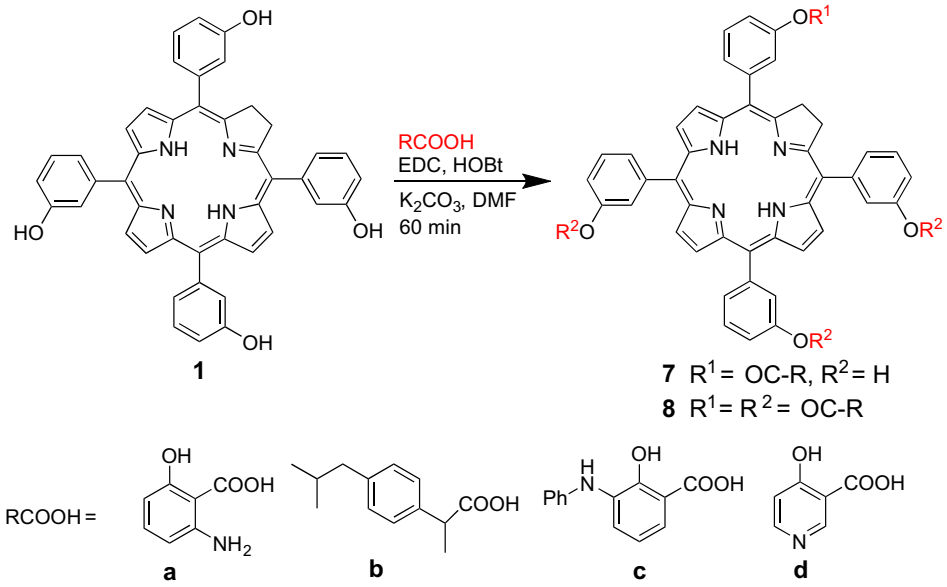

Figure 3. Synthesis of NSAID conjugates of temoporfin.

4-iodobenzaldehyde under Sonogashira conditions gave the tetraaldehyde **15** in 45% yield which exhibited an enhanced two-photon absorption cross section compared to temoporfin indicating the possibility of using such derivatives in two-photon induced PDT (61).

An alternative method to achieve monofunctionalization is to use *m*THPC/*m*THPP derivatives carrying one functionality that can be addressed directly (62). This was exemplified by Staegemann *et al*. who prepared *m*THPP analogues, where one meso-hydroxyphenyl residue was replaced by a pentafluorophenyl group. The *p*-position in the latter can easily be substituted under conditions not affecting the hydroxyphenyl groups, e.g. via reaction with amines (63). The use of amines with terminal alkynyl groups then allowed an entry into click-chemistry, which was used to link the chromophore with stimuli-responsive hyperbranched polyglycerols.

Related porphyrinoids

The range of related compounds, *i.e*, with similar substituent patterns or functional groups, is ever expanding (64). In the following, we highlight selected examples that have been directly compared with temoporfin (see also below) or conceptional approaches which could also be applied to *m*THPP/*m*THPC systems.

An interesting approach, albeit realized only for the 5,10,15,20-tetraphenylporphyrin framework, was reported by Nykong *et al*. (65). Using a standard sequence via Michael addition of dimethyl malonate with 2-nitro-5,10,15,20-tetraphenylporphyrin, they prepared the 'cyclopropanochlorins' **16** and **17** (Fig. 6). The compounds showed high photostability and *in vitro* and *in vivo* studies indicate promise for the treatment of cholangiocarcinoma. Another chlorin of interest is disulfonated 5,10,15,20-tetraphenylchlorin **18**. Prepared by Berg *et al*. via diimide reduction of the precursor porphyrin, **18**, as a mixture of three isomers ($TPCS_{2a}$), was used for photochemical internalization (PCI) (66) of bleomycin (67). *In vivo* studies with a CT26.CL25 subcutaneously growing mouse carcinoma model showed that it effectively facilitated import and activation of the toxin, induced siRNA-based gene silencing, and resulted in tumor growth delay superior to *m*THPC PDT.

At the bacteriochlorin level, we note a broad study by Dabrowski *et al*. on photostable sulfonamides of halogenated bacteriochlorins (68). With either chlorine or fluorine atoms in the *o*-phenyl positions, these compounds (**19**) absorb in the near-IR, and show high cellular uptake, localization in the ER. Together with low cyto- and high phototoxicity these photosensitizers operate both Types I and II photochemical reactions. One of these compounds (Redaporfin, **20**) has progressed to the clinical trial stage, as preclinical data showed it to be a potent photoactivated antineoplastic that also facilitates indirect immune-dependent destruction of malignant tissue (69). Due to the presence of the sulfonamide groups, these compounds are formed as atropisomeric mixtures. Depending on the relative orientation of these groups four different atropisomers are possible (α_4: ↑↑↑↑, $\alpha_3\beta$: ↑↑↑↓, $\alpha_2\beta_2$: ↑↑↓↓, αβαβ:↑↓↑↓). Investigation of the individual redaporfin atropisomers showed the α_4 atropisomer, where the sulfonamide substituents are on the same side of the tetrapyrrole macrocycle, to exhibit the highest cellular uptake and phototoxicity as the most amphiphatic rotamer (70). Thus, atropisomerism as a drug design principle must be taken into account for *m*THPC derivatives with at least two *o*-phenyl residues (provided the rotation barrier is high enough).

Going back to the porphyrin level the range of compounds is much wider. An interesting study from 2009 investigated 5,15-diarylporphyrins with only one *m*-hydroxyphenyl group (**21**). The compounds induced apoptosis in HCT111 human colon carcinoma cell, generated ROS and $NO^{\bullet}$, and showed a higher photodynamic effect compared to *m*THPC, most likely due to higher uptake (71). Interestingly, related tetraarylporphyrins and -chlorins with 3,4-dihydroxyphenyl residues – in a sense a composite of *m*THPC and *p*THPC – were reported by Marydasan

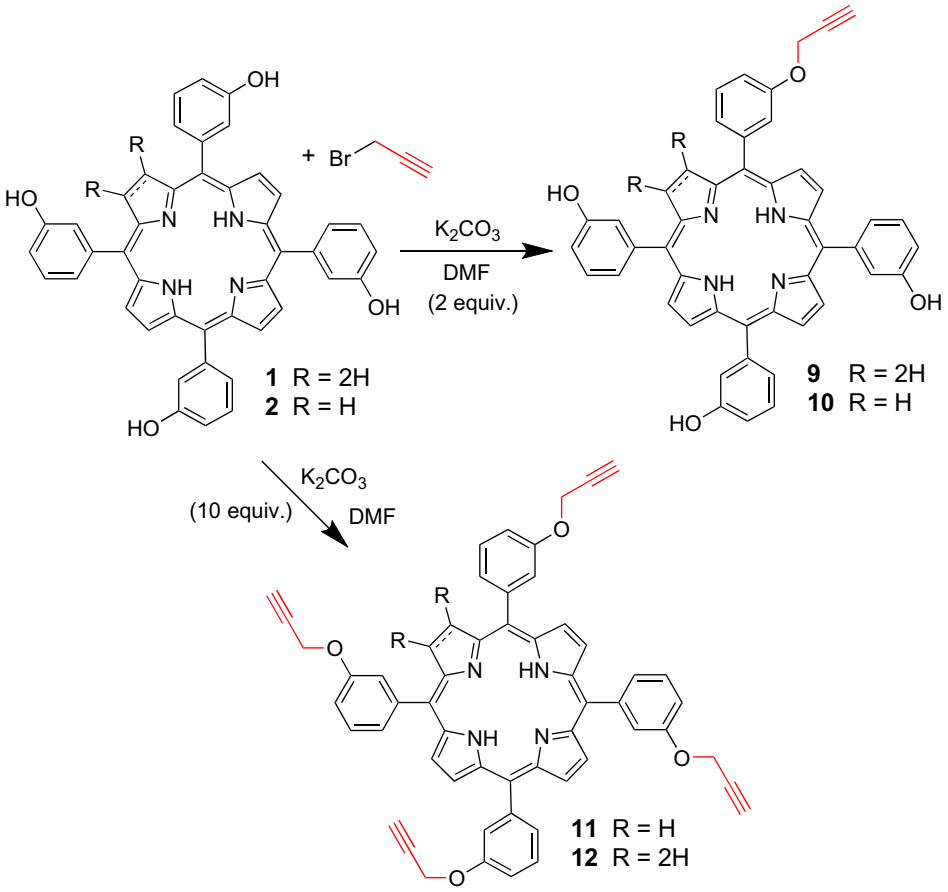

Figure 4. Synthesis of propargylic derivatives of *m*THPP and *m*THPC.

et al. (72). The chlorin **22** was prepared via diimide reduction of the respective dimethoxyphenylporphyrin, followed by demethylation with BBr_3. Water solubility of **22** was increased 6-fold compared to *m*THPC, with excellent triplet excited state and singlet oxygen yields. *In vitro* studies with human ovarian cancer cells (SKOV-3) and *in vivo* studies in a mouse model confirmed high photodynamic activity. Di- and trisubstituted phenyl substituents were also employed by Rojkiewicz *et al*. (73). They prepared a range of 5,10,15,20-tetraarylporphyrins of the general type **23** using a combination of pyrrole condensation and hydroxy group substitution reactions to generate amphiphilic systems. All compounds exhibited singlet oxygen quantum yields in the range of 0.6–0.7.

Other compounds of interest are the hydrophobic 5,10,15,20-tetrakis(quinolin-2-yl)porphyrin (74), water-soluble phosphorous (V) 5,10,15,20-tetraalkylporphyrins (75), water-soluble 5,10,15,20-tetracarboxyporphyrins (76) and temocene, the porphycene analogue of *m*THPP (77). The latter absorbs stronger in the red spectrum compared to *m*THPC, is more photostable, has lower dark toxicity, and, depending on the delivery means, localizes in mitochondria or lysosomes (78). Its singlet oxygen quantum yield is lower compared to *m*THPC, and the DFT study relates this to the slightly higher spin-orbit coupling matrix elements (SOCME) in the former (79).

Computational methods are increasingly used to suggest suitable photosensitizers or to explain features of existing ones. For example, DFT calculations of a range of synthetic, expanded bacteriochlorins gave higher computed SOCME compared to temoporfin thus suggesting the PDT potential of such compounds (80). In one study DFT was used to design new candidate molecules with strong red-shifted absorption bands. The spectra were shown to depend on the substituent pattern and one chlorin with four propenoic acid groups (λ_{max} = 755 nm) was suggested as a lead compound (81), while time-dependent DFT using long-range corrected functionals accurately predicted the long-wavelength absorption of temoporfin (82). However, a theoretical quantitative structure property relationships (QSPR) study which aimed to correlate λ_{max} of the Q band with eight descriptors (*e.g.* aromaticity, electrostatics, reactivity) showed that the wavelength is a multidimensional parameter and cannot be correlated with a single descriptor. This approach gave good agreement between theoretical and experimental data (83).

A quantum chemical study investigated the *m,o,p*THPC isomers (84). While most features (chemical hardness, ionization potential, triplet energy level, and UV spectra) are similar for the isomers, differences in the dipole moment confirmed the greater lipophilic character of *m*THPC over the *o*- and *p*-isomers.

Photochemistry

A study by Brault and coworkers used laser flash photolysis to investigate the reaction of the *m*THPC triplet state with antioxidants (85). Both the antioxidant Trolox and the anesthetic Propofol reacted with the photosensitizer triplet state in

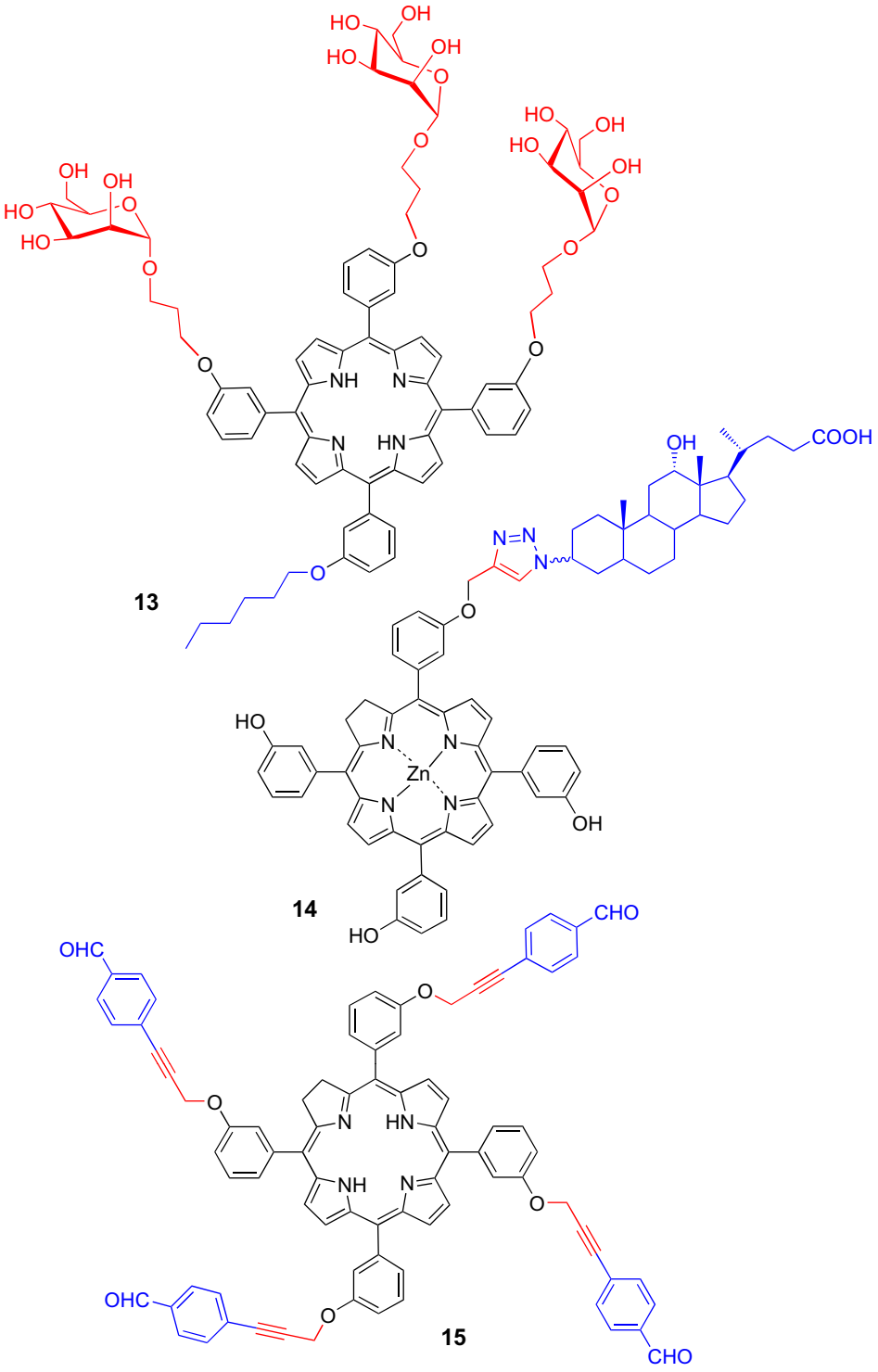

Figure 5. Selected bioconjugates and derivatives of *m*THPC.

solution regenerating the ground state. In the latter case, a unimolecular reaction was observed, while in the former a bimolecular reaction with intermediary detection of a Trolox radical and *m*THPC radical anion was observed. The reaction kinetics with Propofol indicated that quenching of triplet state *m*THPC could occur under clinical conditions when using this anesthetic.

PHARMACOLOGY AND BIOCHEMISTRY

In vitro tests

The first step in the evaluation of any drug candidate for its medicinal potential is characterization at the *in vitro* level. This serves to establish its uptake mechanism, intracellular localization, (dark)

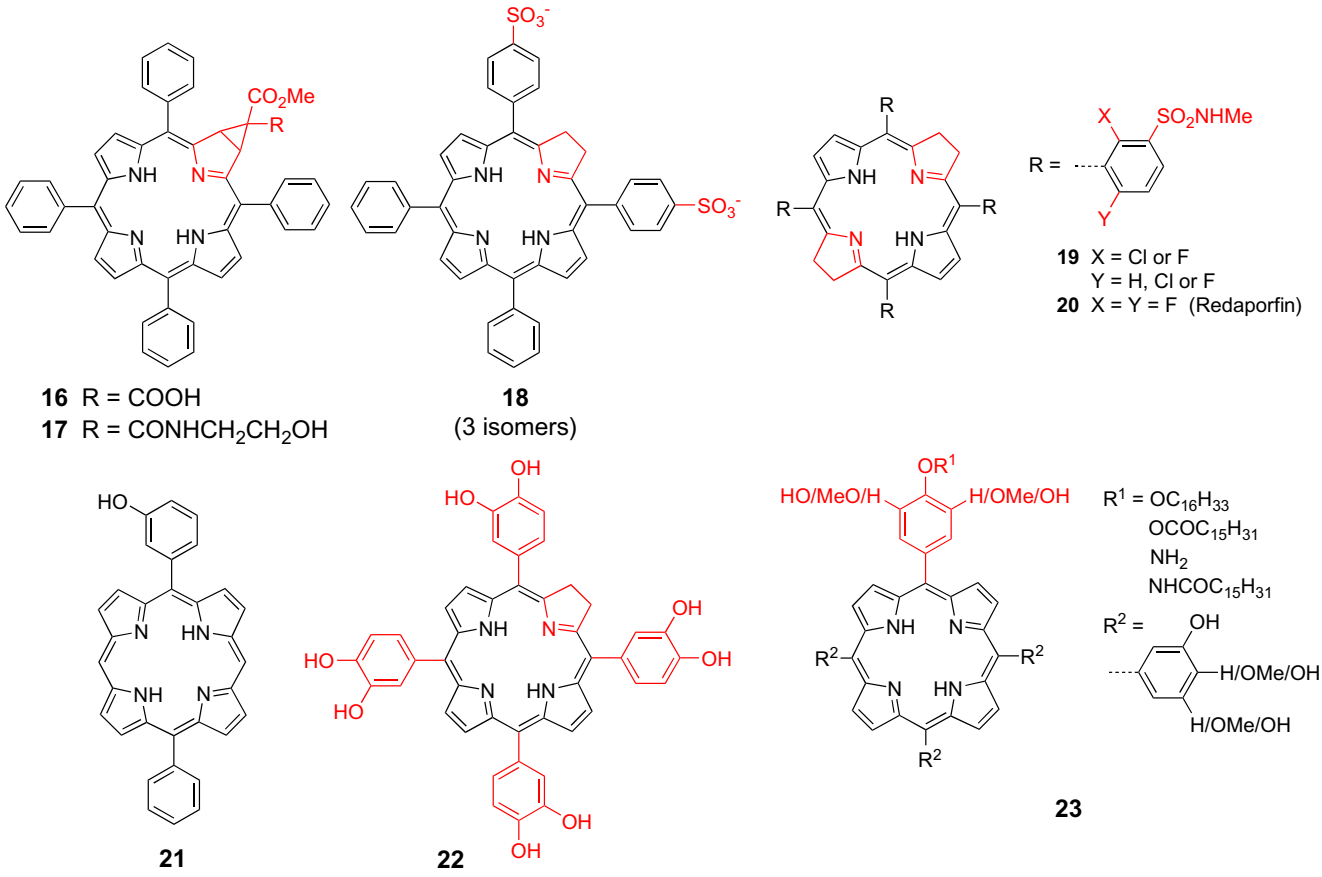

Figure 6. Representative examples of novel photosensitizers.

cytotoxicity, phototoxicity upon illumination, and modes of cell death. The relevant classic studies related to temoporfin have been discussed before (42). Still, the field does not stand still, and the decade of work covered in this review has seen numerous additional *in vitro* studies with temoporfin and its congeners. These were aimed at expanding clinical applications to other types of cancer or diseases, improving PDT protocols, assessing the impact of co-administration of other effectors, evaluating new targeting strategies, validating new formulations, and more.

While facile and cheap, simple 2D *in vitro* cell tests have their pitfalls (86). There may be changes in cell morphology, different interactions of the cellular and extracellular environments, altered polarity or cell division. 2D cell cultures do not reflect the 3D tissue environment, neglect interactions and influence with other cells, cannot mimic influences such as anti-angiogenesis, immune effects, etc. As a result, the predictive power of 2D *in vitro* studies within the translational pipeline, or even for transition to *in vivo* animal models, is very limited (87).

The same issues affect PDT studies, *i.e.* simple 2D systems cannot provide information on the migration and invasiveness of cancer cells (88) or the influence of the tumor vasculature (89). Different Human cancer cell lines can give drastically different responses to PDT (90). Another problem is the adherence of photosensitizers to the culture microplates used in the cell tests (91). Plaetzer and coworkers investigated a range of hydrophilic and hydrophobic photosensitizers with respect to their adherence to the surfaces of 96-well microplates (92). Lipophilic compounds (temoporfin, hypericin, Photofrin®) exhibited strong adherence to the microplates. Using lysis and fluorescence measurements they showed that 50–90% of the fluorescence signal was caused by PS adherence. The composition of the medium can impact the PDT efficacy as well. Pretreatment of the medium (RPMI 1640 supplemented with fetal calf serum (FCS)) with Rose Bengal or temoporfin (and light) used for the growth of rat glioma cells reduced cell survival by 40% upon irradiation of the cell suspension (93). In the medium pre-treated with Rose Bengal and light the presence of oxidizing species was detected suggesting the formation of such long-lasting oxidizing species, *e.g.* peroxides, as the result of initial ROS formation in the medium (93).

By now 3D cell systems have become the standard of analysis and have been employed in a wider range of PDT studies (see Table 1) (236,237). Amongst others, they have been used to evaluate the use of extracellular vesicles for drug delivery (211,212). They have also been used to evaluate how the stroma-rich microenvironment affects the uptake and activity of lipid-based nanoformulations (219,220). Often such studies show that the PS (as indicated by fluorescence) is confined to the external cell layers of spheroids (205). A quantitative means to determine the penetration in tumor spheroids with the high spatial resolution is the use of laser ablation coupled to inductively coupled plasma mass spectrometry (238). This requires incubation with metal complexes and Pd-tagged *m*THPP was used in this context.

3D cell systems also offer the advantage of using different cell types within one system (236). For example, Philipps *et al.*

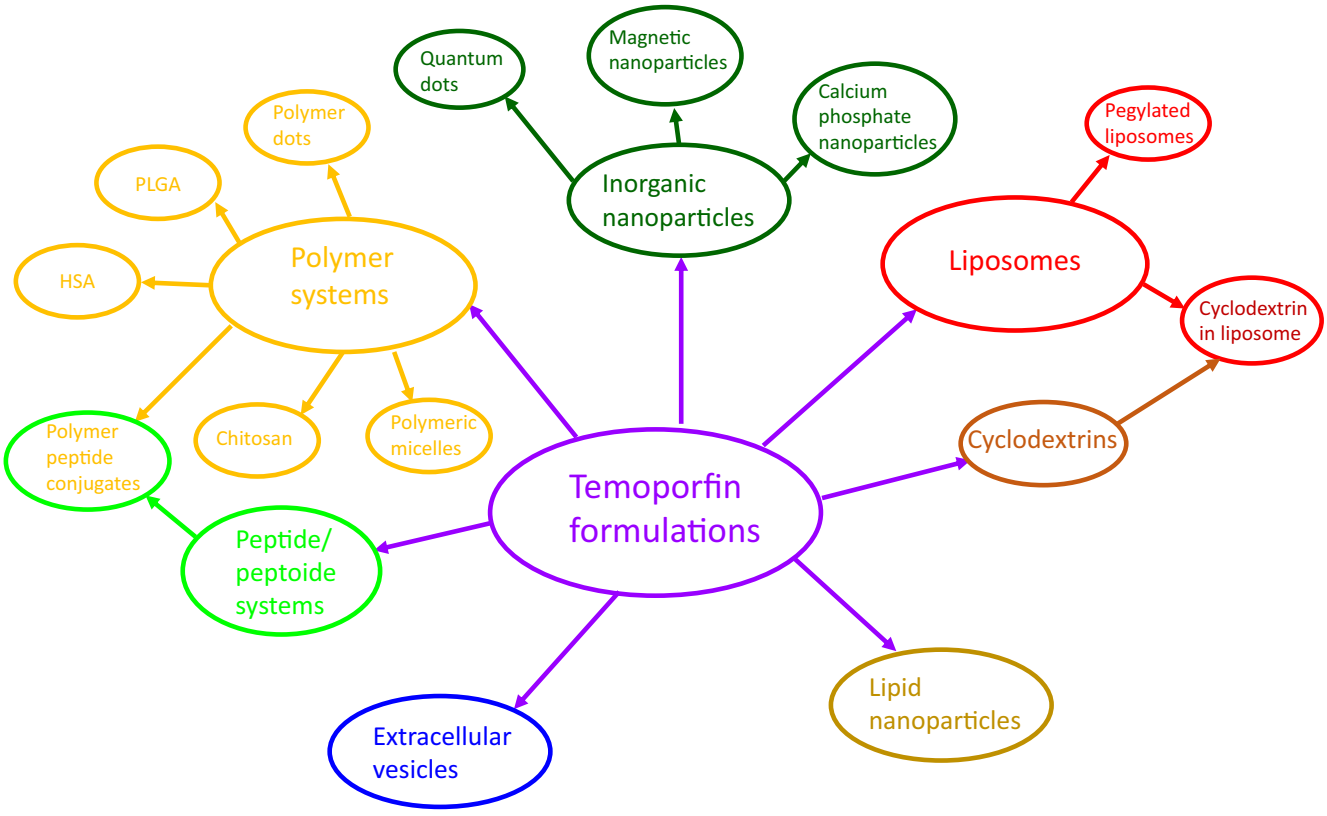

Figure 7. Graphical illustration of pharmaceutical formulation systems explored with temoporfin.

studied the peripheral neural cell sensitivity to temoporfin in a 3-dimensional collagen gel culture system and found MCF-7s and satellite glia to be more sensitive to PDT than neurons (207). A similar system comprised only of the glia cells showed that inhibition of antioxidant pathways increased the sensitivity of neurons to PDT (225).

In tandem with new developments in using 3D cell methods, screening methods are advancing as well. Thus, high content screening and analysis are slowly replacing standard assays (51,58,75,158,239). Such assays require the identification of cellular parameters (*e.g.* nuclear area, reciprocal form factor, cell area, cell number, PS integrated area, and PS area) which can be used to determine the phototoxic effects of porphyrin compounds. Using esophageal cell lines Vaz *et al*. evaluated parameters such as these in a screen of five photosensitizers, including temoporfin (240). This proof of principle study showed that the HCS assay offers significant advantages and correlated with MTT data.

Temoporfin as a comparator

As an established clinical photosensitizer temoporfin and its various formulations often serve as a comparator, *i.e.* are used to evaluate the PDT potential of novel compounds and other drug candidates. Without going into the details or analyzing all other photosensitizer classes, compounds from almost all of them have been compared with temoporfin and related formulations (151). Some individual representative examples include BODIPYs (241), bacteriochlorins such as redaporfin (109), unsymmetrically 5,15-disubstituted porphyrins (119,242), picolyl-functionalized porphyrin zinc(II) complexes (243), new chlorin e_6 derivatives (155,213), chlorin e_6 derivative liposomal formulations (134), gallium(III) corroles (125), tetra(3,4-pyrido)porphyrazines embedded in cationic cages (100), and phthalocyanines and tetrapyrazinoporphyrazines (244). The most relevant data relating to temoporfin are compiled in Table 1.

Such studies reveal differences in the PDT efficacy and mode of action and cell death between photosensitizers. For example, a comparison with redaporfin showed different susceptibilities of A549 and CT26 cells to the two photosensitizers (Table 1) indicating that e.g. A549 cells are more susceptible to PDT operating via Type I. Using redaporfin in combination with ascorbate and inhibition of antioxidant enzymes significantly improved its effect against such cells (109).

Mechanistic aspects

The basic mechanism of action of photosensitizers is quite well understood. It relies on the formation of reactive oxygen species (ROS) generated by Type I or Type II photoreactions. In the case of temoporfin, the dominant mechanism is the Type II reaction leading to the formation of singlet oxygen (42,109,245). This singlet oxygen reacts, depending on the photosensitizer localization in the cell, with surrounding biomolecules, thereby damaging the cells and provoking cell death *via* apoptosis, autophagy or necrosis, though other cell death pathways like paraptosis also play a role (110,246–250). These direct effects on the tumor cells are important for PDT, however, they cannot

Table 1. Cell lines used for selected *in vitro* studies with *m*THPC or derivatives thereof in solution.

Cell line	Compound/Formulation	Study	Comments/Phototoxicity	Year	References
African green monkey kidney cells CCL-81	Styrene maleic acid copolymer (SMA) micelle encapsulating *m*THPC; SMA@mTHPC	PDT study	Phototoxicity: IC50 SMA@mTHPC = 0.15 μg mL^{-1}; dark toxicity: IC50 SMA@mTHPC = 20 μg mL^{-1}	2021	(94)
Head and neck squamous cell carcinoma SCC19	*m*THPC	Cell death mechanism	Enhanced apoptosis with fenretinide via de novo sphingolipid biosynthesis pathway	2016	(95)
Head and neck squamous cell carcinoma SCC19	*m*THPC (+C6-pyridinium ceramide or Fenretinide)	Combination with anti-cancer agents C6-pyridinium ceramide/Fenretinide	Fumonisin B1 inhibits apoptosis after PDT	2017	(96)
Head and neck squamous cell carcinoma UMB-SCC 745 (and 969)	Foslipos	Cell death mechanism; combined used with hypericin	Necrosis; upregulation of heat shock proteins	2013	(97)
Head and neck squamous cell carcinoma UMB-SCC 745 (and 969)	Foslipos+hypericin (1:1)	Dark toxicity	Combination has no dark toxicity, unlike individual PS	2012	(98)
HeLa	*m*THPC	Comparison with temocene	Temocene is more stable, has lower dark toxcitiy, but is less active than *m*THPC	2011	(77)
HeLa	*m*THPC	Comparison with 5,10,15,20-tetracarboxyporphyrin	IC_{50} = 1.6 μM	2019	(76)
HeLa	*m*THPC *m*THPC SOF1 mTHPC SOF2 *m*THPC SOF3	Temoporfin supramolecular framework (SOF) PDT [	IC_{50}: 54.2 μg L^{-1} IC_{50}: 13.7 μg L^{-1} IC_{50}: 24.2 μg L^{-1} IC_{50}: 23.0 μg L^{-1}	2022	(99)
HeLa	*m*THPC	PDT comparison with tetra(3,4-pyrido)porphyrazines	EC_{50} = 0.045 μM (λ > 570 nm, 12.4 mW cm^{-2}, 15 min, 11.2 J cm^{-2}); > comparator	2016	(100)
HeLa	*m*THPC-S-S-PEG-Folate conjugate *m*THPC-PEG-Folate conjugate	Development of releasable conjugate systems	Redox-responsive folate targeting PS *m*THPC-S-S-PEG-Folate showed slightly higher phototoxicity than *m*THPC-PEG-Folate	2019	(50)
HeLa	*m*THPC loaded folate-PEOz-PLA micelles	PDT study		2012	(94)
HeLa	*m*THPC loaded P(CL_x-TMC-Bz_y)-PEG micelles *m*THPC	PDT study	Photocytotoxicity: EC_{50} = 5–13 μg mL^{-1}; free *m*THPC = ~1.5 μg mL^{-1}	2020	(101)
HeLa	*m*THPC loaded PCLn-PEG micelles decorated with EGFR targeting nanobody (EGa1)	EGFR targeting PS	EGa1-conjugated micelles are internalized upon specific binding of the NP with the EGFR receptor overexpressed on the surfaces of A431 cells, resulting in enhanced cellular uptake and photocytotoxicity on A431 cells, as compared to EGFR low-expressing HeLa cells	2020	(102)
HeLa	*m*THPP loaded P(Glu-b-NADA), amphiphilic block-co-polypeptides	amphiphilic co-polypeptides as drug delivery systems	No dark toxicity, *m*THPP release in controlled manner	2012	(103)
HeLa	*m*THPC + iron oxide magnetic NP + doxoruicin in liposomes	PDT/photothermal study	Almost complete elimination of cancer cells; effect of magnetic hyperthermia = PDT > chemotherapy	2016	(104)
HeLa	mTHPC covalently linked to LiYF4: Tm3+/Yb3+ upconverting nanoparticles (UCNPs)	PDT study	70% cell death under 980 nm illumination	2014	(49)
HeLa	*m*THPC	Test of LEDs as light source		2016	(105)
Hep-2	*m*THPC + cisplatin	Synergistic effect of Pt(II) complexes	Improved efficacy with sequential administration	2019	(106)
Human acute myeloid leukemia AML	*m*THPC	*in vitro* $^1O_2$ luminescence measurements		2011 2012	(107,108)

(continues)

Table 1. (continued)

Cell line	Compound/Formulation	Study	Comments/Phototoxicity	Year	References
Human adenocarcinoma SKGT-4	*m*THPC derivative **13**	Impact of bile acid conjugates	Good uptake in cells but no PDT effect	2013	(55)
Human adenocarcinoma SKGT-4	*m*THPC	Comparison with P(V) 5,10,15,20-tetraalkylporphyrins	High content analysis, *m*THPC IC_{50} = 5 μM	2014	(75)
Human adenocarcinoma SKGT-4	*m*THPC-NSAID conjugates	PDT study	Good uptake but no phototoxicity at 2 min illumination	2015	(51)
Human alveolar basal epithelial adenocarcinomic cells A549	*m*THPC	Comparison with 5,10,15,20-tetracarboxyporphyrin	IC_{50} = 0.5 μM	2019	(76)
Human alveolar basal epithelial adenocarcinomic cells A549	*m*THPC	Comparison with redaporfin	LLD_{50} = 20 mJ cm^{-2} at 0.5 μM (*m*THPC) LLD_{50} = 250 mJ cm^{-2} at 5 μM (redaporfin)	2016	(109)
Human alveolar basal epithelial adenocarcinomic cells A549	*m*THPC	Cell death mechanism	*m*THPC initiates paraptosis after ER photodamage	2021	(110)
Human alveolar basal epithelial adenocarcinomic cells A549	*m*THPC *m*THPC SOF1 mTHPC SOF2 *m*THPC SOF3	Temoporfin supramolecular framework (SOF) PDT [	IC_{50}: 45.9 μg L^{-1} IC_{50}: 26.7 μg L^{-1} IC_{50}: 34.6 μg L^{-1} IC_{50}: 17.5 μg L^{-1}	2022	(99)
Human alveolar basal epithelial adenocarcinomic cells A549	*m*THPC-loaded PLGA nanoparticles	Nanoparticles versus free PS	No dark toxicity of temoporfin in nanoparticles; reduced cellular uptake of NP, but similar phototoxicity	2012	(111)
Human alveolar basal epithelial adenocarcinomic cells A549	*m*THPC in micelles + Renilla luciferase-immobilized quantum dots-655 (QD-RLuc8)	Bioluminescence activated PDT	Bioluminescent QD-RLuc8 conjugate exhibits self-illumination at 655 nm after coelenterazine addition which allows activation of the PS	2013	(112)
Human alveolar basal epithelial adenocarcinomic cells A549	Fospeg®	PDT study	Less dark toxicity of Fospeg compared to *m*THPC; internalization via endocytosis and localization in Golgi; 30–40% lower efficiency of uptake	2011	(113)
Human alveolar basal epithelial adenocarcinomic cells A549	*m*THPC in folate-targeted liposomes	Folate targeting	Similar degree of internalization and phototoxicity for folate targeted and non-targeted liposomes	2013	(114)
Human alveolar basal epithelial adenocarcinomic cells A549	*m*THPC	Evaluation of Raman spectroscopy for diagnostics	No interference of irradiation with 785 nm	2021	(115)
Human Barrett's esophagus adenocarcinoma OE33	*m*THPC derivative **13**	Impact of bile acid conjugates	Good uptake in cells but no PDT effect	2013	(55)
Human Barrett's esophagus adenocarcinoma OE33	*m*THPC	Comparison with P(V) 5,10,15,20-tetraalkylporphyrins	High content analysis, *m*THPC IC_{50} = 5.1 μM	2014	(75)
Human Barrett's esophagus adenocarcinoma OE33	*m*THPC-NSAID conjugates	PDT study	Good uptake but no phototoxicity at 2 min illumination	2015	(51)
Human breast adenocarcinoma MCF-7	*m*THPC	Cell death mechanisms	Autophagy contributes to cell death	2011	(116)
Human breast adenocarcinoma MCF-7	*m*THPC	Intracellular localization	ER and Golgi as primary sites of action	2003	(117)
Human breast adenocarcinoma MCF-7	*m*THPC	ER targeting	Development of luciferase reporting system	2014	(118)
Human breast adenocarcinoma MCF-7	*m*THPC *m*THPC SOF1 mTHPC SOF2 *m*THPC SOF3	Temoporfin supramolecular framework (SOF) PDT [	IC_{50}: 43.5 μg L^{-1} IC_{50}: 21.1 μg L^{-1} IC_{50}: 23.3 μg L^{-1} IC_{50}: 12.2 μg L^{-1}	2022	(99)
Human breast adenocarcinoma MCF-7	*m*THPC	Comparison with 5,15-diarylporphyrins	IC_{50} = 5.4 nM; > comparator	2019	(119)
Human breast adenocarcinoma MCF-7	*m*THPC loaded FH-PDots	PDT study of polymer dots		2014	(120)

(continues)

Table 1. (continued)

Cell line	Compound/Formulation	Study	Comments/Phototoxicity	Year	References
			Active; cell viability increase with concentration; more uptake in cancer cells compared to normal ones due to folate receptor targeting		
Human breast adenocarcinoma MCF-7	*m*THPC loaded MEH-PPV and CN-PPV	PDT study of polymer dots	Significant uptake and phototoxicity; more cell damage for Pdots with CN-PPV polymer than with the MEH-PPV polymer	2016	(121)
Human breast adenocarcinoma MCF-7	*m*THPC-LNP (lipid NP)	PDT study	Phototoxicity similar to free *m*THPC, some dark cytotoxicity of LNP	2011 2014	(122,123)
Human breast carcinoma MDA-MB-231	*m*THPC	Cell death mechanism	c-PARP expression is dependent on treatment-induced apoptosis.	2009	(124)
Human breast carcinoma MDA-MB-231	*m*THPC	Comparison with 5,15-diarylporphyrins	IC_{50} = 1.84 nM; ~ comparator	2019	(119)
Human breast carcinoma MDA-MB-231	*m*THPC	PDT comparison with corroles	IC_{50} = 0.87 μM; > comparator	2020	(125)
Human breast carcinoma MDA-MB-231	*m*THPC core shell nano drug: ~80 nm size poly(lactic-co-glycolic acid) (PLGA) nano-core encapsulating *m*THPC and ~20 nm size albumin nano-shell encapsulating tyrosine kinase inhibitor dasatinib	Combination therapy	Blocking of cancer migration: disruption of Src kinase albumin–dasatinib nano-shell and generation of photoactivated oxidative stress by mTHPC-PLGA nano-core; combinatorial photo-chemotherapy resulted in synergistic cytotoxicity in ~99% of motility-impaired metastatic cells	2014	(126)
Human breast carcinoma MDA-MB-231	*m*THPC–T-SLNP; temoporfin-loaded 1-tetradecanol-based thermoresponsive solid LNP/Foscan®	PDT study	Faster accumulation of LNP formulation	2016	(127)
Human breast carcinoma MDA-MB-231	*m*THPC bound to Ce-doped-γ-Fe2O3 maghemite nanoparticles (MNPs)	Magnetic targeting of PDT agents	High uptake and phototoxicity; use of magnetic forces during incubation directed NPs to selected sites given 2× accumulation compared to no magnetic field	2019	(128)
Human breast carcinoma MDA-MB-231 (and 436)	*m*THPC	Evaluation of Raman spectroscopy for diagnostics	No interference of irradiation with 785 nm	2021	(115)
Human Burkitt's lymphoma Raji	*m*THPC–β-cyclodextrins	Effect of β-CD methylation		2021	(129)
Human cervix adenocarcinoma SISO	*m*THPC	Combination of PDT with glutathione peroxidase inhibition		2021	(130)
Human cervix adenocarcinoma SISO	*m*THPC	Cell death mechanism	Apoptosis main mechanism, autophagy can occur as well. Wide variation in PDT response among 5 cell lines	2019	(90)
Human cervix adenocarcinoma SISO	*m*THPC + carboplatin (CBDCA) or cisplatin (CDDP) or oxaliplatin (1-OHP)	Synergistic effect of Pt(II) complexes		2018	(131)
Human cholangiocarcinoma QBC-939	*m*THPC	Comparison with cyclopropanochlorins	IC_{50} = 1.96 μM [1 J cm^{-2}], slightly less effective than other chlorins	2020	(65)
Human cholangiocarcinoma TFK-1	Nanoparticle albumin-bound mTHPC	Nanoparticles versus free PS	Reduced cytotoxicity of NP while retaining phototoxicity	2020	(132)
Human colon carcinoma HCT116	*m*THPC	Comparison with 5,15-diarylporphyrins	IC_{50} = 7.6 nM; slightly less effective than other cmpds.	2009	(71)
Human colon carcinoma HCT116	*m*THPC-loaded PLGA nanoparticles	Nanoparticles versus free PS	No dark toxicity of temoporfin in nanoparticles; reduced cellular uptake of NP, but similar phototoxicity	2012	(111)
Human colon carcinoma HCT116	*m*THPC	Comparison with 5,15-diarylporphyrins	IC_{50} = 3.6 nM; = comparator	2019	(119)
Human colon carcinoma HCT116	*m*THPC multifunctional NPs ((mTHPC@VeC/T-RGD NPs)	PDT and immunotherapy		2021	(133)

(continues)

Table 1. (continued)

Cell line	Compound/Formulation	Study	Comments/Phototoxicity	Year	References
			induced apoptosis and/or necrosis and stimulated systemic immune response; sensitized tumors to PD-L1 blockade therapy		
Human colon carcinoma HCT116	*m*THPC	PDT comparison with chlorin e_6 derivatives in liposomal formulations	IC_{50} = 0.2–1 μM (20 J cm^{-2})); ~ comparator	2020	(134)
Human colon carcinoma HCT116 (and SW480)	*m*THPC	Cell death mechanism	Autophagy via activation of the ROS/JNK pathway	2020	(135)
Human colon carcinoma HCT-15	*m*THPC	Evaluation of low light fluence rate	Significant PDT activity with low light fluence 5–20 J cm^{-2}	2019	(136)
Human colon carcinoma HT29	*m*THPC-loaded PLGA nanoparticles	Nanoparticles versus free PS	No dark toxicity of temoporfin in nanoparticles	2011	(137)
Human colon carcinoma HT29	*m*THPC-loaded PLGA nanoparticles	Nanoparticles versus free PS	Reduced cytotoxicity of NP while retaining phototoxicity	2015	(138)
Human colon carcinoma HT29	*m*THPC loaded PEGMA-*co*-DPA (NPs)	pH sensitive NPs for PDT	*in vitro* release rate of PS within 48 h at pH 5.0 was faster than at pH 7.0 (58% versus 10% released), no cytotoxicity of NP, good photocytotoxicity	2010	(139)
Human colon carcinoma HT29	*m*THPC- Nip-SLrPExx-PLGA100-xx-NP (light sensitive)	Light-responsive NPs for drug release	Improved efficacy using a two-step illumination protocol	2021	(140)
Human colon carcinoma HT29	*m*THPC loaded micelles based on poly (2-ethyl-2-oxazoline)-*b*-poly(D,L-lactide) deblock copolymer	PDT study	pH-sensitive delivery system	2010	(141)
Human colon carcinoma HT29	*m*THPC invasomes	PDT study		2010	(142)
Human colon carcinoma HT29	*m*THPC loaded lipid-DNA micelles (UU11mer)	Lipid DNA as drug solubilizer	Good biocompatibility without irradiation, high PDT efficacy upon irradiation	2018	(143)
Human colon carcinoma HT29	*m*THPC–β-cyclodextrins	PDT study	Improved uptake and phototoxicity compared to free *m*THPC	2016	(144)
Human colon carcinoma HT29	*m*THPC Foslip® *m*THPC-β-CD (methylated) complexes in liposomes (*m*THPC-DCLs)	Evaluation of delivery system	*m*THPC-DCLs ~ Foslip®	2019	(145)
Human colon carcinoma HT29	Fospeg®	PDT study	LD_{50} = 0.4 μg mL^{-1} (3 J cm^{-2})	2015	(146)
Human colon carcinoma HT29-MTX	*m*THPC-(LrPC50%-PEG)-PLGA14 NP (light sensitive) *m*THPC-(PEG-PLA)-PLGA-NP (non light-sensitive)	Light-responsive NPs for drug release	Increased efficacy of light-responsive NPs; mucus-penetrating effect of PEGylated NP compared to free PS	2019	(147)
Human colon carcinoma HT29-MTX	*m*THPC-(LrPC-PEG)-PLGA NP (light sensitive) *m*THPC-(PEG-PLA)-PLGA-NP (non light-sensitive)	Light responsive polymers	Increased drug release after illumination when using light-responsive polymers	2019	(148)
Human colon carcinoma RKO	*m*THPC	Evaluation of low light fluence rate	Significant PDT activity with low light fluence 5–20 J cm^{-2}	2019	(136)
Human colorectal adenocarcinoma HT29	*m*THPC	Cell death mechanism	c-PARP expression is dependent on treatment-induced apoptosis.	2009	(124)
Human colorectal adenocarcinoma HT-29	*m*THPC	Comparison with 2,3-dihydroxychlorins	PDT activity similar to temoporfin	2011	(47)
Human colorectal carcinoma SW480 (and 620)	*m*THPC	Cell death mechanism	Cytoplasmic cytoskeleton destruction	2021	(149)
Human colorectal carcinoma SW480 (and 620)	*m*THPC	PDT study		2018	(150)
Human epidermoid carcinoma A431	*m*THPC (Foscan®)	Comparison of different PSs	Foscan®: LD_{50} = 0.03 μM	2010	(151)

(continues)

Table 1. (continued)

Cell line	Compound/Formulation	Study	Comments/Phototoxicity	Year	References
	*m*THPC (Fospeg®)		Fospeg®: LD_{50} = 0.06 μM		
Human epidermoid carcinoma A431	*m*THPC	Cell death mechanism	Autophagy and apoptotic features	2009	(152)
Human epidermoid carcinoma A431	*m*THPC + doxorubicin	Combination PDT + chemotherapy	Combination more cytotoxic than individual treatments; upregulation of IL-1alpha + VEGF in PDT-treated cells	2014	(153)
Human epidermoid carcinoma A431	*m*THPC	PDT effect on cytokines	Up-regulation of VEGF and IL-1alpha	2012	(154)
Human epidermoid carcinoma A431	*m*THPC loaded P(CL_x-TMC-Bz_y)-PEG micelles *m*THPC	PDT study	Photocytotoxicity: EC_{50} = 4–11 μg mL^{-1}; free *m*THPC = ~1.5 μg mL^{-1}	2020	(101)
Human epidermoid carcinoma A431	*m*THPC	PDT comparison with chlorin e_6 derivatives	IC_{50} = 0.7 μM at 2 J cm^{-2}; > comparator	2019	(155)
Human epidermoid carcinoma A431	$VHH^{[Fluo]}$-decorated *m*THPC loaded micelles	Targeted dual-labeled llama antibody–NP Conjugates	Bioorthogonal VHH (variable heavy chain domains of heavy chain antibodies) modification and conjugation strategy	2017	(156)
Human epidermoid carcinoma A431	*m*THPC loaded PCLn-PEG micelles decorated with EGFR targeting nanobody (EGa1)	EGFR targeting PS	EGa1-conjugated micelles are internalized upon specific binding of the NP with the EGFR receptor overexpressed on the surfaces of A431 cells, resulting in enhanced cellular uptake and photocytotoxicity on A431 cells, as compared to EGFR low-expressing HeLa cells	2020	(102)
Human epidermoid carcinoma A431	*m*THPC loaded lipid-DNA micelles (UU11mer)	Lipid DNA as drug solubilizer	Good biocompatibility without irradiation, high PDT efficacy upon irradiation	2018	(143)
Human epidermoid carcinoma A431	*m*THPC	Investigation of adherence to microplates	Significant adherence to plastic material	2011	(92)
Human epidermoid carcinoma A431	*m*THPC invasomes	PDT study		2010	(142)
Human esophageal squamous cell carcinoma KYSE-70	*m*THPC	Combination of PDT with glutathione peroxidase inhibition	Synergistic effect	2021	(130)
Human esophageal squamous cell carcinoma KYSE-70	*m*THPC	Cell death mechanism	Apoptosis main mechanism, autophagy can occur as well. Wide variation in PDT response among 5 cell lines	2019	(90)
Human esophageal squamous cell carcinoma KYSE-70	*m*THPC loaded silica NP	PDT study	50% reduced uptake of *m*THPC with NP but same concentration-dependent PDT effect and intracellular localization	2009	(157)
Human esophageal squamous cell carcinoma KYSE-70	*m*THPC + carboplatin (CBDCA) or cisplatin (CDDP) or oxaliplatin (1-OHP)	Synergistic effect of Pt(II) complexes		2018	(131)
Human esophageal squamous cell carcinoma OE21	*m*THPC in comparison to porphyrin-glycoconjugates	Carbohydrate bioconjugates	Slower uptake of carbohydrate bioconjugates and no phototoxicity	2012	(58)
Human esophageal squamous cell carcinoma OE21	*m*THPC in PEG-grafted, transferrin (Tf)-conjugated liposomes	Targeting of transferrin receptor	Neither increased uptake nor increases PDT effect	2013	(158)
Human glioma E98	$VHH^{[Fluo]}$-decorated *m*THPC loaded micelles	Targeted dual-labeled llama antibody–NP Conjugates	Bioorthogonal VHH (variable heavy chain domains of heavy chain antibodies) modification and conjugation strategy	2017	(156)
Human head and neck squamous carcinoma um-scc-U2 (and um-scc-U8)	Foscan®, Fospeg®, Foslip® + treatment with bleomycin	PCI study	Significantly increased bleomycin cytotoxicity when Foslip® or Fospeg® PDT was performed before BLM treatment	2014	(159)
Human hepatoma carcinoma Huh7	Fospeg®	PDT study	Effective for killing 80-90% of HCC cells; PDT-induced apoptosis might be due to p53 upregulation	2013	(160)
Human hepatoma HepG2	*m*THPC	Comparison with 5,10,15,20-tetracarboxyporphyrin	IC_{50} = 1.3 μM	2019	(76)
Human immortalized keratinocytes HaCaT	*m*THPP loaded P(Glu-b-NADA), amphiphilic block-co-polypeptides	amphiphilic co-polypeptides as drug delivery systems	No dark toxicity, *m*THPP release in controlled manner	2012	(103)

(continues)

Table 1. (continued)

Cell line	Compound/Formulation	Study	Comments/Phototoxicity	Year	References
Human lung carcinoma A-427	*m*THPC	Combination of PDT with glutathione peroxidase inhibition		2021	(130)
Human lung carcinoma A-427	*m*THPC	Cell death mechanism	Apoptosis main mechanism, autophagy can occur as well. Wide variation in PDT response among 5 cell lines	2019	(90)
Human lung carcinoma A-427	*m*THPC + carboplatin (CBDCA) or cisplatin (CDDP) or oxaliplatin (1-OHP)	Synergistic effect of Pt(II) complexes		2018	(131)
Human mammary breast carcinoma EMT6 (transfected with plasmid pR70/GFP)	*m*THPC	PDT effect on heat shock proteins	Extracellular release of HSP70	2011	(161)
Human mammary breast carcinoma HB4a–Ras	*m*THPC	PDT effect on cytoskeleton	Reduction of the migratory and invasive ability in Ras transfected cells	2017	(162)
Human monocyte THP-1	Foslip® Nanoparticulate N2	Effect on macrophages	Temoporfin nanoparticles induces a shift to M1-like phenotype in M2-polarized macrophages	2018	(163)
Human monocyte THP-1	*m*THPC	Development of extracellular vesicles as theranostic materials	Generation of *m*THPC loaded FVs	2012	(164)
Human nasopharyngeal carcinoma C666-1 (EBV-positive)	Fospeg®	Multidrug resistant cancer	PDT efficiency is independent of MDR1 gene and P-gp protein expression	2015	(165)
Human nasopharyngeal carcinoma C666-1 (EBV-positive)	Fospeg®	Epstein-Barr virus infections	Up-regulation of both LMP1 mRNA and protein	2013	(166)
Human nasopharyngeal carcinoma HK1 (EBV-negative)	Fospeg®	Multidrug resistant cancer	PDT efficiency is independent of MDR1 gene and P-gp protein expression	2015	(165)
Human nasopharyngeal carcinoma NPC/C666-1	Fospeg®	Comparison 2D 3D cell system	Down-regulation of LMP1 mRNA in MCL spheroids; PS uptake in 3D model 50% of 2D; different protein expression patterns in 2D versus 3D models	2020	(167)
Human nasopharyngeal carcinoma NPC/HK1	*m*THPC	Cell death mechanism	Induces early apoptotic responses	2009	(168)
Human nasopharyngeal undifferentiated carcinoma KJ-1 was used	*m*THPC	Test of cell migration in Matrigel invasion assay	Decrease in migration distance of KJ-1 cells	2014	(88)
Human neuroblastoma SH-SY5Y	*m*THPC-AuNP	PDT study	Better PDT effect of gold NPs; no dark toxicity	2018	(53)
Human non-tumorigenic lung epithelial cells BEAS-2G	*m*THPC	Comparison with 5,10,15,20-tetracarboxyporphyrin	IC_{50} = 1.9 μM	2019	(76)
Human oral adenouscarcinoma CAL27	*m*THPC	Cell death mechanism; damage-associated molecular pattern (DAMP)	Presentation of ceramide and sphingosine-1-phosphate (S1P) on the cell surface after PDT	2014	(169)
Human oral squamous cell carcinoma BHY	*m*THPC	Combination of PDT with glutathione peroxidase inhibition		2021	(130)
Human oral squamous cell carcinoma BHY	*m*THPC	Cell death mechanism	Apoptosis main mechanism, autophagy can occur as well. Wide variation in PDT response among 5 cell lines	2019	(90)
Human oral squamous cell carcinoma BHY	*m*THPC + carboplatin (CBDCA) or cisplatin (CDDP) or oxaliplatin (1-OHP)	Synergistic effect of Pt(II) complexes		2018	(131)
Human oral adenosquamous carcinoma CAL27	*m*THPC loaded lipid-DNA micelles (UU11mer)	Lipid DNA as drug solubilizer	Good biocompatibility without irradiation, high PDT efficacy upon irradiation	2018	(143)

(continues)

Table 1. (continued)

Cell line	Compound/Formulation	Study	Comments/Phototoxicity	Year	References
Human oral adenosquamous carcinoma CAL27	*m*THPC in calcium phosphate nanoparticles conjugated with RGDfK peptide and DY682-NHS	PDT study	Combined near-IR imaging and PDT	2015	(170)
Human oral adenosquamous carcinoma CAL27	Foslip	Uptake study		2013	(171)
Human ovarian carcinoma SKOV-3	*m*THPC	Comparison with 5,15-diarylporphyrins	IC_{50} = 2.9 nM; > comparator	2019	(119)
Human ovarian carcinoma SKOV-3	*m*THPC + magnetic NP loadead EVs	Development of extracellular vesicles as theranostic materials	Translation to *in vivo*	2012	(164)
Human ovarian carcinoma SKOV-3	*m*THPC + iron oxide magnetic NP in liposomes	PDT/photothermal study	Complete cancer cell death	2015	(172)
Human ovarian carcinoma SKOV-3	*m*THPC–MWCNT complex (multi-walled carbon nanotubes)	PDT/photothermal study	Different signaling pathways leading to cell apoptosis for PDT and PTT	2016	(173)
Human ovarian carcinoma SKOV-3	*m*THPC formulated in tetraether liposomes	PDT study		2020	(174)
Human ovarian carcinoma SKOV-3	Lipid-enveloped PLGA NP with *m*THPC + pirarubicin	Combination of PDT and chemotherphy	THP nanoparticles coated with *m*THPC liposomes yielded lipid-coated nanoparticles (LCNPs) with good activity	2021	(175)
Human promonocytic cells U937	*m*THPC-loaded PLGA nanoparticles	Nanoparticles versus free PS	No dark toxicity of temoporfin in nanoparticles; reduced cellular uptake of NP, but similar phototoxicity	2012	(111)
Human prostate carcinoma LNCaP	*m*THPC (+ *P. halepensis* extracts)	Effect of natural antioxidants on PDT	*P. halepensis* bark extracts are cytotoxic and enhanced the PDT effect	2022	(176)
Human prostate carcinoma LNCaP	Fospeg®	PDT study	LD50 = 0.15 μg mL^{-1} at 180 mJ cm^{-2}; improved compared to Foscan® (1.2 μg mL^{-1})	2009 2012	(177,178)
Human prostate carcinoma LNCaP	*m*THPC	Time resolved sub-cellular singlet oxygen detection		2012	(179)
Human prostate carcinoma PC-3	*m*THPC	Cell death mechanism	Release of extracellular vehicles 1 h after illumination	2016	(180)
Human prostate carcinoma PC-3	*m*THPC	PDT effect on intracellular trafficking	Depolymerization of microtubule network; 100-fold lower endosomal trafficking	2013	(181)
Human prostate carcinoma PC-3	Foslipos	Cell death mechanism		2011	(182)
Human prostate carcinoma PC-3	*m*THPC + magnetic NP loadead EVs	Development of extracellular vesicles as theranostic materials	Translation to *in vivo*	2012	(164)
Human retinoblastoma RB Y79	Liponanoparticles consisting of a poly (D,L)-lactide (PDLLA) NP coated with a phospholipid (1-palmitoyl-2-oleoyl-sn-glycero-3-phosphocholine/ 1,2-dioleoyl-3-trimethylammonium-propane) bilayer + loaded with anticancer drug beta-lapachone (β-Lap) and *m*THPC	Combined chemotherapy + PDT	LNPs are cytotoxic at lower doses of the two encapsulated compounds as compared to the single therapies	2019	(183)
Human squamous carcinoma 14C	*m*THPP loaded NOCCS/PMAA NP	*In vitro* release study	High loading capacity and stability	2011	(184)
Human tumor cells A-231 (submaxillary salivary gland)	*m*THPC encapsulated in Eudragit® RS 100 (NPs)	Evaluation of upscaling of NP production for peroral PDT	Successful process development	2015	(185)
Human umbilical vein endothelial cells HUVEC	*m*THPC Foscan® *m*THPC loaded magnetic nanoparticles	Development of extracellular vesicles as theranostic materials	EVs encapsulating iron oxide nanoparticles and PS as biocamouflaged agents for PDT, MRI, magnetic manipulation, and hyperthermia	2017 2018	(186,187)
	*m*THPC	PDT comparison with corroles		2020	(125)

(continues)

Table 1. (continued)

Cell line	Compound/Formulation	Study	Comments/Phototoxicity	Year	References
Human umbilical vein endothelial cells HUVEC			IC_{50} = 1.50 μM; < comparator free bases; > comparator Ga complexes		
Human urinary bladder transitional cell carcinoma RT-4	*m*THPC	Combination of PDT with glutathione peroxidase inhibition	Synergistic effect	2021	(130)
Human urinary bladder transitional cell carcinoma RT-4	*m*THPC	Cell death mechanism	Apoptosis main mechanism, autophagy can occur as well. Wide variation in PDT response among 5 cell lines	2019	(90)
Human urinary bladder transitional cell carcinoma RT-4	*m*THPC + carboplatin (CBDCA) or cisplatin (CDDP) or oxaliplatin (1-OHP)	Synergistic effect of Pt(II) complexes		2018	(131)
Human-transformed breast cells MCF10A neoT	*m*THPC-loaded PLGA nanoparticles	Nanoparticles versus free PS	No dark toxicity of temoporfin in nanoparticles; reduced cellular uptake of NP, but similar phototoxicity	2012	(111)
Jurkat cells (human T-cell lymphocytes)	*m*THPC loaded HSA nanoparticles	Photophysical study		2010	(188)
Jurkat cells (human T-cell lymphocytes)	*m*THPC loaded HSA nanoparticles *m*THPP loaded HSA nanoparticles	Drug release study	$^1O_2$ production in cells	2010	(189)
Jurkat cells (human T-cell lymphocytes)	*m*THPC loaded HSA nanoparticles *m*THPP loaded HSA nanoparticles	Drug release study	*m*THPC-NP: high phototoxicity 5-24 h after incubation, 70-85% apoptosis *m*THPP-NP: max. phototoxicity 1 h after incubation, then no further release of *m*THPP	2011	(190)
Jurkat cells (human T-cell lymphocytes)	*m*THPC	Time resolved sub-cellular singlet oxygen detection		2012	(179)
KB Cells	*m*THPC containing discoidal NP with folate/*m*THPC containing vesicular NP with folate	Impact of delivery system morphology on PDT	Better PDT effect with discoidal carriers compared to spherical ones	2019	(191)
KB cells	*m*THPC in folate-targeted liposomes	Folate targeting	Low level internalization of folate-targeted liposomes via specific endocytosis; however, doubled *m*THPC and increased phototoxicity compared to untargeted liposomes	2013	(114)
Mouse colon adenocarcinoma CT29	*m*THPC	Comparison with redaporfin	LLD_{50} = 5 mJ cm^{-2} at 0.5 μM (*m*THPC) LLD_{50} = 500 mJ cm^{-2} at 5 μM (redaporfin)	2016	(109)
Mouse colon carcinoma C26	Styrene maleic acid copolymer (SMA) micelle encapsulating *m*THPC; SMA@mTHPC	PDT study	pH-dependent release profile; lower dark and light toxicity than *m*THPC; phototoxicity: IC50 SMA@mTHPC = 0.015 μg mL^{-1}; *m*THPC = 0.0005 μg mL^{-1}	2021	(192)
Mouse hepatoma 1c1c7	*m*THPC	Cell death mechanism	*m*THPC initiates paraptosis after ER photodamage	2021	(110)
Mouse mammary carcinoma 4T1	*m*THPC	PDT resistance	Generation of PDT-resistant clones; resistance based on a mechanism based on sequestration of the drug to lysosomes; resistance can be overcome by using other PSs	2017	(193)
Mouse mammary carcinoma 4T1	*m*THPC	PDT comparison with corroles	IC_{50} = 0.05 μM; < comparator	2020	(125)
Mouse mammary carcinoma 4T1	*m*THPC–T-SLNP; temoporfin-loaded 1-tetradecanol-based thermoresponsive solid LNP/Foscan	PDT study	Faster accumulation of LNP formulation	2016	(127)
Mouse mammary carcinoma 4T1	*m*THPC loaded silica NP	PDT study	Better PDT effect compared to *m*THPC	2018	(194)
Mouse squamous cell carcinoma SCCVII	*m*THPC	Cell death mechanism; damage-associated molecular pattern (DAMP)	Presentation of ceramide and sphingosine-1-phosphate (S1P) on the cell surface after PDT	2014	(169)
Mouse squamous cell carcinoma SCCVII	*m*THPC (+acid ceramidase inhibitor LCL521)	Cell death mechanism	LCL521-promoted PDT-mediated cell killing	2020	(195)
Murine cervical carcinoma TC-1	*m*THPC + magnetic NP loadead EVs		Translation to *in vivo*	2012	(164)

(continues)

Table 1. (continued)

Cell line	Compound/Formulation	Study	Comments/Phototoxicity	Year	References
		Development of extracellular vesicles as theranostic materials			
Murine colon carcinoma CT26	*m*THPC multifunctional NPs ((mTHPC@VeC/T-RGD NPs)	PDT and immunotherapy	Induced apoptosis and/or necrosis and stimulated systemic immune response; sensitized tumors to PD-L1 blockade therapy	2021	(133)
Murine colon carcinoma CT26	EVs fused with liposomes carrying *m*THPC (Foslip®)	Development of extracellular vesicles as theranostic materials	Fusion of EV with Foslip liposomes generates hybrid-EVs with 3-4 improved cellular delivery efficiency compared to Foscan or Foslip	2018	(187)
Murine embryonic fibroblasts	*m*THPC loaded FH-PDots	PDT study of polymer dots	Active; cell viability increase with concentration; more uptake in cancer cells compared to normal ones due to folate receptor targeting	2014	(120)
Murine endothelial cells C166	*m*THPC loaded Ben-PCL-mPEG micelles	Effect on macrophages	RAW264.7 macrophages degrade micelles faster and activate the PS earlier than C166 cells, allowing for selective killing of macrophages	2017	(196)
Murine fibroblasts L929	*m*THPC loaded lipid-DNA micelles (UU11mer)	Lipid DNA as drug solubilizer	Good biocompatibility without irradiation, high PDT efficacy upon irradiation	2018	(143)
Murine fibroblasts L929	*m*THPC organic crystalline NPs	Preparation and testing of neat PS NPs	Preferential uptake in macrophages compared to fibroblasts	2018	(197)
Murine glioma C6	*m*THPC loaded PLGA NPs	PDT study	Reduced cytotoxicity of *m*THPC-NP but higher phototoxicity compared to *m*THPC	2019	(198)
Murine glioma C6	*m*THPC loaded FH-PDots	PDT study of polymer dots	Active; cell viability increase with concentration; more uptake in cancer cells compared to normal ones due to folate receptor targeting	2014	(120)
Murine hematopoiesis monocytic macrophages J774A.1	*m*THPC loaded lipid-DNA micelles (UU11mer)	Lipid DNA as drug solubilizer	Good biocompatibility without irradiation, high PDT efficacy upon irradiation	2018	(143)
Murine hematopoiesis monocytic macrophages J774A.1	*m*THPC organic crystalline NPs	Preparation and testing of neat PS NPs	Preferential uptake in macrophages compared to fibroblasts	2018	(197)
Murine hepatoma MH22	*m*THPC	Cell death mechanism	Apoptosis associated with caspase activation	2009	(199)
Murine Lewis lung carcinoma LLC1	*m*THPC	PDT effect	CD50 at 60 mJ cm^{-2} with 400 ng mL^{-1} mTHPC	2010	(200)
Murine melanoma cells B16-F10	*m*THPC *m*THPC SOF1 mTHPC SOF2 *m*THPC SOF3	Temoporfin supramolecular framework (SOF) PDT [	IC_{50}: 58.8 μg L^{-1} IC_{50}: 26.7 μg L^{-1} IC_{50}: 47.1 μg L^{-1} IC_{50}: 25.0 μg L^{-1}	2022	(99)
Murine mesenchymal stem cell line C3H/10T1/2 (mMSC)	*m*THPC	Development of extracellular vesicles as theranostic materials	Generation of *m*THPC loaded FVs	2021	(201)
Murine prostate TRAMP-C1	*m*THPC + IR780 loaded PFOB@IMHNPs ; tumor acidity-responsive lipid membrane-enclosed perfluorooctyl bromide oil droplet NPs surface modified with *N*-acetyl histidine-modified D-α-tocopheryl polyethylene glycol 1000 succinate	PDT/photothermal study	Effective killing of hypoxic cancer cells *in vitro*	2020	(202)
Murine RAW264.7 macrophages	*m*THPC loaded Ben-PCL-mPEG micelles	Effect on macrophages	RAW264.7 macrophages degrade micelles faster and activate the PS earlier than C166 cells, allowing for selective killing of macrophages	2017	(196)
Rat glioma F98	mTHPC (+Rose Bengal)	Pretreatment of medium	Pretreatment reduced cell survival by 40%	2009	(93)

(continues)

Table 1. (continued)

Cell line	Compound/Formulation	Study	Comments/Phototoxicity	Year	References
3D systems/spheroids					
Biliary Tract Cancer Cell Lines	Foscan®	Comparison with Photofrin; influence of miRNA	Identification of miRNAs which improve susceptibility to PDT. cell lines EGI-1, GBC, MzChA-1, SkChA-1, and TFK-1 showed relatively low phototoxic effects; CCSW-1, BDC, and MzChA-2 have significantly higher phototoxic efficiency cells with a low cytokeratin-19 (ductal differentiation), high vimentin (mesenchymal marker), and high proliferative phenotype show higher uptake of *m*THPC and phototoxicity	2014 2010	(203,204)
HeLa multicellular spheroids	Foscan® Foslip® Fospeg®	PDT study	Localization mainly in outer area of spheroids, PDT effect comparable for all three	2016	(205)
HeLa multicellular spheroids	Foscan®	Evaluation of LED illumination	PDT outcome is more efficient with violet light followed by red light	2020	(206)
Human breast adenocarcinoma MCF-7 + neural and satellite glial cells in a collagen matrix	*m*THPC	PDT study	MCF-7s and satellite glia are more sensitive to PDT than neurons	2009	(207)
Human colon carcinoma HCT116	*m*THPC	PDT study, effect on fluorouracil resistant cells	PDT overcomes resistance	2017	(208)
Human colon carcinoma HT29	*m*THPC	Cell death mechanism	c-PARP expression is dependent on treatment-induced apoptosis.	2009	(124)
Human colon carcinoma HT29	Foslip®	PDT study	IC_{50} = 2 ng mL^{-1} with 2 J cm^{-2}; Foslip® PDT effect on HT29 cells was independent to 5-FU resistance	2020	(209)
Human colon carcinoma HT29 – multicellular spheroids	*m*THPC–β-CD complexes in liposomes	Evaluation of drug-β-CD in liposomes concept	Homogenous accumulation across spheroid volume	2017	(210)
Human colon carcinoma HT29 – multicellular spheroids	*m*THPC Foslip® *m*THPC-β-CD (methylated) complexes in liposomes (*m*THPC-DCLs)	Evaluation of delivery system	*m*THPC-DCLs > Foslip®	2019	(145)
Human colon carcinoma HT29FU (fluorouracil resistant)	Foslip®	PDT study	IC50 = 2 ng mL^{-1} with 2 J cm^{-2}; Foslip® PDT effect on HT29 cells was independent to 5-FU resistance	2020	(209)
Human colorectal adenocarcinoma HT29 – Multicellular spheroids	*m*THPC loaded in endothelial extracellular vesicles Foslip®	*m*THPC nanovectorization using extracellular vesicles	*m*THPC-EVs are stable in murine plasma; better mTHPC accumulation and penetration in MCTS compared to Foslip®; light dose required for 50% cell death was 4 and 2.5-times lower than free and liposomal *m*THPC	2018	(211)
Human colorectal adenocarcinoma HT29 – Multicellular spheroids	*m*THPC loaded in endothelial extracellular vesicles Foslip®	*m*THPC nanovectorization using extracellular vesicles	Deeper penetration after 24h incubation compared to Foslip®	2020	(212)
Human esophageal carcinoma *Eca 109*	*m*THPC	PDT comparison with chlorin e_6 derivative	PDT efficacy < comparator	2018	(213)
Human glioblastoma U87MG spheroids	*m*THPC)-loaded NP, based on vitamin-E-succinate-grafted chitosan oligosaccharide and cyclic (arginine-glycine-aspartic acid-D-phenylalanine-lysine) (c [RGDfK])-modified D-a-tocopheryl polyethylene glycol 1000 succinate, were prepared (RGD-NPs)	Targeting integrin-rich tumors	Deep penetration into spheroids and enhanced targeting	2017	(214)

(continues)

Table 1. (continued)

Cell line	Compound/Formulation	Study	Comments/Phototoxicity	Year	References
Human glioblastoma LN229	*m*THPC in liposomes formulated with DMPC and a cationic gemini surfactant	Effect of surfactant	Stereochemistry of the spacer of the gemini surfactant strongly affects uptake, interaction with cell membrane and intracellular distribution of PS	2010	(215)
Human monocyte THP-1	*m*THPC + magnetic NP + doxorubicin + $TPCS_{2a}$ + tissue plasminogen activator (t-PA) in EV	PS + magnetic NPs in cell-derived microvesicles	Hybrid cell microvesicles were magnetically responsive + MRI-detectable; PS action could be modulated by magnetic targeting	2015	(216)
Human nasopharyngeal carcinoma NPC/C666-1/3D model	Fospeg®	Comparison 2D 3D cell system	Down-regulation of LMP1 mRNA in MCL spheroids; PS uptake in 3D model 50% of 2D; different protein expression patterns in 2D versus 3D models	2020	(167)
Human osteosarcoma 143B (metastatic)	Foscan® Foslip®	PDT study	Time- and dose-dependent uptake, light dose-dependent phototoxicity associated with apoptosis	2017	(217)
Human osteosarcoma 143B (metastatic)	*m*THPC	PDT study	LD_{50} = 0.012 to 0.047 μg mL^{-1} with 652 nm laser light (2.5–10 J $cm)^2$	2012	(218)
Human pharynx squamous cell carcinoma FaDu	*m*THPC Foslip® *m*THPC-DCL (PS-in-cyclodextrin-in-liposome) *m*THOC-EV	Influence of stromal microenvironment	Generation of stroma-rich 3D HNSCC spheroids; *m*THPC-EVs best uptake; PDT efficiency comparable to other NPs	2021	(219)
Human pharynx squamous cell carcinoma FaDu	*m*THPC	Development of 3D spheroid pre-clinical *in vitro* system	Improved uptake and PDT efficiency of *m*THPC	2019	(220)
Human pharynx squamous cell carcinoma FaDu	*m*THPC–β-cyclodextrins	Evaluation of cross-linked cyclodextrins as carrier system	Improved penetration of spheroids with cross-linked CD system but lower cellular uptake of PS	2020	(221)
Human pharynx squamous cell carcinoma FaDu	Foslip®	O_2 measurements during PDT	Simultaneous use of time resolved NIR luminescence and spectrally resolved UV/VIS fluorescence	2020	(222)
Human squamous cell carcinomas of the tongue CAL-33	*m*THPC–LNP	PDT study	Similar phototoxicity compared to *m*THPC but lower dark toxicity; necrosis and apoptosis with *m*THPC-PDT, apoptosis with 50 nm *m*THPC–LNP	2016	(223)
Murine glioblastoma C6	*m*THPC in liposomes formulated with DMPC and a cationic gemini surfactant	Effect of surfactant	Stereochemistry of the spacer of the gemini surfactant strongly affects uptake, interaction with cell membrane and intracellular distribution of PS	2010	(215)
Murine melanoma cells B16-F10	*m*THPC + oxygen-carrying perfluorocarbon encapsulated into cRGD peptide modified multilayer liposomes (C-ML/HPT/O_2), which are then loaded into live neutrophils ("Acous-cyte/O_2")	PS-neutrophils for sonodynamic therapy	Selective accumulation in tumors, enhancement of tumor O_2 levels, triggering of anticancer sonodynamics upon ultrasound stimulation	2022	(224)
Murine osteosarcoma K7M2	Foscan® Foslip®	PDT study	Time- and dose-dependent uptake, light dose-dependent phototoxicity associated with apoptosis	2017	(217)
Neural and satellite glial cells in a collagen matrix	*m*THPC	PDT study	Inhibition of anti-oxidant pathways increases sensitivity of neurons to PDT	2012	(225)
Other					
Hen's egg test on chorioallantoic membrane (HET-CAM) model with HuTu-80 or HT29-MTX-E12 tumor spheroids	*m*THPP loaded PLGA NPs + others	Vascularized intestine tumor model	Assay is suitable link between standardized *in vitro* models and animal models	2022	(226)
Anti-microbial					
Candida albicans		Anti-bacterial PDT	59% inhibition with 15 min illumination	2021	(227)

(continues)

Table 1. (continued)

Cell line	Compound/Formulation	Study	Comments/Phototoxicity	Year	References
	*m*THPP-ethyl cellulose/chitosan nanocomposite				
Clostridium difficile	*m*THPC	Anti-bacterial PDT	<3 log unit reduction	2015	(228)
Enterococcus faecalis	*m*THPC	Anti-bacterial PDT, endodontic infections	50 mM PS, 100 J cm^{-2}: complete eradication; 10 mM PS: reduction in CFU by 5.8 log-units	2011	(229)
Enterococcus faecalis	*m*THPC containing biomaterial for periodontal regeneration	Anti-bacterial PDT	3.1–3.7 log unit reduction	2018	(230)
Escherichia coli	*m*THPP-nanodiamond conjugates	Anti-bacterial PDT	56% inhibition	2021	(52)
Porphyromonas gingivalis	*m*THPC containing biomaterial for periodontal regeneration	Anti-bacterial PDT	Total suppression	2018	(230)
Pseudomonas aeruginosa	Liposomal formulation: *m*THPC + antimicrobial peptide WLBU2	Anti-bacterial PDT	3.3 log unit reduction	2011	(231)
Pseudomonas aeruginosa	Liposomal formulation *m*THPC conjugated with wheat germ agglutinin (WGA)	Anti-bacterial PDT	2 log unit reduction	2012	(232)
Pseudomonas aeruginosa	Temoporfin	Anti-bacterial PDT	Less than 1 log reduction after 20 min illumination	2021	(233)
Pseudomonas aeruginosa	*m*THPP-ethyl cellulose/chitosan nanocomposite	Anti-bacterial PDT	71% inhibition with 15 min illumination	2021	(227)
Staphylococcus aureus	Fospeg®	Anti-bacterial PDT	100 nM PS, 5 min incubation, 30 min illumination at 75 mW cm^{-2} → 4–5 log unit reduction	2010	(234)
Staphylococcus aureus	Temoporfin	Anti-bacterial PDT	12.5 μM mTHPC resulted in complete eradication	2021	(233)
Staphylococcus aureus	*m*THPP-ethyl cellulose/chitosan nanocomposite	Anti-bacterial PDT	74% inhibition with 15 min illumination	2021	(227)
Staphylococcus aureus (MRSA)	Liposomal formulation: *m*THPC + antimicrobial peptide WLBU2	Anti-bacterial PDT	Complete eradication	2011	(231)
Staphylococcus aureus (MRSA)	Liposomal formulation *m*THPC conjugated with wheat germ agglutinin (WGA)	Anti-bacterial PDT	Complete eradication	2012	(232)
Streptococcus mutans	Foslipos	Anti-bacterial PDT, dental caries	Significant dark toxicity at 10–1.25 mg mL^{-1}; complete eradication with a mixture of Foslipos/hypericin (0.625 mg mL^{-1}, each), 15 min incubation, 120 s illumination	2009	(235)
Streptococcus sobrinus	Foslipos	Anti-bacterial PDT, dental caries	Complete eradication with 5 mg mL^{-1}, 15 min incubation, 120 s illumination	2009	(235)

Table 2. Animal models used for *m*THPC and related compounds (sorted by animal model and by publication year).

Animal model	Compound/Study	Comments	Year	References
Mouse				
Male C57 mice bearing B16-F10 tumors (melanoma)	*m*THPC loaded on supramolecular organic frameworks (nanoparticles): PDT efficacy	Suppression of tumor growth	2022	(99)
Male C57BL/6 mice bearing B16F10 tumors	Perfluorocarbon-oxygen carrier and *m*THPC in peptide-modified liposomes combined with neutrophils: characterization and sonodynamic application	Apoptosis induced by ROS generated under ultrasound treatment, tumor growth inhibition	2022	(224)
Female BALB/c mice bearing CT26 tumors	*m*THPC-loaded vitamin-E-succinate-grafted chitosan oligosaccharide/D-α-tocopheryl PEG succinate nanoparticles (RGDfK peptide-modified) combined with anti-PD-L1: PDT and immune effects	Combination of PDT and anti-PD-L1 checkpoint blockade inhibited growth of local and distant tumors	2021	(133)
Female BALB/c and C57BL/6 mice bearing CT26 and ID8-Luc tumors, respectively	*m*THPC *vs*. liposomal *m*THPC (Foslip®) and extracellular vesicles derived from mesenchymal stem/stromal cells loaded with *m*THPC: PDT efficacy	Enhanced tumor selectivity and anti-cancer efficacy of the *m*THPC in extracellular vesicles, promotion of antitumor immune cell infiltration	2021	(201)
Female albino (BALB/c) mice	Combination of Pirarubicin PLGA nanoparticles and liposomal *m*THPC: Acute toxicity and particle characterization	Cytotoxicity synergism, lower toxicity compared to the free drugs	2021	(175)
Male ddY mice bearing S180 mouse sarcoma	*m*THPC in styrene maleic acid copolymer micelles: characterization, release profile, PDT efficacy	Similar anti-tumor efficacy as free *m*THPC, less side effects	2021	(192)
Female NMRI$^{nu/nu}$ mice bearing HT-29 tumors	Extracellular vesicles loaded with *m*THPC *vs*. liposomal *m*THPC (Foslip®): PDT efficacy	Efficient tumor volume reduction with *m*THPC in extracellular vesicles	2020	(212)
Female Balb/c nude mice bearing A431 tumors	*m*THPC loaded polymeric micelles: Pharmacokinetics and tumor accumulation	Long circulating micelles resulted in significantly higher tumor accumulation compared to short circulating micelles	2020	(280)
Female Balb/c nude mice bearing A431 tumors	Polymeric micelles loaded with *m*THPC and EGFR targeting: Formulation and pharmacokinetics	Prolonged blood circulation kinetics for the nanoparticles, independent of antibody presence	2020	(102)
Female Balb/c nude mice	*m*THPC and *m*THPC loaded on polymeric micelles: Comparison of biodistribution	π-π stacking interactions to improve cargo retention in polymeric micelles *in vitro*, differences to *in vivo* distribution	2020	(101)
Male C57BL/6 mice bearing TRAMP-C1 tumors	Combined photothermal and *m*THPC-PDT with oil droplet nanoparticles: Antitumor efficacy	Inhibition of tumor growth	2020	(202)
MaleBALB/c mice	Effect of *m*THPC-PDT on tumor growth of HCT116 xenografts, role of autphagy	Inhibition of tumor growth, importance of autophagy	2020	(135)
Female athymic nude mice	*m*THPC encapsulated in (folate) nanodiscs vs. liposomal *m*THPC: antitumor efficacy	Highest tumor reduction with the *m*THPC-loaded folate nanodiscs	2019	(191)
Female NMRI$^{nu/nu}$ mice bearing HT-29 tumors	*m*THPC/cyclodextrin inclusion complexes in liposomal *m*THPC *vs*. liposomal *m*THPC (Foslip®): PDT efficacy	Similar PDT efficacy of liposomal mTHPC (Foslip®) and double-loaded liposomes	2019	(145)
Male Hsd:Athymic Nude-Foxn1 mice bearing MDA-MB231 tumors	*m*THPC-loaded Ce-doped maghemite nanoparticles: PDT efficacy	Faster accumulation compared to free *m*THPC, tumor regression	2019	(128)
Nu/Nu mice bearing MDA-MB-231 tumors (human breast carcinoma)	*m*THPC (Foscan®) *vs*. silica nanoparticles loaded with *m*THPC: PDT efficacy	Efficient intracellular delivery of silica nanoparticles, passage of blood brain-barrier, *m*THPC silica nanoparticles more effective, partial tumor relapse in all cases	2018	(194)
Nude mice bearing HeLa tumors	*p*THPP vs. *p*THPP polyhedral oligomeric silsesquioxanes with PEG: PDT efficacy	Superiority (biocompatibility, tumor volume reduction) of the nanoparticle formulation	2018	(60)
Female BALB/c athymic nude mice bearing HT-29 tumors	Combination of *m*THPC-PDT and anti-VEGF monoclonal neutralizing antibody bevacizumab: Efficacy	PDT treatment followed by bevacizumab more effective than opposite combination (bevacizumab treatment decreased *m*THPC tumor accumulation)	2018	(281)
BALB/c mice bearing fibrosarcoma	*m*THPC: pharmacokinetics		2018	(282)

(continues)

Table 2. (continued)

Animal model	Compound/Study	Comments	Year	References
		Rebound effect (new local drug accumulation)		
Subcutaneous-U87MG tumor-bearing nude mice	*m*THPC-loaded vitamin-E-succinate-grafted chitosan oligosaccharide/D-α-tocopheryl PEG succinate nanoparticles (RGDfK peptide-modified) *vs*. unmodified nanoparticles: PDT efficacy	Higher anti-tumor efficacy, less systemic toxicity for the modified nanoparticles	2017	(214)
SCID (143B/SCID, human xenograft mouse model) and BALB/c mice (K7M2L2/BALB/c, syngeneic mouse model), intratibial mouse model	*m*THPC (Foscan®) and liposomal *m*THPC (Foslip®): PDT efficacy, immune effects	Uptake of both formulations higher in tumor than in healthy control tissue, significant tumor growth inhibition by PDT, significant immune system-dependent suppression of lung metastasis in the K7M2L2/BALB/c model	2017	(217)
BALB/c syngeneic mice bearing 4T1 tumors and tumors derived from cells of PDT-resistant clones	Ethylene glycol derivatives of tetraphenylporphyrin and *m*THPC: Investigation of resistance to PDT	Different resistance mechanisms, for *m*THPC: sequestration to lysosomes	2017	(193)
Nu/Nu mice bearing MDA-MB-231 tumors	*m*THPC (Foscan®) *vs*. *m*THPC in 1-tetradecanol thermoresponsive solid-lipid nanoparticles: PDT efficacy	Improved anti-cancer efficacy of the nanoparticle formulation	2016	(127)
CD1-Foxn1^{nu} nude mice bearing CAL-33 tumors	*m*THPC *vs*. liposomal *m*THPC (Foslip®) and *m*THPC lipid nanoparticles: PDT efficacy	Better biocompatibility of both nanoparticle formulations, highest tumor volume reduction with liposomal *m*THPC	2016	(283)
Syngeneic C3H/HeN mice bearing murine SCC (SCCVII)	Combination of anti-GR1 antibody and *m*THPC-PDT: Tumor response, immune effects	Better anti-tumor effect with delayed anti-GR1 treatment	2016	(284)
NMRI male nude mice bearing PC-3 prostate carcinoma	Effect of mTHPC PDT and doxorubicin on release of extracellular vesicles	Release of large amounts of extracellular vesicles (higher for PDT)	2016	(180)
Radiation-induced fibrosarcoma tumor mouse model	Benzoporphyrin derivative monoacid ring A, Photofrin® and *m*THPC: PDT threshold dose	*In vivo* $^1O_2$ threshold doses for Photofrin®, BPD, and *m*THPC ~ 20 times smaller than those observed *in vitro*	2015	(285, 286)
NMRI nude mice bearing A431 tumors	Liposomal *m*THPC, with iron oxide nanoparticles in the aqueous core: combination of PDT and magnetic hyperthermia	Synergistic effect, complete tumor ablation	2015	(172)
NMRI$^{nu/nu}$ mice bearing HT-29 tumors	Pegylated liposomal *m*THPC (Fospeg®): Pharmacokinetics and biodistribution *via* optical imaging	Good correlation between *ex vivo* tissue fluorescence and reflectance imaging and chemical extraction	2015	(287)
Athymic Nude-Foxn1^{nu} mice bearing CAL-27 tumors	*m*THPC-loaded calcium phosphate nanoparticles modified with RGDfK peptide and NIR fluorescence dye: PDT efficacy	Decrease in tumor vascularization and tumor volume	2015	(170)
Female NCRNu mice, dorsal skin-fold window chamber tumor model (luciferase- and green fluorescent protein-transduced gliosarcoma)	*m*THPC (Foscan®): Correlation tumor response and singlet oxygen luminescence	$^1O_2$ luminescence as dosimetric technique for PDT in tumor tissue	2015	(288)
Female C57BL/6 mice with azoxymethane/dextran sulfate sodium -induced colitis and tumors	Liposomal *m*THPC (Foslip®): Effect of low-dose-PDT on colitis and colitis-associated carcinogenesis	Reduction of tumor growth, expression decrease of inflammatory mediators, lowering neutrophil influx	2015	(289)
Female NMRI$^{nu/nu}$ mice bearing HT-29 tumors	Liposomal *m*THPC (Foslip®) and pegylated liposomal *m*THPC (Fospeg®): Distribution and PDT efficacy	Enhanced permeability and retention-based tumor accumulation and circulation stability for Fospeg®	2013	(290)
Female athymic nude-Foxn1^{nu} mice bearing Cal-27 tumors	Fluorescence optical imaging of liposomal *m*THPC (Foslip®) in combination with DY-734 annexin V	Detection of apoptotic cells shortly after treatment, reduction of tumor vascularization at later time points	2013	(171)
Female nude NMRI mice bearing TC-1 tumors	*m*THPC *vs*. extracellular vesicles loaded with *m*THPC and maghemite (iron oxide) nanoparticles: PDT efficacy and imaging	Improved anti-cancer efficacy (reduction of tumor growth) of the nanoparticle formulation, dual imaging by fluorescence and MRI	2013	(164)
Female BALB/cAnN.Cg-Foxn1^{nu}/CrlNarl nude mice bearing A549 tumors	Luciferase-immobilized quantum dots combined with *m*THPC loaded micelles: PDT efficacy, ROS generation	bioluminescence resonance energy transfer for PDT, delayed tumor growth	2013	(112)

(continues)

Table 2. (continued)

Animal model	Compound/Study	Comments	Year	References
Male Hsd:Athymic Nude-Foxn1 mice bearing HCT-116-luc tumors	*m*THPC *vs.* *m*THPC in PLGA and pegylated PLGA nanoparticles: PDT efficacy	Reduced dark toxicity for the nanoparticles, improved tissue distribution for pegylated PLGA nanoparticles	2012	(111)
SCID mice bearing LNCaP tumors	Interstitial PDT with pegylated liposomal *m*THPC (Fospeg®): Effect of natural antioxidants	Prevention of photosensitivity with the natural antioxidants	2012	(291)
Female BALB, cAnN.Cg-Foxn1^{nu} and CrlNarl nude mice bearing KB and HT-29 tumors	*m*THPC *vs.* *m*THPC loaded on folate-conjugated polymeric micelles: PDT efficacy	Folate-conjugated micelles have higher PDT efficacy than *m*THPC or *m*THPC polymeric micelles without folate	2012	(94)
Male Balb/C mice bearing SIRCC1.15 (kidney) tumors	*m*THPC: PDT efficacy against kidney tumors	Renal tumor destruction, *m*THPC uptake and PDT sensitivity increased in endothelial cells compared renal cell carcinoma and renal cells	2012	(292)
Female BALB/c mice bearing hsp70-GFP/EMT6 tumors	*m*THPC: Investigation of tumor efficacy and heat shock protein levels	Maximum heat shock protein levels at PDT doses corresponding to 30% cell survival	2011	(161)
Syngeneic C3H/HeN mice bearing murine SCC (SCCVII)	*m*THPC in combination with ceramide analog (LCL29): Effect on PDT	Increase of cancer cell apoptosis by combination of LCL29 and *m*THPC-PDT	2011	(273)
Female NMRI$^{nu/nu}$ mice bearing HT-29 tumors	Pegylated liposomal *m*THPC (Fospeg®): Drug quantification	Fluorescence imaging (time-resolved fluorescence white Monte Carlo simulations combined with the Beer–Lambert law)	2011	(293)
Female syngeneic C3H/HeN mice bearing SCCVII tumors	*m*THPC in combination with ceramide analog (LCL29): Effect on PDT	Combination improved long-term tumor cure, changes in sphingolipid profile	2011	(275)
Female SKH-1 mice	Liposomal *m*THPC in collagen matrix: antibacterial photodynamic inactivation	Faster wound healing (scab detachment) with *m*THPC loaded an illuminated collagen implant	2011	(294)
Female Swiss (nu/nu) mice bearing RB-102-FER, RB-109-LAK and RB-111-MIL xenograft tumors	*m*THPC and Verteporfin: PDT efficacy, xenograft model for retinoblastoma	Transient response to *m*THPC for RB102-FER and response with partial regression to *m*THPC for RB111-MIL	2010	(295)
Female BALB/c mice bearing EMT6 tumors	*m*THPC: PDT efficacy using fractionation of drug administration	Investigation *m*THPC biodistribution profile and regional distribution of apoptosis; improved tumor cure with fractionated drug administration	2010	(296)
Hybrid DBA/2 × BALB/c male mice bearing L1210 ascitic tumors	Combination of *m*THPC PDT, adoptive immunotherapy, and chemotherapy: Efficacy study	Synergistic anti-tumor effect	2010	(297)
Male C57BL/6 mice bearing Lewis lung carcinoma	*m*THPC: PDT efficacy	0.25 mg kg^{-1} *m*THPC, 24 h DLI: Inhibition of tumor growth, prolonged survival	2010	(200)
Female athymic Foxn^{1nu}/Foxn^{1nu} mice bearing HT-29 tumors	*m*THPC treatment: Apoptosis and caspase activity	Different expression pattern of caspase-3 and caspase-7 in *m*THPC treated tumors	2009	(124)
Female Foxn1$^{nu/nu}$ mice bearing EMT6 tumors	*m*THPC vs. liposomal mTHPC (Foslip®): Pharmacokinetics and PDT efficacy	Highest tumour to muscle ratios at 6 and 15 h post-administration, best tumor response for 6 h DLI	2009	(298)
Rat				
Male Wistar rats (HsdCpb:W) bearing 4NQO-induced tumors	*m*THPC (Foscan®), liposomal *m*THPC (Foslip®) and pegylated liposomal *m*THPC (Fospeg®): Tumor accumulation *vs.* normal tissue	Higher *m*THPC fluorescence of Fospeg® in normal and tumor tissue compared to Foscan® and Foslip®, significant differences between tumor and normal tissue for all formulations	2013	(299)
Male Wistar rats bearing Walker-256 tumors	*m*THPC: pharmacokinetics, distribution, and elimination in orthotropic liver cancer model	Highest tumor/normal tissue-ratio at 24 h	2013	(300)
Female Wistar rats and Female HL rats bearing MC28 tumors	Pegylated liposomal *m*THPC (Fospeg®): distribution, effect of different degrees of pegylation	Longer elimination half-life for higher degree of pegylation	2012	(301)
Female Fisher-344 rats bearing transplanted R3230AC tumors	*m*THPC (Foscan®), liposomal *m*THPC (Foslip®) and pegylated liposomal *m*THPC (Fospeg®): Tumor accumulation vasculature kinetics	Skin-fold observation chamber model, maximum tumor fluorescence 8 h for Fospeg®, 24 h for Foslip® and Foscan®, higher bioavailability of liposomal formulations	2011	(302)
Female Fischer-344 rats bearing transplanted R3230AC tumors			2011	(303)

(continues)

Table 2. (continued)

Animal model	Compound/Study	Comments	Year	References
	*m*THPC: *in vivo* quantification/ pharmacokinetics *via* fluorescence, method development	Skin fold observation chamber model, dual wavelength excitation, NIR imaging		
Fisher-344 rats bearing tumors	*m*THPC: *in vivo* quantification/ pharmacokinetics by fluorescence measurement	Skin-fold observation chamber model, correction for autofluorescence	2009	(304)
Male Wistar rats	*m*THPC: *in vivo* quantification/ pharmacokinetics by fluorescence differential path length spectroscopy	Good correlation with chemical extraction	2009	(305)
Male Wistar rats	*m*THPC: Fluorescence and reflectance spectroscopic monitoring of interstitial PDT	Decrease in fluence rate during PDT, observation of differences in vascular response even between animals of the same treatment group	2009	(306)
Male Wistar rats	*m*THPC and other PS: Determination of PDT threshold dose depth of necrosis and superficial necrosis	Determination of PDT threshold dose by measurement of necrosis depth and superficial necrotic area	2009	(307)
Dog				
Male beagles	*m*THPC: Dosimetry for interstitial PDT in the canine prostate	Light-dose escalation plan, less damage to surrounding tissue with dosimetry planning, light energy dose-response relationship	2016	(308)
Sheep				
Swiss white alpine sheep	*m*THPC: Pharmacokinetics by blood sampling and fluorescence, optimization of oesophagus PDT	Similar pharmacokinetics and sensitivity to *m*THPC-PDT compared to humans	2009	(309)
Cat				
Cats bearing SCC (animal PDT)	*m*THPC: PDT treatment of feline SCC (63 lesions in 38 cats)	Complete remission 61%, partial remission 22%, mean progression-free interval of 35 months, median overall survival time 40 months	2018	(310)
Horse				
Horse sarcoid (animal PDT)	Pegylated liposomal *m*THPC (Fospeg®): PDT and surgical treatment of equine sarcoid (case report)	Local treatment, tumor remission or tumor growth stagnation	2012	(311)

account for the extent of tumor eradication observed *in vivo*. Here indirect effects, mainly on the tumor vasculature (42,251), are critical for long-term tumor control (42,245). In addition, PDT effects on the immune system contribute to tumor eradication (42,245,252–254). PDT can provoke the formation of antitumor inflammatory cells and can result in a persistent antitumor immune response (8,42,252–257). A significant body of research effort has been done addressing these effects and processes related to PDT at the molecular and cellular level as well as at the systemic level of the organism.

Photosensitizers rely on the ability to generate singlet oxygen and other ROS when irradiated with light in the presence of oxygen. The photophysics and basic photochemistry of temoporfin have therefore been investigated in various surroundings and under various conditions (42). In recent years, de Vetta *et al*. (258,259) and de Oliveria *et al.* (84) studied the photophysics of temoporfin using quantum chemical methods. Whereas the former analyzed temoporfin in a polar solvent (258), and later also in liposomes (see below) (259), the latter compared temoporfin to its corresponding *ortho*- and *para*-isomers concluding that the high efficacy of temoporfin – the *meta*-isomer – is not due to photophysical parameters but the better localization in tumor cells and tissues (84). Quantum chemistry (*vide supra*) has also been used for photophysics optimization approaches of porphyrins and chlorins for PDT involving temoporfin (81–83). Quantum chemical methods were also used to satisfactorily explain the higher photodynamic activity of temoporfin compared to its porphycene analogue, temocene (79). Also, the two-photon absorption properties of temoporfin have been analyzed (see below under 'Dosimetry and Detection') (61,260–262).

Only a limited number of investigations studied different frequently used photosensitizers under the same conditions. In one of those, Berlanda *et al*. (151) tested Foscan®, Fospeg® (a liposomal formulation of temoporfin containing pegylated lipids, see below), hypericin, aluminium(III) phthalocyanine tetrasulfonate chloride ($AlPcS_4$), δ-aminolevulinic acid (ALA) and Photofrin® in the A431 cell line with wavelength-specific LED-based illumination, finding distinct differences between them. They confirmed that temoporfin in both formulations is a very effective photosensitizer that induced high phototoxicity already at very low concentrations giving the lowest LD_{50} value under PDT of all tested photosensitizers (151). The efficiency of several photosensitizers including temoporfin, measured as the depth of necrosis was hypothesized to be correlated with their photostability in solution; however, a clear correlation could not be established (263). Already in 2005 Mitra and Foster compared the PDT efficacy of Photofrin® and temoporfin in EMT6 tumor cell spheroids and found that the higher efficacy of temoporfin is due to its photophysical properties (enhanced redshift absorption compared to Photofrin®) but also due to its ability to sequester tightly in (tumor) cells (264).

The photophysical properties of temoporfin in different carrier systems have been investigated as well (see also 'Formulation Development'). In a comparative investigation of three chlorin systems (temoporfin, disulfonated tetraphenylchlorin ($TPCS_{2a}$), chlorin e_6) in solution and in liposomes, the order of efficacy followed the sequence given above. This was attributed to the embedding of the different photosensitizers in the liposomal membrane (265). In human serum albumin (HSA) nanoparticles the ability of temoporfin to generate singlet oxygen depended on the loading ratio with only particles of lower loading able to generate singlet oxygen (188). However, after incorporation in Jurkat cells, all particles generated singlet oxygen based on the release of temoporfin. Also, the influence of antioxidants on the photophysics of temoporfin has been investigated (85). The phototoxicity in cells and photophysics of halogenated bacteriochlorins carrying sulfonic acids and sulfonamide moieties have been investigated in comparison with temoporfin. Whereas the PDT effect of temoporfin was associated primarily with a Type II reaction, the PDT effect of investigated bacteriochlorins was concluded to rest on Type I and Type II photochemical reactions (68). In a series of publications, the photosensitizing mechanism of temoporfin – serving as a model photosensitizer – has been analyzed with field-induced droplet ionization mass spectrometry at the air-water interface using lipids and on-purpose designed lipid-like molecules (266–268). The authors observed the formation of allyl hydroperoxides by oxidation of unsaturated lipid chains rationalized by the Type II mechanism (266). Later, evidence for the involvement of Type I photoreaction was found as well (267). This oxidation could be hindered by host-guest complexation of such amphiphilic molecules (268).

At the cellular level, PDT elicits a multitude of effects and affects numerous intracellular pathways (245). In addition, such effects observed on the cellular level depend on the light dose and the time after illumination (42,116). Therefore, sometimes seemingly contradictory results originate from different cell testing parameters and different observation windows. For PDT with temoporfin, the ER and the Golgi apparatus have been identified as primary sites of action in the cell (116,117,247,269,270). This cellular targeting of the ER has been studied in detail for three different photosensitizers (hypericin, temoporfin and methylene blue) using multifunctional luciferase reporter systems, confirming the ER targeting for hypericin and temoporfin (118). Mitochondrial oxidative stress followed by cytochrome c release and caspase activation resulting in an apoptotic cell response was determined for PDT with temoporfin (42,152,168,271), though this is not always observed in cellular assays (110). The change from apoptotic events to autophagy has been investigated in MCF-7 cells subjected to temoporfin and light (116). The importance of autophagy for temoporfin PDT has also been shown in colorectal cancer cells and *in vivo* in mice (135). The ROS generated by PDT were found to activate the signaling pathway *via* the c-Jun N-terminal kinases (135). PDT-induced cell damage results in the release of large numbers of extracellular vesicles, an effect that has been observed *in vitro* as well as *in vivo* (180). These extracellular vesicles can be exploited themselves as carriers for photosensitizers (see below under 'Formulation development').

PDT is also associated with the increased expression of heat shock proteins (97,272). Mitra *et al*. (161) found a correlation between long-term tumor control *in vivo* in mice and extracellular release of heat shock protein 70. This up-regulation of selected heat shock proteins has also been observed in two head and neck cancer cell lines (UMB-SCC 745 and 969) and the increased expression of heat shock proteins was used for specific targeting with verteporfin as a photosensitizer (272). PDT with the liposomal temoporfin formulation Fospeg® increased the P-glycoprotein expression – which is an important protein with respect to multidrug resistance in cancer cells – in human nasopharyngeal carcinoma cells (165). However, as temoporfin was no substrate to this transporter protein the PDT efficacy was not affected. The same authors also investigated the effect of Fospeg® on Epstein-Barr virus positive nasopharyngeal carcinoma cells (166). Temoporfin PDT led to an up-regulation of the cytokines VEGF and IL-1alpha in A431 carcinoma cells (154). Apart from such effects on specific proteins temoporfin has been observed to have a more general impact, e.g. on microtubules and cell endosomal transport (181). Other recent publications found phenotype shifts in macrophages elicited by temoporfin nanoparticles (163) and in Ras-transfected mammary cells, where a reduction of the migratory and invasive ability was observed for cells treated with PDT using different photosensitizers including temoporfin (162). Sphingolipids and their ceramide subgroup are building blocks of membranes, but also fulfil numerous other functions in the cell and have been shown to be involved in PDT (95,169). In a series of publications, Korbelik and Separovic (95,96,169,195,273–275) analyzed the relevance of sphingolipids for PDT with temoporfin and investigated the synergistic effect of combination therapies, e.g. with the ceramide analogue LCL29, the synthetic retinoide derivative fenretinide and a ceramidase inhibitor.

Cell death mechanisms and pathways have been and are still a matter of debate in PDT (8,110,248–250). Whereas for a long time the modes of unregulated cell death *via* necrosis or the programmed cell death *via* apoptosis in combination with autophagy were the main focus, recently, other modes of cell death have found increased attention with respect to PDT, specifically cell death triggered by the bodies' immune response (249). Induction of apoptosis by temoporfin PDT has been shown in many cellular assays (42,90,116,124,135,149,150,152,168,199). This cell death by apoptosis is often found to be accompanied by autophagy (90,116,135,152). In a comparative investigation, Lange *et al*. (90) investigated cellular death pathways after temoporfin PDT in five cancer cell lines (A-427, BHY, KYSE-70, RT-4, and SISO cells). In this case, cells were treated with equitoxic concentrations of temoporfin. Mitochondrial photodamage and ROS formation were observed in all cases. Apoptosis was identified as the dominant cell death mechanism, accompanied by autophagy. Lipid peroxidation and cell death due to loss of membrane integrity were found to be less important. However, there were considerable differences between the cell lines and the times when certain effects were found, and the authors suggest an interplay of different cell death mechanisms. That other cell death mechanisms also play a role for temoporfin has also recently been shown by Kessel who reported on the induction of paraptosis following temoporfin PDT-induced ER photodamage (110).

As mentioned above, the effects of PDT on the immune system contribute to the tumor control effect observed *in vivo*, and this has been discussed in numerous reviews (8,249,252,253,255–257,276,277). By activation of the T-cell adaptive immune response PDT can trigger immunogenic cell death (249). In the treatment of actinic keratosis and squamous

cell carcinoma, PDT has been found to activate the innate and adaptive immune system, following the local inflammatory response (277). Theodoraki *et al*. (254) analyzed blood samples from nine head and neck cancer patients treated with PDT for changes in different immune-cell subsets. Samples were taken before, during and after PDT and were compared to samples from age-matched healthy donors. They observed a systemic inflammatory immune response and found altered profiles of immune cell populations and cytokine concentrations (increased number of Treg and NK cells). The authors suggest that a combination of PDT with immune checkpoint modulators could lead to an improved anti-tumor response. Looking at the systemic effects of PDT resistance to PDT comes into focus as well, which was discussed in a recent review (278). Possible resistance mechanisms to PDT with temoporfin were investigated by Kralova *et al*. in cells and in mice bearing tumors grown from PDT-resistant cancer cells (193). Apart from temoporfin, ethylene glycol derivatives of 5,10,15,20-tetraphenylporphyrin were used as well. Interestingly, different resistance mechanisms were found; the more polar porphyrin ethylene glycol derivatives showed increased drug efflux through ABCB1 P-glycoprotein, whereas for the more lipophilic temoporfin a sequestration to lysosomes was observed.

Animal testing

Animal testing is still an indispensable measure in the preclinical development of pharmaceuticals though there is of course intense research going on to reduce, refine and replace such experiments according to the three R's principle (279). Quite a number of animal tests have been performed in recent years with temoporfin and its formulations (see Table 2). Of the many investigations listed in the review by Senge and Brandt from 2011 (42), many focused on elucidating the basic pharmacokinetic and pharmacodynamic properties of temoporfin in precedence of the marketing authorization application. As can be seen from the studies listed in Table 2 the newer *in vivo* investigations are to a large extent focused on the development of new formulations, new (tumor) indications and new treatment regimens. More than half of the investigations cited in Table 2 studied the *in vivo* behavior of new pharmaceutical formulations of temoporfin. Consequently, those publications are reviewed in the chapter about formulation development.

Animal experiments with temoporfin have almost exclusively been performed in rodents, predominantly in mice and also in rats. Single studies have been done in beagle dogs (308) and sheep (309), the two animal species chosen due to the specific requirements of the tumors to be treated, prostate and esophagus, respectively. Special cases are the treatment of cats (310) and horses (311). In these cases, a curative tumor treatment was intended, showing that PDT is also a treatment option for certain tumors in animals (*vide infra*).

A number of publications investigated the pharmacokinetics and the PDT effect of temoporfin with respect to specific tumors. Etcheverry *et al*. looked at the pharmacokinetics of the PS in mice bearing fibrosarcoma *via* fluorescence measurements (282). They observed a 'rebound effect', *i.e*. a fluorescence increase in certain parts of the tumor compared to that measured immediately after illumination. Fluorescence detection has also been used in other cases to investigate pharmacokinetics *in vivo* (303–306). In an investigation of rats, Kruijt *et al*. found a good correlation between quantification by fluorescence and chemical extraction (305). Also, singlet oxygen luminescence has been used as a dosimetric technique *in vivo* showing a good correlation between tumor response and singlet oxygen luminescence (288). Ferraz *et al*. determined the PDT threshold dose for different photosensitizers including porfimer sodium, bremachlorin (Radachlorin®) and temoporfin using a model employing the depth and width of necrosis in rat liver. They determined a value of 5.3 (±2.0) J cm^{-2} at a temoporfin dose of 0.3 mg kg^{-1}, considerably smaller than for porfimer sodium (28.0 (±2.0) J cm^{-2}, dose 2.0 mg kg^{-1}) (307). In a similar approach, *in vivo* necrosis experiments in mice combined with modelling were used to determine singlet oxygen threshold doses for PDT for different photosensitizers including temoporfin (285,286,312). Garrier *et al*. investigated the effectiveness of a compartmental targeting in xenografted tumors in mice, finding that fractionated double-injection of temoporfin with 24-h and 3-h drug-light intervals (DLI) yielded 100% tumor cure (296).

In a study with cellular assays and in mice the effect of temoporfin PDT on the induction and release of heat shock protein 70 was analyzed, showing that there was a clear correlation between temoporfin PDT doses achieving long-term tumor cure and those that effect high levels of surface exposed or extracellularly released HSP70 (161). In a mechanistic investigation, the apoptosis and activity of different caspases has been studied in cell cultures and in mice (124). The authors observed that photosensitized tumors had a higher number of cells with active caspase-3 and poly-ADP-ribose polymerase 1, suggesting that polymerase expression was mediated by treatment-induced apoptosis. A similar mechanistic investigation has been addressing the importance of autophagy in cells and in mice (135). As mentioned above (cf. 'mechanistic aspects'), resistance to PDT was investigated by Kralova *et al*. (193) in mice bearing tumors grown from PDT-resistant cancer cells and found to differ depending on the photosensitizer structure.

Temoporfin in a liposomal formulation was combined with natural antioxidants derived from *Pinus halepensis* in an investigation in mice to assess the use of such antioxidants to prevent photosensitizer-induced (skin) photosensitivity (291). The combination allowed to eliminate the tumor in this murine prostate cancer model while at the same time reducing photosensitivity. Similar protective effects of *P. halepensis* extracts were observed in *in vitro* experiments in the LNCaP prostate cancer cell line (176). Korbelik *et al*. (273,275) investigated the combination of temoporfin and a ceramide (LCL29) for PDT in a murine tumor model with squamous cell carcinoma. They found that this combination increased cancer cell apoptosis and long-term tumor cure. In addition, specific changes in the sphingolipid profile were observed during and after PDT (275). The authors also addressed the role of ceramides and sphingosines in PDT in several *in vitro* investigations (95,96,169,195,273,274).

In addition, the combination of PDT with antibody treatments has been tested in murine models. Korbelik *et al*. (284) analyzed whether an immunodepletion of granulocytic myeloid regulatory cells by administration of the anti-GR1 antibody would improve the effect of PDT and PDT-generated anti-cancer vaccines. They found that this strongly depended on the timeframe, immediately after PDT the administration of the anti-GR1 antibody eliminated the curative PDT effect in the mice, whereas after 1 h an

increased tumor response was observed. Temoporfin PDT has also been combined with chemotherapy and immune lymphocytes collected from mice pre-treated with PDT to cure advanced L1210 tumors in mice, showing a synergistic anti-tumor effect (297). A similar synergistic effect was observed for the combination of temoporfin PDT with the anti-VEGF antibody bevacizumab; however, only if PDT preceded the administration of bevacizumab (281).

One of the fields, where the clinical use of PDT is explored is liver cancer (see below). Wang *et al*. looked at temoporfin pharmacokinetics, distribution and elimination in an orthotropic liver cancer model in the rat in preparation for clinical investigations (300). The plasma concentration over time could be fitted with a two-compartment model. Tissue distributions showed the highest accumulation in the tumor with a subsequent decrease to liver, heart, spleen, muscle, and skin, the tumor-to-normal tissue localization ratio being highest at 24 h. PDT with temoporfin was studied in cell cultures and in mice bearing Lewis lung carcinoma and effectively inhibited tumor growth and prolonged survival. However, tumors regained their growth potential after nine days (200). PDT with temoporfin (0.6 mg kg^{-1}) and verteporfin (1 mg kg^{-1}) was tested in a mouse xenograft model for retinoblastoma, using an irradiation wavelength of 514 nm for temoporfin and 689 nm for verteporfin. The retinoblastoma xenografts derived from different patient cell lines reacted differently to the PDT treatment, with temoporfin showing a significant but transient response and verteporfin PDT being effective in xenografts where temoporfin was not (295). Temoporfin has also been investigated in mice with kidney tumors, suggesting it may be suitable as a nephron-sparing therapeutic option for small tumors (292).

While the majority of pre-clinical animal testing is done in rodents, sometimes specific indications require different animal models. *e.g*. Glanzmann *et al*. (309) assessed a sheep animal model for a PDT treatment of esophagus lesions with temoporfin. Sheep and human esophagus are closely comparable histologically and the pharmacokinetics of temoporfin were investigated by blood sampling and fluorescence *in vivo* measurements using the clinically approved dosage of 0.15 mg kg^{-1}. The maximum temoporfin concentration in plasma was observed after 10 h, and the maximum temoporfin fluorescence was observed in the oral cavity between 30 and 50 h. As the sheep and human tissue sensitivity to temoporfin PDT was found to be similar as well, the model was deemed suitable for optimizing esophagus PDT with temoporfin (309). In a similar way, the canine prostate was used as a model to perform light dosimetry during interstitial PDT with temoporfin (308). Again, temoporfin was used in a dose of 0.15 mg kg^{-1} and administered 72 h prior to illumination. The PDT effect was assessed by magnetic resonance imaging, pathology and histopathology of excised tissue. The results allowed to determine a threshold dose of 20 to 30 J cm^{-2} to induce prostate tissue necrosis.

Formulation development

Temoporfin is a quite lipophilic substance with an estimated octanol-water partition coefficient (logP) of >9, rendering it practically water-insoluble (313). The combination of the tetrapyrrole skeleton with NH-groups, together with the polar hydroxyphenyl groups gives the molecule a high affinity to membranes, proteins and lipoproteins, which is desirable with respect to the mode of action – the photodynamic damage to tumor cell structures. The affinity of temoporfin and other photosensitizers to membranes, proteins, and lipoproteins is also important with respect to their transport to the tumor tissue after intravenous administration (42,314). However, this poses a challenge for their pharmaceutical formulation (315,316). Of course, the problem of the pharmaceutical formulation of highly lipophilic, water-insoluble drug molecules is not unique to photosensitizers but a general issue for many new drug substances (317,318).

The presently approved drug formulation of temoporfin (Foscan®) is a solution of temoporfin in a mixture of ethanol and propylene glycol (319). This formulation shows a delayed pharmacokinetics profile, which is why the PDT treatment is performed 96 hrs after injection (42,319). Hence, numerous publications deal with possible new formulations of temoporfin (see below) (320,321). As for many other anti-cancer drugs, nanoparticles and nanoparticle formulations play an important role in this respect (322), often with reference to the EPR (enhanced permeability and retention) effect (323,324). Hence, nanoparticles have been specifically exploited as carriers for photosensitizers (24,315,316,321,323,325–331). Apart from serving as carriers, the nanoparticulate formulation of photosensitizers can additionally be used to enhance the singlet oxygen generation (332) or may be used to switch the operating photochemical mechanism (333).

The studies related to the delivery of temoporfin *via* nanoparticles have quite recently been reviewed expertly by Yakavets *et al*. (320). Investigations on the incorporation of temoporfin in nanoparticles cover a broad range of materials comprising systems such as extracellular vesicles (186,211,212), supramolecular organic frameworks (99), or polymer-*block*-peptides (334,335), hydrogels (336–338), as well as carrier systems for which there is already considerable pre-clinical and clinical experience. Examples for the latter are PLGA [poly(lactic-co-glycolic acid)] (111,137,138) and HSA nanoparticles (132,189,190) and liposomes (42,298,320) (Fig. 7).

Chitosan nanoparticles

*m*THPP has been used as a model substance for temoporfin in the incorporation into polymethacrylic acid (PMAA)-modified chitosan nanoparticles finding a high loading capacity for the substance and uptake into 14C cells (184). Temoporfin itself has been incorporated into polyplex nanoparticles consisting of sodium alginate and a chitosan polymer or oligomer (339). The nanoparticle size distribution could be modified by the concentration of the solutions, order of addition, the ratio of addition and the pH. Chitosan oligosaccharides were used in the formation of core-shell nanoparticles loaded with temoporfin and targeted with an RGD peptide to address integrin-rich tumors (214). The targeted core-shell nanoparticles showed a deeper penetration into U87MG tumor spheroids and had a higher anti-tumor efficacy than non-modified nanoparticles in U87MG tumor-bearing mice. Recently, these nanoparticles were combined with checkpoint inhibitors (anti-PD-1/PD-L1 antibodies) for PDT and immunotherapy for colorectal cancer inhibiting primary and distant tumor growth in mice (133). *m*THPP–ethylcellulose/chitosan nanoparticles have also been studied for their antibacterial action (227).

Human serum albumin nanoparticles

Wacker *et al*. (189) reported on the preparation of temoporfin-loaded HSA nanoparticles, the photophysical properties of which were later investigated in more detail (188). For these particles, a freeze-drying method was developed which is important with respect to the storage of a future pharmaceutical formulation (189). In photophysical investigations in D_2O only particles with low temoporfin loading generated singlet oxygen; however, in Jurkat cells all formulations generated singlet oxygen suggesting that the particles were successfully taken up by the cells releasing temoporfin (188,189). The release of temoporfin from the HSA nanoparticles was found to occur via lysosomal decomposition of the nanoparticles with the HSA nanoparticles exhibiting a higher phototoxicity than free temoporfin (190). Quite recently, an optimized protocol for albumin nanoparticles loaded with temoporfin was published making use of the nanoparticle albumin-bound (*nab*)-technology which is also applied for the medicinal product Abraxane®. The nanoparticles were effectively taken up in the TFK-1 cholangiocarcinoma cell line and showed high phototoxicity (132). Recently, pulsed dipolar electron paramagnetic resonance (EPR) has been used to investigate the binding of *m*THPP to BSA (bovine serum albumin) and identified the proton-rich pocket of HSA subdomain IIIA and the main binding site (340).

PLGA nanoparticles

The incorporation of photosensitizers in nanoparticles often results in a reduced dark (cyto)toxicity compared to the free photosensitizer. The same was also observed for the incorporation of temoporfin in PLGA nanoparticles (137). The lysosomal decomposition and release of the temoporfin were faster for PLGA than for HSA nanoparticles (341). Rojnik *et al*. (111) compared pegylated and non-pegylated PLGA nanoparticles in cells and in mice. Both kinds of nanoparticles were found to be distributed in the cytoplasm in MCF10AneoT cells shortly after incubation with a preference for endoplasmic reticulum and Golgi apparatus, whereas at later time points temoporfin fluorescence was observed in lysosomal-endosomal compartments. Differences were observed for *in vivo* distribution, e.g. in colon tissue the temoporfin delivery was highest for the pegylated PLGA nanoparticles whereas in lung tissue it was highest for the non-pegylated nanoparticles (111). The rational design and scale-up manufacture of temoporfin-loaded pegylated PLGA nanoparticles has been investigated in more detail, again revealing reduced dark toxicity but efficient phototoxicity of the final formulation (138). The nanoparticles also exhibited an altered pharmacokinetic behavior: With Foscan®, precipitation of the compound at the injection site (the tail vein) and a delayed distribution was observed. This was not the case for the nanoparticle formulation (138). Temoporfin-loaded PLGA nanoparticles were employed for the fabrication of core-shell nanoparticles with a temoporfin-PLGA-core and an albumin shell (126). Similar systems were prepared with *m*THPP (342). Boeuf-Muraille *et al*. (198) found in *in vitro* release studies in a buffer of temoporfin-loaded PLGA nanoparticles that approx. 50% of temoporfin was retained in the nanoparticles after 5 days. Cell testing in the murine C6 glioma cell line revealed apoptosis as the main cell death mechanism. Elberskirch *et al*. (226) used the HET-CAM model with the duodenum adenocarcinoma cell line HuTu-80 employing temoporfin-loaded PLGA nanoparticles as well as nanoparticles with two porphyrin-based photosensitizers, finding that the model was suitable to simulate *in vivo* endoscopic irradiation. PLGA nanoparticles coated with a phospholipid bilayer have also been tested for co-encapsulation of temoporfin and a chemotherapeutic, exhibiting an additive effect against a retinoblastoma cell line (183).

Polymer systems

Different polymer systems (343) have been used for the encapsulation of *m*THPP (344) and temoporfin and for studying the PDT effect of the resulting nanoparticle formulations. Temoporfin has been loaded on Eudragit® nanoparticles – which is an approved pharmaceutical ingredient – and up-scaling for this formulation has been investigated (185). In addition, the drug release from these particles was studied using mathematical models (345). One of the advantages of polymeric carriers is the broad variation of functionalities allowing the inclusion of specific linkers that enable the release of – sometimes covalently bound – photosensitizers based on specific triggers (346). pH-sensitive nanoparticles based on hyperbranched polyglycerol and 2-(diisopropylamino)ethyl methacrylate loaded with temoporfin have been prepared (63,139) while polyglycerol-based nanogels with the temoporfin congener *m*THPP have also been specifically tested for dermal delivery (347). Such systems are of interest for the local administration of photosensitizers specifically in skin cancer (348). Systems with a disulfide linker have been prepared as well, which make use of the difference in the redox potentials between the cellular membrane and the bloodstream (50,63). It is known that the bloodstream has a global potential that is mildly oxidative whereas the intracellular potential is mildly reductive (63).

Recently, the concept of light-responsive polymers (349) as delivery systems for temoporfin has come into focus (148). Light-sensitive polycarbonates were combined with PLGA to encapsulate temoporfin. Light-induced nanoparticle degradation then led to the local release of the photosensitizer. Upon irradiation, with UV light a decreasing particle count rate and an increased release of temoporfin compared to standard PLGA nanoparticles were found (350). Pegylation was used to obtain particles with mucus-penetrating properties (351,352) for intestinal PDT (147). Later this concept was extended to other polymers (140).

Temoporfin has also been incorporated in polymeric micelles based on different polymers. For example, Fang *et al*. (192) prepared styrene maleic acid copolymer micelles loaded with temoporfin and tested their in cell cultures and in mice. They observed a lower dark toxicity *in vitro* and reduced side effects *in vivo*; concomitantly, the polymeric micelles maintained their antitumor PDT effect longer as compared to free temoporfin. Similar results were obtained for poly(2-ethyl-2-oxazoline)-*b*-poly(*D,L*-lactide) diblock copolymer micelles loaded with temoporfin (141). For folate-conjugated polymeric micelles loaded with temoporfin, an enhanced PDT efficacy compared to free photosensitizer or polymeric micelles without folate conjugation was observed in *in vitro* and in a murine model (94). Polymeric micelles based on ε-caprolactone have been described in several publications. Wennink *et al*. (196) prepared specific temoporfin-loaded ε-caprolactone micelles which were degraded faster by macrophages than by endothelial cells thereby releasing

temoporfin and exhibiting higher phototoxicity for this cell type – in the context of a selective macrophage elimination by PDT. However, as the temoporfin was found to be rapidly released from the micelles in plasma this selectivity could not be exploited *in vivo*. ε-Caprolactone micelles loaded with temoporfin were also tested in two other *in vivo* investigations in mice investigating the effect of aromatic groups on the polymer (101) as well as that of dithiolane-crosslinking and pegylation (280). The presence of aromatic groups in the polymer and non-crosslinked micelles resulted in higher temoporfin retention. This polymeric micelle approach has also been employed to produce antibody-nanoparticle conjugates with a Llama or an EGFR-targeted antibody (102,156).

Peptides

Peptides have been used for a long time as targeting units for photosensitizers (353). However, the combination of peptides and polymers has also been exploited as drug transporters for temoporfin. Ahmadi *et al*. (103) used amphiphilic block-*co*-polypeptides as carriers for dermal drug delivery, again taking the temoporfin congener *m*THPP as a model drug. In another approach polymer-*block*-peptides were exploited for drug delivery. Combinatorial chemistry methods were used to select small peptide sequences to specifically bind small drug molecules, using temoporfin as an example (334,335,354–357).

As in many other cases, temoporfin proved to be a very suitable compound for investigating the encapsulation of hydrophobic drug molecules in nanoformulations, as its encapsulation and release can easily be followed by means of optical spectroscopy (355). The loading capacity of the formulation as well as release kinetics were found to be strongly influenced by the specific peptide sequence, and transfer from the nanoformulation to BSA, as a model for HSA, could be observed (355). Switchable release profiles with these systems could be realized by introducing disulfide linkers into the peptide sequence (334) and the pharmacokinetics could be further modified by PEGylation (335,354). The concept has also been applied to the preparation of nanogels suitable for dermal drug delivery (356). The utility of the concept was further tested by comparing the solubilization of three related tetrapyrrole-based photosensitizers, temoporfin, chlorin e_6, and pheophorbide a, finding significant binding capacity differences (357). Apart from peptides, the concept was additionally investigated, using temoporfin as a model drug, with lipid-DNA (143), thiolactone polymers (358), peptoid sequences (359), and alternating co-polymers (360).

Resonance energy transfer can be used to excite photosensitizer molecules. This has been exploited in *m*THPP containing quantum dots (361,362) and the combination of semiconducting polymer dots (Pdots) with temoporfin. Zhang *et al*. (120) prepared Pdots functionalized with folic acid and horseradish peroxidase. The fluorescent polymer backbone served as a light antenna and as a hydrophobic carrier for temoporfin. In this system, after luminol-H_2O_2 activation, indications for chemoluminescence resonance energy transfer were found. In another system, Pdots with coatings of different pegylated lipids were synthesized, the polymer backbone serving again as the light antenna and the lipid coating ensuring close contact to the photosensitizer temoporfin, enabling efficient fluorescence energy transfer (121,363). Both compositions were effectively taken up in cancer cells (120,121,363).

Extracellular vesicles

Extracellular vesicles (EVs) have recently found considerable interest as new carrier systems (364). Aubertin *et al*. (180) showed that PDT with temoporfin as well as chemotherapeutic treatment with doxorubicin resulted in a high production and release of extracellular vesicles from cancer cells, an effect that was also observed *in vivo* in mice. The effect was more pronounced for PDT than for chemotherapy (180). Such cell-released vesicles could be loaded simultaneously with temoporfin and magnetic nanoparticles (164). Piffoux *et al*. (186) prepared extracellular vesicles loaded with temoporfin and iron oxide nanoparticles as theranostic agents for PDT, MRI and hyperthermia and compared different methods for their production. They identified starvation of cells in a serum-free medium followed by ultracentrifugation as a suitable method for production and purification of the vesicles. The same authors later modified the extracellular vesicles by fusion with liposomes (187). Loading with hydrophobic or hydrophilic molecules was possible without leakage of the intrinsic load of the vesicles. Temoporfin-loaded extracellular vesicles have been compared to liposomal temoporfin in multicellular tumor spheroids and *in vivo* in HT29 xenografted mice (211,212). The authors observed deeper penetration of temoporfin into the tumor spheroids and an improved biodistribution and PDT efficacy *in vivo* (212). In the context of a PDT-immunotherapy combination extracellular vesicles have been prepared from mesenchymal stem/stromal cells targeting peritoneal metastasis in mice, where the authors observed a promotion of antitumor immune cell infiltration in addition to the primary PDT effect (201). Temoporfin-loaded extracellular vesicles have also been tested in comparison to a liposomal temoporfin formulation and a liposomal formulation additionally containing cyclodextrin-bound temoporfin (see also below) (219). In this investigation of stroma-rich head and neck cancer tumor spheroids (220) the extracellular vesicles demonstrated the highest loading capacity and deep penetration into the tumor spheroids (219).

Cyclodextrins

Pronounced differences in pharmacokinetics in mice were observed between free temoporfin and temoporfin inclusion complexes with cyclodextrins (CDs) (144). The photosensitizer forms 1:2 inclusion complexes with β-cyclodextrins in a 2-step-mechanism (365). With temoporfin-β-cyclodextrin complexes, a faster and increased accumulation in the tumor of HT29 tumor-bearing mice were found, together with a decreased level of temoporfin accumulation in skin and muscles (144). The release of temoporfin from the CD inclusion complexes and transfer to serum components could be studied making use of the Soret band shape which was found to be sensitive to changes in the immediate surroundings of the molecule (366). However, other optical methods amended by computational modelling can be used for such analyses (367,368). Similar to the above-mentioned extracellular vesicles, β-cyclodextrin complexes led to a higher accumulation and deeper penetration in HT29 multicellular tumor spheroids compared to free temoporfin (210). However, the temoporfin–β-CD complexes are sensitive to dilution; therefore, hyper-crosslinked cyclodextrin monomers were prepared, capable of forming inclusion and non-inclusion complexes (221). With *m*THPP it was shown that covalently linked PS-β-

cyclodextrin compounds had better PDT activity *in vitro* against glioblastoma cells compared to inclusions complexes (369). The affinity of temoporfin to cyclodextrin could also be influenced by methylation of the cyclodextrin carrier (129,365). Temoporfin and β-cyclodextrins have also been combined with liposomes as a second carrier to obtain 'drug-in-cyclodextrin-in-liposome' nanoparticle systems. In these, most of the temoporfin was bound to cyclodextrins in the inner aqueous liposome core (370). Later this system was modified to obtain lipid vesicles containing temoporfin β-cyclodextrin inclusion complexes in the inner aqueous core as well as lipid compartments of the vesicles (145). However, in an *in vivo* test in mice with xenografted HT29 tumors, the PDT efficacy was similar to that of a liposomal temoporfin formulation (145).

Lipid nanoparticles

Lipid nanoparticles (371) have been used as carrier systems for temoporfin as well. Navarro *et al*. (122,123) reported on the preparation, characterization and cell testing of solid lipid nanoparticles encapsulating temoporfin. The lipid nanoparticles were composed of a lipid core, stabilized by phospholipids and pegylated surfactants. The temoporfin-loaded lipid nanoparticles exhibited photocytotoxicity in MCF7 cells; however, there was also some toxicity induced by the empty lipid nanoparticles. Hinger *et al*. (223) evaluated these lipid nanoparticles in two different sizes (50 and 120 nm) in 3D CAL-33 cancer cell spheroids, where the 50 nm lipid nanoparticles exhibited the same PDT efficacy as free temoporfin. Later, the same authors compared the temoporfin-loaded lipid nanoparticles with the approved drug formulation (Foscan®) and a liposomal formulation (Foslip®, see below) in CAL-33 tumor-bearing mice (283). With respect to tumor response, Foslip® gave the best results, whereas the temoporfin-loaded lipid nanoparticles were better tolerated and gave less side effects. Brezaniova *et al*. (127) compared the *in vitro* and *in vivo* efficacy of 1-tetradecanol-based and copolymer stabilized solid lipid nanoparticles loaded with temoporfin with Foscan®. In the experiments in mice, certain formulation variants performed considerably better than the approved drug formulation. However, partial tumor relapse was observed, mostly at the periphery of the original tumor (127). Rad *et al*. (191) compared temoporfin-loaded lipid vesicular (liposomal) and discoidal nanoparticles with and without folate targeting for their PDT efficacy in cellular assays and in mice. The authors found a clear morphology effect with the folate-decorated discoidal nanoparticles being more effective than the folate-decorated vesicular nanoparticles.

In a combined photothermal and PDT approach oil droplet nanoparticles were loaded with temoporfin and the photothermal agent IR780 (202). The combined photothermal/PDT efficacy was investigated *in vitro* and *in vivo*. Irradiation at 808 nm (for IR780) and 660 nm (for temoporfin) effectively suppressed tumor growth in TRAMP-C1 tumor-bearing mice. Lipid nanoparticles have also been used in release studies (372,373). Trimyristin lipid nanoparticles or phospholipid liposomes were loaded with substances of different polarity, including temoporfin, and transfer from these donor nanoparticles to oil-in-water emulsions was studied by flow cytometry and separation of donor and acceptor by ultracentrifugation (372). Flow cytometry proved to be a suitable method to investigate dye transfer.

Inorganic nanoparticles

Inorganic nanoparticles have been used for loading with or encapsulation of temoporfin, *e.g.* temoporfin PDT and fluorescence imaging have been combined with RGDfK peptide targeting in CAL-27 cells and in mice with calcium phosphate nanoparticles (170). Haimov *et al*. (53) covalently conjugated temoporfin to gold nanoparticles and tested their PDT efficacy in SH-SY5Y human retinoblastoma cells. Temoporfin has been loaded on maghemite nanoparticles and magnetic targeting followed by PDT was investigated in mice (128). Silva *et al*. (164) prepared cell-derived vesicles loaded with temoporfin and magnetic nanoparticles and tested them *in vivo* in a murine tumor model. The distribution in the animals could be followed by fluorescence as well as MRI. Temoporfin and iron oxide nanoparticles were also incorporated in liposomes – temoporfin in the lipid bilayer and the iron oxide particles in the aqueous core – and these liposomes were successfully tested on mice for a combined hyperthermia-PDT application (172). Shah *et al*. (104) used a similar approach of liposomes incorporating temoporfin and magnetite nanoparticles but additionally encapsulated the chemotherapeutic doxorubicin. They investigated the separate and combined effect in HeLa cells finding the combination to be more effective than the individual treatments. Silva *et al*. (216) employed cell-derived vesicles to load them with doxorubicin, a tissue-plasminogen activator and the two photosensitizers temoporfin and disulfonated tetraphenylchlorin (Fimaporfin, $TPCS_{2a}$). They could show *in vitro*, using photosensitizer fluorescence, that the microvesicles are taken up by cancer cells (SKOV-3, TC1 and PC-3 cells) and that the vesicles can be magnetically manipulated. The two photosensitizers localize in different cellular compartments; temoporfin was found in the cytoplasm whereas $TPCS_{2a}$ accumulated in endosomes (181). Silica nanoparticles have successfully been tested as well *in vitro* (157,194) and *in vivo* (194) as carriers for temoporfin. In the *in vivo* tests in mice, it was found that the temoporfin-loaded silica nanoparticles were able to cross the blood-brain barrier (194). Silica nanoparticles containing carbon dots have also been simultaneously loaded with temoporfin and a nitric oxide photodonor (374). Hsu *et al*. (112) prepared luciferase-immobilized quantum dots which were activated by addition of coelenterazine. These bioluminescent quantum dots served as an internal light source for temoporfin PDT. The PDT effect was studied in cancer cell cultures and in mice. *In vivo*, a delayed tumor growth due to tumor cell apoptosis was observed (112). Yu *et al*. (49) performed a chemical modification of temoporfin with 4-(bromomethyl)benzoic acid to connect it to the surface of $LiYF_4$:Tm^{3+}/Yb^{3+} upconverting nanoparticles. Upon irradiation, with light of 980 nm the particles generated singlet oxygen and photocytotoxicity in HeLa cells was detected. Timor *et al*. (375) reported on the solubilization of CdSe/CdS quantum rods by decoration with lecithin and pegylated phospholipids. This solubilizing layer was capable of carrying temoporfin allowing close contact with the quantum rods and enabling efficient fluorescence resonance energy transfer and singlet oxygen generation.

Liposomes

Liposomes are by far the carrier system employed most widely for the pharmaceutical formulation of temoporfin (320). This is not unexpected as liposomes are long established as carrier

systems for pharmaceuticals, including anti-cancer drugs (376–378), and are of specific interest as carriers for photosensitizers (379–384). Moreover, liposomes carry the option of additional functionalization for drug targeting (378,379,385,386). Liposomes are unilamellar vesicles consisting of an aqueous core surrounded by a lipid bilayer. This structure allows hydrophilic compounds to be included in the aqueous core or lipophilic compounds to be incorporated in the lipid bilayer (377,386). Of course, both functions can be combined to simultaneously transport hydrophilic compounds in the aqueous core and lipophilic compounds in the lipid bilayer (see also the examples mentioned above). Temoporfin as a lipophilic membrane-affine compound is transported in the lipid compartment of the liposomes (145,368). The interaction of temoporfin with the liposomal membrane has also been studied by computational methods (259).

From a practical point of view, liposomes have the additional advantage that they can be freeze-dried – with the addition of suitable cryo-protectants – and then re-constituted prior to use, which is beneficial with respect to transport and stability. Visudyne®, which contains the photosensitizer verteporfin as the active substance and is used in the treatment of the age-related macular degeneration, is such a freeze-dried liposomal formulation to be re-constituted before administration to the patient (387). Various liposomal formulations of temoporfin have been prepared and related photosensitizers have been incorporated into liposomes as well (226), *e.g.* the temoporfin analogue temocene (78). There is also a special interest in liposomal formulations with respect to applications in dermatology and topical delivery (371,384,388,389).

Two liposomal temoporfin formulations are often mentioned in the publications under their tradenames, one is Foslip®, the other is Fospeg®. Foslip® are unilamellar vesicles (liposomes) consisting of dipalmitoylphosphatidylcholine (DPPC) with the addition of 10% dipalmitoylphosphatidylglycerol (DPPG) and temoporfin at a concentration of 1.5 mg mL^{-1}. The molar drug: lipid ratio is approximately 1:12 (290,320,390). Fospeg® is similar to Foslip®, but additionally contains pegylated lipids (290). Incorporation of temoporfin in liposomes (or other carrier systems) changes the optical properties of temoporfin (265,368) and can alter the cellular response compared to simple administration of the PS (182). On the other hand, the properties of the phospholipid membrane are also affected by temoporfin (390,391).

Temoporfin-loaded liposomes based on dipalmitoylphosphatidylcholine/-glycerol have a phase transition temperature near body temperature (390). Computational studies suggested that temoporfin in the lipid membrane acts as a hydrogen donor in hydrogen-bonding interactions with the polar groups of the phospholipids (259). The generation of singlet oxygen of the photosensitizers temoporfin, fimaporfin ($TPCS_{2a}$) and chlorin e_6 – which was similar in ethanolic solution – is different when incorporated into liposomes (265). As liposomes serve as carrier system for the photosensitizer the release and transfer of temoporfin from liposomes to acceptor compartments, to membranes, or to plasma components, has been extensively studied. Different methods have been employed to study this transfer, e.g. optical methods (392,393), radioactively labelled temoporfin or lipids (391,394–396) or by flow-field-flow fractionation (391,394,397,398). The latter method has also been used for related tetrapyrrole systems (399–401). Flow field-flow fractionation was found to reliably recover liposomes loaded with temoporfin (drug recovery ~ 80%); however, drug loss was much higher for drugs with a lower octanol-water partition coefficient (397).

Methods to rapidly screen and characterize different liposomal formulations, *e.g.* for size and incorporation efficiency, have been developed as well (402). Chen *et al*. investigated the transfer of a hydrophilic model drug (carboxyfluorescein) and temoporfin from vesicular systems to skin *in vitro*. They found the vesicular systems capable to improve the transfer of carboxyfluorescein into the skin, but not for temoporfin (403). Hefesha *et al*. (404) analyzed the transfer mechanism of temoporfin between liposomal membranes of different compositions. Finding apparent first-order kinetics, the transfer rates strongly depended on temperature, with positively charged donor liposomes exhibiting faster transfer than negatively charged ones. The maximum amount of temoporfin transferred was nearly the same in both cases and a model describing the release kinetics was developed (405). A strong influence of the membrane composition on temoporfin release was observed in other investigations as well (394).

The rigidity of the liposomal membrane can be influenced by membrane additives. A comparative investigation of cholesterol and temoporfin as membrane additives revealed that cholesterol increases the rigidity of the membrane whereas temoporfin lowers it (391,396,398). Reshetov *et al*. compared the transfer of temoporfin from pegylated and non-pegylated liposomes to proteins and model membranes (406,407). Using fluorescence quenching and fluorescence polarization they determined that in Fospeg® a part of the temoporfin is also in the PEG shell and not only in the lipid bilayer. They stated that at short incubation time redistribution from Foslip® and Fospeg® occurred via drug release and liposome destruction whereas at longer periods drug release is dominant (407). In a similar investigation on the transfer of temoporfin from pegylated liposomes to human plasma proteins, the authors additionally evaluated phosphatidyl oligoglycerols. These alternatives to pegylated lipids resulted in a lower transfer rate compared to pegylated liposomes (396). Using ^{14}C-labelled temoporfin in transfer experiments with human plasma, Kaess and Fahr could show that approximately 15% of temoporfin is retained in the liposomes after 48 h (395). The main acceptors in plasma were HDL and LDL, whereas albumin played only a minor role (395,397). Recently, a dispersion releaser technology combined with a four-step-model has recently been described for such release experiments using temoporfin and temoporfin-loaded liposomes as the test systems (408).

The pharmacokinetics of liposomal temoporfin were investigated in mice (298) and in rats (299,302). A study in mice bearing EMT6 xenografted tumors with i.v. administration of 0.3 mg kg^{-1} temoporfin (as Foslip®) found that plasma pharmacokinetics and biodistribution could be described with a three-compartment model. The highest tumor-to-muscle ratios for temoporfin were observed at 6 and 15 h post administration with the best tumor response for 6 h DLI (298). In a pharmacokinetic investigation in rats using fluorescence detection with the window-chamber tumor model at a temoporfin dose of 0.15 mg kg^{-1} de Visscher *et al*. (302) compared Foscan®, Foslip® and Fospeg®. They observed maximum tumor fluorescence at 8 h for Fospeg® and at 24 h for Foscan® and Foslip® with higher fluorescence from the liposomal formulations, suggesting a higher bioavailability for these formulations. Similar results were obtained by de Visscher *et al*. (299) with the 4NQO carcinogenesis model in rats. Fospeg® showed higher fluorescence differences in tumor vs. normal tissue at earlier time points. Decker

et al. (409) studied the pharmacokinetics of temoporfin and the lipid carrier in rats using radioactively labelled compounds. The pharmacokinetic data showed that part of the temoporfin is released from the liposomes before leaving the bloodstream. This release increased with decreasing bilayer fluidity. Liposomes modified with pegylated lipids or oligo-glycerols showed an increased temoporfin loss from the liposomal carrier (409,410).

Other pharmacokinetic studies of Foslip® have been reviewed earlier (42). Additionally, predictive models for pharmacokinetics and biopharmaceutics have been developed using Foslip® and Fospeg® as test formulations (411,412). Comparing the simulation to the plasma-concentration-time profiles from a phase I clinical trial with Foslip®, the authors showed that their model was able to adequately describe the pharmacokinetic profile in humans (411). Xie *et al*. (293) developed a method to quantify temoporfin from Fospeg® in HT29 tumor-bearing mice tissue samples using fluorescence imaging and correlated this with HPLC determination after tissue extraction. For Fospeg®, a higher plasma peak concentration, a longer circulation time, and a better tumor-to-skin ratio compared to data for Foslip® were found (287). Reshetov *et al*. compared Foslip® and Fospeg® with respect to, e.g. pharmacokinetics, tumor uptake and PDT efficacy *in vitro* an in HT29 tumor-bearing mice (290). Temoporfin release from Foslip® was found to be faster than from Fospeg®. The highest temoporfin levels were found in the spleen and liver for both formulations. The highest concentration in the tumor was reached earlier for Fospeg® (6 h) than for Foslip® (15 h).

The PDT efficacy testing of Foscan® and Fospeg® in the LNCaP prostate cancer cell line revealed a higher temoporfin fluorescence and a higher photocytotoxicity after incubation with Fospeg® (177,178). Foslip® was found to be effective in 5-fluorouracil-resistant HT29 cancer cells (209), similar to results with temoporfin in HCT116 cells (208). An increased tumoricidal effect for Fospeg® compared to Foslip® has been observed in the EMT6 CAM model (413). In comparative *in vivo* tests in MC28 tumor bearing rats with Foscan® and temoporfin-loaded liposomes with different degrees of pegylation, the latter reached the maximal tumor-to-skin ratio at earlier time points and also resulted in higher tumor necrosis (301). A higher PDT efficacy of liposomal temoporfin was also found in tests in CAL-33 tumor bearing mice (283). Related studies in osteosarcoma cells and osteosarcoma mouse models (217,218) revealed an immune-system dependent suppression of lung metastasis in the K7M2L2 mouse tumor model (217). Liposomal temoporfin and hypericin were tested in combination on head and neck SCC, finding synergistic effects of the combination (97,98). An investigation in HeLa tumor cell spheroids found temoporfin fluorescence from all three formulations (Foscan®, Foslip®, Fospeg®) only in the outer cell layer of the spheroids, with a little higher accumulation for the liposomal formulations (205). The liposomal delivery of temoporfin reduced dark toxicity effects (205). A lower dark toxicity for temoporfin in pegylated liposomes was also observed in cellular assays in CCD-34Lu fibroblasts and in A549 lung cancer cells (113). Temoporfin PDT with Fospeg® effectively triggered apoptosis in HT29 tumor cells (146). It has also been used against nasopharyngeal carcinoma cells and tumor spheroids (165–167) and Huh7 hepatocellular carcinoma (160). A photochemical internalization approach in um-scc-U2 and um-scc-U8 head and neck cancer cells showed the cytotoxicity of bleomycin to be considerably increased when PDT with Foslip® and Fospeg® was performed prior to the treatment with the drug (159). Low-dose PDT with liposomal temoporfin reduced tumor growth in a colitis-associated murine carcinogenesis model (289). This low-dose PDT had a strong effect on inflammatory markers and was able to effectively decrease inflammation.

Apart from pegylation, other modifications have been used in connection with liposomal temoporfin formulations. *e.g.* temoporfin has been studied in DPPC monolayers investigating the effect of folate conjugation (414). A comparison of pegylated liposomes loaded with temoporfin with and without folate-targeting showed that folate-modified liposomes are taken up more in folate receptor-positive cells (114). In a similar study transferrin-conjugated liposomes loaded with temoporfin were tested with transferrin receptor-positive OE21 esophageal cancer cells. In this case, an increased uptake or increased photocytotoxicity could not be observed (158). ROS generated by the photosensitizer can in principle also attack the carrier system, *e.g.* the lipids of liposomal carriers. This has been used as an option for photo-triggered liposome membrane alteration with several photosensitizers, including *m*THPP (415).

The addition of gemini surfactants (dimeric surfactants) was tested as a measure to improve the delivery efficiency of temoporfin-loaded liposomes (215). Recently, tetraether liposomes were proposed as a new carrier system for temoporfin (174). Another option for modifying the liposomes is the combination of two carriers, like in the abovementioned cyclodextrin-liposome systems, where temoporfin was complexed by cyclodextrin within the aqueous core of the liposome (370) or additionally included in the lipid compartment of the liposomal carrier (145). Of course, liposomes can be used to combine two therapeutic or diagnostic principles as well. For example, PLGA nanoparticles containing the chemotherapeutic pirarubicin have been coated with a lipid bilayer loaded with temoporfin (175). These dual function particles were then tested in SKOV3 ovarian tumor cells and in mice. The *in vitro* tests suggested a synergistic effect (175). As already discussed above with the inorganic nanoparticles, liposomes have been loaded with temoporfin in the lipid bilayer and iron oxide particles in the aqueous core for combined hyperthermia-PDT application (172). In a similar approach, liposomes incorporating temoporfin and magnetite nanoparticles were prepared encapsulating additionally the chemotherapeutic doxorubicin, thus combining PDT, chemotherapy and hyperthermia (104).

Temoporfin has also been incorporated into liposomes with additives to enhance the penetration properties, e.g. to allow *i.a.* better skin penetration (384). Skin penetration has been investigated with neutral, anionic and cationic flexible liposomes based on phosphatidylcholine (416). Of these, cationic liposomes, containing additional stearylamine showed the highest penetration efficacy. As an alternative temoporfin-containing liposomal gels were prepared using carbomer as the gelling agent (417,418). So-called invasomes (419) containing ethanol and terpenes as penetration enhancers have been investigated in a series of publications (142,388,420,421). The effect of the different enhancers was analyzed, *e.g.* with respect to ethanol as a penetration enhancer the formulation with the highest ethanol content (20%) had the highest penetration efficacy, and the PDT efficacy was evaluated in cellular assays against HT29 and A431 tumor cells (142,388,421).

Liposomal formulations of temoporfin have also been tested for photodynamic antimicrobial chemotherapy (see also 'Antimicrobial PDT'). Garrier *et al*. (294) tested collagen and collagen incubated with Foslip® as a means for wound healing in a

Table 3. Selected clinical investigations (sorted by cancer type/clinical target and by publication year).

Cancer type/Clinical target	Treatment	Conditions	Sample size*	Result/Tumor response	Side effects/comments	Year	References
Gastrointestinal							
Anal intraepithelial neoplasia, grade III	*m*THPC (i.v.)	0.03, 0.075, or 0.15 mg kg^{-1} *m*THPC, 48 h, λ = 652 nm or λ = 532 nm, starting at 50 mW cm^{-2}, 20 J cm^{-2}, later 105 mW cm^{-2}, 105 J cm^{-2}, finally 105 mW cm^{-2}, 340 J cm^{-2}	15 (25 treatments)	Initial response 28%, initial partial response 16%, 16% persistent complete response (at 532 nm)	Red light illuminations caused more significant side effects combined with no persistent complete response	2012	(460)
Anal intraepithelial neoplasia, grade III	*m*THPC (i.v.)	0.03 or 0.075 mg kg^{-1} *m*THPC, 48 h, λ = 652 nm, 45–50 mW cm^{-2}, 10–17 J cm^{-2}	4	Development of a light applicator, monitoring blood saturation, blood volume, fluorescence and fluence (rate) in situ	No influence of the applicator on the fluence rate profile of the light treatment fiber	2010	(461)
Anal intraepithelial neoplasia, grade III	Fosgel (topical)	0.75 mg mL^{-1} (3 mm) *m*THPC, 8 h, λ = 652 nm, 50 mW cm^{-2}, 20 J cm^{-2}, 2 × treatment after 7 d	9	No response	No effect attributed to limited penetration in AIN III	2009	(462)
Cholangiocarcinoma	*m*THPC (i.v.)	0.032–0.063 mg kg^{-1} *m*THPC, 20 h and 67–72 h, λ = 652 nm, 200 mW cm^{-1}, 50 J cm^{-1}	13	Median survival time 13 months	Add. fluorescence measurements; *m*THPC fluorescence at tumor site clearly detectable, no significant fluorescence contrast of tumor to adjacent healthy tissue	2013	(463,464)
Biliary tract cancer	*m*THPC (i.v.)	0.15 mg kg^{-1} *m*THPC, 96 h, λ = 652 nm	20	Primary endpoint: feasibility and safety, combination PDT + chemotherapy + stenting feasible, progression free survival numerically longer in PDT group	Randomized controlled trial (10 patients per group), chemotherapy + stenting vs. chemotherapy + stenting + PDT, number of cholangitis equal in both groups, two abscesses in PDT group	2016	(465)
Biliary tract cancer	*m*THPC (i.v.)	0.15 mg kg^{-1} *m*THPC, 96 h, λ = 652 nm, 28.2 J cm^{-2}	29	PDT with *m*THPC compared to PDT with porfimer sodium: prolonged time to local tumor progression, fewer PDT treatments needed, higher 6-month survival rate.	Adverse events: 4 cholangitis, 2 liver abscesses, 2 cholecystitis, 5 phototoxic skin and 7 injection site reactions	2015	(466, 467)
Hilar bile duct cancer	*m*THPC (i.v.)	0.15 mg kg^{-1} *m*THPC, 72-96 h, λ = 652 nm, 28.2 J cm^{-2}	11	Overall median survival time 18 months after 1st PDT; doubled depth of local tumor ablation compared to porfimer sodium	Adverse events: 4 phototoxic skin reaction, 3 cholangitis, and 3 liver abscesses	2013	(468)
Bone							
Hyoid chondrosarcoma	*m*THPC (i.v.)	0.15 mg kg^{-1} *m*THPC, 96 h, λ = 652 nm, interstitial treatment output per fiber 0.5 W, 20 J.cm^{-2} per site	1 (case study)	Tumor shrinkage, 2nd PDT treatment after 11 months	Ultrasound guidance for needle insertion	2009	(469)
Brain							
Primary brain tumors	*m*THPC (i.v.) and porfimer sodium	0.15 mg kg^{-1} *m*THPC, 96 h, λ = 652 nm, 20 J cm^{-2}	41	Median progression-free survival: 10 months for glioblastoma, 26 months for anaplastic astrocytoma, and 43 months for oligodendroglioma	Administration of PS, craniotomy, surgical resection and laser illumination of the surgical bed combined with temozolomide-based chemotherapy and	2015	(470)

(continues)

Table 3. (continued)

Cancer type/Clinical target	Treatment	Conditions	Sample size*	Result/Tumor response	Side effects/comments	Year	References
					radiotherapy; side effects: pain, neurologic post-operative deficits in 5 patients		
Prostate							
Prostate cancer (dosimetry)	*m*THPC (i.v.)	0.15 mg kg^{-1} *m*THPC, 96 h, λ = 652 nm, 5 J cm^{-2}	4	Incomplete treatment	Threshold dose too low, fiber output power attenuated by heterogeneities	2010	(471)
Prostate cancer (dosimetry)	*m*THPC (i.v.)	652 nm, interstitial treatment	not spec.	Reconstruction of spatial distribution of fluorescent photosensitizer (*m*THPC)	Fluorescence measurements, photosensitizer tomography	2009	(472)
Skin							
Non-melanoma skin cancers (SCC and BCC)	*m*THPC (i.v.)	BCC: 0.05 mg kg^{-1} *m*THPC, 48 h, λ = 652 nm, 20 J cm^{-2}, SCC: 0.1 mg kg^{-1} *m*THPC, 96 h, λ = 652 nm, 20 J cm^{-2}	18	SCC patients: complete response, BCC patients: 12 complete response, 2 complete response after 2nd PDT	4 Hypopigmentation, 1 hyperpigmentation	2020	(473)
Non-melanoma skin cancer (SCC)	*m*THPC (i.v.)	0.05 mg kg^{-1} *m*THPC, 48 h, λ = 652 nm	22	3-Year follow-up: complete repsonse in 20/22 patients (1 PDT treatment), recurrence in 2 patients (treated by surgical resection)	Side effects: local paresthesia (1), local hyperesthesia (1), full recovery of both within 3 months post-PDT, hypopigmentation of treatment site (3)	2019	(474)
Non-melanoma skin cancers (BCC)	*m*THPC (i.v.)	0.05 mg kg^{-1} *m*THPC, 48 h, λ = 652 nm, 20 J cm^{-2}	62	116 Lesions, 60 patients complete response, after 5 years 92% complete response rate	Both superficial and nodular types responded better than invasive type	2017	(475)
Non-melanoma skin cancers (SCC and BCC)	*m*THPC (i.v.)	0.05-0.15 mg kg^{-1} *m*THPC, 24 h, λ = 652 nm and λ = 514 nm (1 case), 10-40 J cm^{-2} (for 652 nm)	4	Complete remission for 105 out of 106 lesions, no response for treatment at 514 nm	Blisters, lipodystrophy, urinary tract infection, leg infection, severe itching	2015	(476)
Non-melanoma skin cancers (BCC)	*m*THPC (i.v.)	0.06–0.15, 0.05, 0.04, and 0.03 mg kg^{-1} *m*THPC, 1–6, 24, 48, and 72–96 h, λ = 652 nm, 20, 40, 50, 60, and ≥100 J cm^{-2}	117	460 Lesions, sustained clearance rate 93.7%, overall treatment success rate 90.7%	Favorable long-term outcome for 'difficult to treat' BCCs with high-dose (0.06–0.15 mg kg^{-1}) and reduced-dose (0.05 mg kg^{-1}); optimized low-dose parameters: 0.05 mg kg^{-1}, 24 h, ≥40 J cm^{-2}	2008/2009/ 2012	(477–479)
Non-melanoma skin cancer (SCC)	*m*THPC (i.v.)	0.05 mg kg^{-1} *m*THPC, 48 h, λ = 652 nm	1 (case report)	Complete response, no recurrence	Optical coherence tomographic guided PDT (assessment of tumor extent and margins)	2011	(480)
Non-melanoma skin cancers (SCC and BCC)	*m*THPC (i.v.)	0.05 mg kg^{-1} *m*THPC, 24 h, λ = 652 nm, 40 J cm^{-2}	9	152 Lesions, 117 complete response, 35 partial response	No adverse clinical and serological effects	2011	(481)
Head and neck							
Different head and neck pathologies	*m*THPC (i.v.)	Different doses of *m*THPC	38	Study on the quality of life of patients after PDT with *m*THPC	Improvement of quality of life (visual symptoms, breathing, speaking and swallowing), main side effect: pain	2022	(482)
Oral and oropharyngeal carcinoma	*m*THPC (i.v.)	0.15 mg kg^{-1} *m*THPC, 72–120 h, λ = 652 nm, interstitial and superficial illumination,	26	76% Complete response, local control in 42.3%, median overall survival 24 months	Retrospective cohort analysis, multiple but transient adverse events, mostly PDT specific	2021	(483)

(continues)

Table 3. (continued)

Cancer type/Clinical target	Treatment	Conditions	Sample size*	Result/Tumor response	Side effects/comments	Year	References
		mean total energy 0.66 W per spot					
Head and neck cancer	*m*THPC (i.v.)	0.15 mg kg^{-1} *m*THPC, 96 h, λ = 652 nm, 100 mW cm^{-2}, 20 J cm^{-1}	1 (case report)	Follow-up at 6 weeks: tissue healing and regeneration with no clinical evidence of recurrence, tumor-free 3 months after treatment	PDT treatment (*m*THPC) as additional treatment after chemotherapy (Bleomycin) combined with photochemical internalization with disulfonated tetraphenyl chlorin $TPCS_{2a}$	2020	(484)
Paranasal sinuses tumors (dosimetry)	*m*THPC (i.v.)	0.15 mg kg^{-1} *m*THPC, 96 h, λ = 652 nm, 100 mW cm^{-2}, 20 J cm^{-2} (target fluence and fluence rate)	11	Major temporal and spatial variations in fluence rate and fluence		2020	(485)
Head and neck cancer	*m*THPC (i.v.)	0.15 mg kg^{-1} *m*THPC, 96 h, λ = 652 nm, 100 mW cm^{-2}, 20 J cm^{-2} (range: 10–30 J cm^{-2})	54	Primary endpoint: Progression-free survival; 2-year progression-free survival rate 30%; 2-year overall survival was 51%. Disease-free survival was significantly better for time interval between surgery and PDT was ≥6 weeks.	Retrospective cohort analysis, PDT as adjuvant therapy for tumor positive resection margins, no adverse events in 78% of patients, most common adverse events localized skin burn (grade I–II) and dysphagia	2018	(505)
Head and neck carcinoma	*m*THPC (i.v.)	*m*THPC, 96 h,	9	Investigation on the effect of PDT treatment on immune cell subsets, systemic inflammatory immune response with altered peripheral immune cell populations and cytokine concentrations		2017	(254)
Nasopharyngeal carcinoma	*m*THPC (i.v.)	0.15 mg kg^{-1} *m*THPC, 96 h, λ = 652 nm, 20 J cm^{-2}	21	20 Patients (95%): Complete response 10 weeks post-treatment; 2-year local control rate 75%, progression free survival 49%, overall survival 65%.	Phase II study, local recurrent or residual nasopharyngeal carcinoma after curative intent (chemo-)radiation, no serious adverse events	2015	(486)
Oral carcinoma (base of tongue)	*m*THPC (i.v.)	0.15 mg kg^{-1} *m*THPC, 96 h, λ = 652 nm, 100 mW cm^{-2}, 20 J cm^{-2}	2	Disease free at 42 and 24 months of follow-up	Adjuvant treatment after salvage surgery to treat the remaining microscopic disease at resection margins	2015	(487)
Paranasal sinuses tumors	*m*THPC (i.v.)	0.15 mg kg^{-1} *m*THPC, 96 h, λ = 652 nm, 100 mW cm^{-2}, 20 J cm^{-2}	15	Complete response in 5 patients, 6 patients with short progression-free intervals	PDT as additional tool for the treatment of recurrent tumors of the paranasal sinuses and the anterior skull base, main side effects: pain and edema	2015	(488)
Early laryngeal cancer	*m*THPC (i.v.) and porfimer sodium	0.15 mg kg^{-1} *m*THPC, 96 h, λ = 652 nm, interstitial treatment, 30 J cm (fiber), 20 J cm^{-2}	10	7 Patients tumor-free on PDT alone (6 *m*THPC, 1 porfimer sodium followed by *m*THPC), 2 after add. radiotherapy	Descriptive, retrospective study, no unexpected side effects or airway problems; most common symptom hoarseness	2014	(489)
Head and neck cancer	*m*THPC (i.v.)	0.15 mg kg^{-1} *m*THPC, 96 h, λ = 652 nm, interstitial treatment, 20 J cm^{-2}	1 (case report)	Use of endoluminal tracheal stenting prior to PDT	Counter measure against possible post operative swelling following PDT	2014	(490)

(continues)

Table 3. (continued)

Cancer type/Clinical target	Treatment	Conditions	Sample size*	Result/Tumor response	Side effects/comments	Year	References
Nasopharyngeal carcinoma	*m*THPC (i.v.)	0.15 mg kg^{-1} *m*THPC, 96 h, λ = 652 nm, interstitial and superficial illumination, 100 mW cm^{-2}, 20 J cm^{-2}	6	Patients receiving transnasal direct illumination postero-superior recurrence disease-free for 38 and 71 months	Coupling with ear, nose, throat (ENT) magnetic navigation system	2014	(491)
Head and neck cancer	*m*THPC (i.v.)	0.15 mg kg^{-1} *m*THPC, 96 h, λ = 652 nm, interstitial treatment	1	Treatment simulation of MR- and CT-assisted interstitial PDT	Method development	2013	(492)
Head and neck cancer	*m*THPC (i.v.)	0.15 mg kg^{-1} *m*THPC, 96 h, λ = 652 nm, interstitial and superficial illumination, 100 mW cm^{-2}, 20 J cm^{-2}	88	Airway management vital for planning PDT treatment for tongue-based tumors, specifically for location at higher risk site: Floor of mouth/posterior tongue/tongue base or multiple oral sites being treated	Retrospective clinical study on the role of airway management in PDT for head and neck cancer	2013	(493)
Oral SCC	*m*THPC (i.v.)	0.15 mg kg^{-1} *m*THPC, 96 h, λ = 652 nm, 100 mW cm^{-2}, 20 J cm^{-2}	214 (treatments; 156 PDT, 58 surgery)	T1 tumors: similar results for PDT or transoral surgery, T2 tumors: PDT seemed less effective; PDT and surgery: similar overall survival rates for both T1 and T2 tumors	Comparison PDT vs. surgical treatment	2013	(494)
Oral and oropharyngeal carcinoma	*m*THPC (i.v.)	0.15 mg kg^{-1} *m*THPC, 96 h, λ = 652 nm, 100 mW cm^{-2}, 20 J cm^{-2}	15	14 Complete responses, 1 partial response, overall survival 72% at 1 year and 36% at 5 years, disease-specific survival 82% at 1 year was 82% and 45% at 5 years.	Side effects: pain in all cases, 2 burns, 1 edema (tongue base)	2013	(495)
Early oral cavity carcinoma	*m*THPC (i.v.)	Not spec.	98 (55 PDT, 43 surgery)	Primary endpoint: local disease-free survival, PDT comparable to trans-oral resection in terms of disease control and survival	Matched cohort comparison	2013	(496)
Kimura disease	*m*THPC (i.v.)	0.15 mg kg^{-1} *m*THPC, 96 h, λ = 652 nm, interstitial treatment, 20 J cm^{-2}	1 (case report)	Reduction of disease volume, 2nd PDT 14 months later similar reduction of disease volume	Ultrasound-guided PDT	2012	(497)
Nasopharyngeal carcinoma	*m*THPC (i.v.)	0.15 mg kg^{-1} *m*THPC, 96 h, 0.10 mg kg^{-1} *m*THPC, 48 h, and 0.075 mg kg^{-1} *m*THPC, 24 h λ = 652 nm, 100 mW cm^{-1}, 20 J cm^{-1}	22	Biopsy in 17 of the 22 patients after 40 weeks showed no tumor in all 17 biopsies, highest clinical efficiency in group 0.15 mg kg^{-1} *m*THPC, 96 h DLI	Feasibility study, most common side effect: headache (33%), no skin burn or other skin adverse reactions caused by the photosensitizer	2012	(498)
Nasopharyngeal carcinoma (T4N0M0)	*m*THPC (i.v.)	0.15 mg kg^{-1} *m*THPC, 96 h, λ = 652 nm	1 (case report)	Treatment of residual T4 nasopharyngeal tumor, no tumor recurrence for five years after PDT	Special nasopharyngeal applicator	2012	(499)

(continues)

Table 3. (continued)

Cancer type/Clinical target	Treatment	Conditions	Sample size*	Result/Tumor response	Side effects/comments	Year	References
Solitary neurofibroma (neck)	*m*THPC (i.v.)	0.15 mg kg^{-1} *m*THPC, 96 h, λ = 652 nm, 20 J cm^{-2}	1 (case report)	Reduction of large neurofibroma, reduction of pain, dysphagia and shortness of breath issues	Ultrasound-guided light delivery	2012	(500)
Nasopharyngeal carcinoma	*m*THPC (i.v.)	0.15 mg kg^{-1} *m*THPC, 96 h, λ = 652 nm, 20 J cm^{-2}	7	Palliative treatment of recurrent advanced carcinoma, moderate to significant response, symptom reduction, control of disease progression	Case series, naso-endoscopic guidance	2012	(501)
Base of tongue cancer	*m*THPC (i.v.)	0.15 mg kg^{-1} *m*THPC, 96 h, λ = 652 nm, interstitial treatment, 100 mW cm^{-1}, 30 J cm^{-1}	20	9 Patients complete response (6 months), with 4 patients free of disease after 46–80 months	No short-term complications, pharyngo-cutaneous fistula (6 patients), bleeding (1 patient, cutaneous metastasis (2 patients)	2012	(502)
Proliferative verrucous leukoplakia	*m*THPC (i.v.)	not spec.	1 (case report)	not spec.	Bisphosphonate-related osteonecrosis (parallel treatment with bisphosphonates)	2011	(503)
Vascular anomalies of the head and neck	*m*THPC (i.v.)	0.15 mg kg^{-1} *m*THPC, 96 h, λ = 652 nm, interstitial treatment, 100 mW cm^{-2}, 10 –20 J cm^{-2}	43	Clinical assessment: 50% 'good treatment response', moderate clinical response 30.2%, radiological assessment (6-week post-PDT) moderate response 25.6%, significant response 34.9%	Ultrasound guidance, post-operative infection, peripheral oedema, skin ulceration, skin burn, fistula, hemorrhage	2011	(504)
Base of tongue cancer	*m*THPC (i.v.)	0.15 mg kg^{-1} *m*THPC, 96 h, λ = 652 nm, interstitial treatment, 20 J cm^{-2}	33	Moderate to significant tumor response (> 50% reduction) in 20/33 patients, improvement of breathing, swallowing, and speech in the majority of patients	End-stage base of tongue cancer, ultrasound guidance, side effect: skin burns	2011	(505) cf. f. also (506)
Head and neck cancer, vascular anomalies	*m*THPC (i.v.)	0.15 mg kg^{-1} *m*THPC, 96 h, λ = 652 nm, interstitial treatment, 100 mW cm^{-2}, 20 J cm^{-2}	110	App. 50% of patients showed 'good response' to treatment, 5 patients became disease free; improvement of breathing (27/32), improvement of swallowing (30/37), speech improvement (22/29) reduction of disfigurement caused by their pathology (43/52)	Prospective evaluation, ultrasound guidance	2011	(507)
Extramedullary plasmacytoma (nasopharynx)	*m*THPC (i.v.)	0.15 mg kg^{-1} *m*THPC, 96 h, λ = 652 nm, 100 mW cm^{-1}, 20 J cm^{-1}	1 (case report)	Surgical debulking combined with PDT, patient disease free since 6 years	Dedicated PDT nasopharyn × applicator	2011	(508)
Oral carcinoma (OSCC, T1/T2)	*m*THPC (i.v.)	0.15 mg kg^{-1} *m*THPC, 96 h, λ = 652 nm, 100 mW cm^{-2}, 10–20 J cm^{-2}	38	Most recent clinical review post PDT: in 26/38 patients normal clinical appearance of oral	Multiple PDT treatments on patients	2011	(509)

(continues)

Table 3. (continued)

Cancer type/Clinical target	Treatment	Conditions	Sample size*	Result/Tumor response	Side effects/comments	Year	References
				mucosa, overall recurrence rate 15.8%, 5-year survival 84.2%			
Base of tongue cancer	*m*THPC (i.v.)	0.15 mg kg^{-1} *m*THPC, 96 h, λ = 652 nm, interstitial treatment, 20 J cm^{-2}	21	>50% 'good response' and ~ 1/3 'moderate response' to treatment, improvement of breathing (9/11), improvement of swallowing (19/21), speech improvement (11/13)	Multiple PDT treatments on patients, 85% of patients: no problems post PDT, side effects: skin burns (3), skin necrosis (1), airway treatment (2), fistula (1)	2011	(506) cf. also (505)
Oral dysplasia	*m*THPC (i.v.) and 5-ALA (topical)	0.1 mg kg^{-1} *m*THPC, 96 h, λ = 652 nm, 20 J cm^{-2}	147	Complete response in 119/147 patients (81%), partial response in 12 (8.2%), stable disease in 5 (3.4%), and progressive disease in 11 (7.5%) patients	Prospective study, side effects: mild-to-moderate pain in 126 (85.7%) patients, mild-to-moderate skin photosensitivity for 22 (15%) patients	2011	(510)
Base of tongue cancer	*m*THPC (i.v.)	0.15 mg kg^{-1} *m*THPC, 96 h, λ = 652 nm, interstitial treatment, 20 J cm^{-2} and 100 J cm^{-2}	1 (case report)	Improvement of dysphagia and dysphonia	Ultrasound guidance, 2nd treatment with increased light dose	2011	(511)
Oral and oropharyngeal carcinoma	*m*THPC (i.v.)	0.15 mg kg^{-1} *m*THPC, 96 h, λ = 652 nm, 100 mW cm^{-2}, 20 J cm^{-2}	170	Complete response rate of 70.8%, median local disease-free interval (for complete response cases) 102.0 months, 2- and 5-year local disease-free survival 74 and 61%, respectively	Retrospective analysis	2011	(512)
Oral carcinoma	*m*THPC (i.v.)	0.15 mg kg^{-1} *m*THPC, 96 h, λ = 652 nm, 100 mW cm^{-2}, 20 J cm^{-2} (for the patients)	3 (+ 8 healthy volunteers)	Monitoring PDT by fluorescence differential path length spectroscopy	Monitoring of PDT by fluorescence differential path length spectroscopy is feasible	2011	(519)
Oropharyngeal/laryngeal carcinoma	*m*THPC (i.v.)	0.15 mg kg^{-1} *m*THPC, 96 h, λ = 652 nm, interstitial treatment, 20 J cm^{-2}	1 (case report)	Palliative treatment, 6 months follow-up stable disease with no progression	Radiologically inserted endoluminal carotid stenting prior to PDT for vessel protection	2010	(513)
Head and neck cancer	*m*THPC (i.v.)	0.15 mg kg^{-1} *m*THPC, 96 h, λ = 652 nm, interstitial treatment 100 mW cm^{-1}, 30 J cm^{-1}	Not spec.	Fluorescence differential path length spectroscopy for monitoring *m*THPC-PDT for interstitial treatment of head and neck cancer		2010	(514)
Subglottic carcinoma	*m*THPC (i.v.)	0.15 mg kg^{-1} *m*THPC, 96 h, λ = 652 nm, 20 J cm^{-2}	1 (case report)	Surgery with adjuvant PDT, patient disease free 18 months post PDT	Elective tracheostomy performed due to the airway risk as a result of the postoperative swelling, 3 consecutive PDT treatments	2010	(515)
Head and neck cancer	*m*THPC (i.v.)	0.15 mg kg^{-1} *m*THPC, 96 h, λ = 652 nm, 100 mW cm^{-2}, 20 J cm^{-2}	39	Response rate 54%, median survival significantly longer for responders (37 months) than for non-responders (7.4 months), 9 patients were alive at 3.7 to 6.5 years (median, 4.8 years) post-treatment, 7 free of disease	Multicenter study, most frequent adverse events: cancer pain (21%), pain in general (13%), dysphagia (13%), and photosensitivity reactions (10%)	2010	(516)

(continues)

Table 3. (continued)

Cancer type/Clinical target	Treatment	Conditions	Sample size*	Result/Tumor response	Side effects/comments	Year	References
Cystic hygroma	*m*THPC (i.v.)	0.15 mg kg^{-1} *m*THPC, 96 h, λ = 652 nm, interstitial treatment, 20 J cm^{-2}	1 (case report)	50% Size reduction of cystic hygroma	Ultrasound-guided PDT	2010	(517)
Head and neck cancer	*m*THPC (i.v.)	0.15 mg kg^{-1} *m*THPC, 96 h, λ = 652 nm, 100 mW cm^{-2}, 20 J cm^{-2}	35	Local control in 21 patients (60%), partial remission in 10 patients (28.5%), 4 patients were non-responders, 1-year survival rate was 53.4% for all patients, 62.4% for patients with complete local control, and 30% for patients with partial remission	Side effects: pain at injection site 83%, pain associated with necrosis in the illuminated area 46%	2009	(518)
Tumors and malformations (mainly oropharyngeal region, face and limbs)	*m*THPC (i.v.)	0.15 mg kg^{-1} *m*THPC, 96 h, λ = 652 nm, interstitial treatment, 20 J cm^{-2}	68	App. 50% of patients showed 'good response' to treatment, 1/3 'moderate response', 2 patients became disease free; improvement of breathing (14/17), improvement of swallowing (25/30), speech improvement (16/22) reduction of disfigurement caused by their pathology (33/40)	Prospective study, ultrasound guidance	2009	(519)
Hemangiomas and other malformations							
Hemangioma	*m*THPC (i.v.)	0.15 mg kg^{-1} *m*THPC, 96 h, λ = 652 nm, interstitial treatment, 20 J cm^{-2}	1 (case report)	Size reduction of hemangioma, increased function of the leg with the angioma	Ultrasound-guided PDT, skin burn on left arm following inadvertent sun exposure	2010	(520)
Non-tumorous malformations	*m*THPC (i.v.)	0.15 mg kg^{-1} *m*THPC, 96 h, λ = 652 nm, interstitial treatment, 20 J cm^{-2}	21	At the 6-week follow-up review, significant shrinkage (50–80%) detected in all patients with hemangiomas, lymphangiomas, arteriovenous malformations and neurofibromas	Ultrasound guidance, up to 10 treatments per patient	2009	(521)

*Number of protocol compliant patients.

murine model. The mice implanted with temoporfin-treated collagen and subsequent illumination showed earlier scab detachment and elastin neosynthesis. PDT with liposomal temoporfin in combination with hypericin has been used against cariogenic bacteria the *Streptococcus mutans* and *Streptococcus sobrinus* (235), and PDT with temoporfin in the liposomal formulation was tested on *Enterococcus faecalis* which is often found in endodontic infections (229,422). With 10 μM of temoporfin a bacterial reduction (measured in CFU, colony forming units) of *E. faecalis* of 5.8 log units was achieved (229). Engelhardt *et al*. (234) tested water-soluble formulations of hypericin and temoporfin (Fospeg®) as aqueous sprays for the inactivation of *Staphylococcus aureus*. With 100 nM of photosensitizer, a bacterial count reduction of 4-5 log units was observed. In terms of a better bacterial targeting Yang *et al*. (231,232) modified temoporfin-loaded liposomes either with an antimicrobial peptide or with a lectin (wheat germ agglutinin) and tested them on *S. aureus* and *Pseudomonas aeruginosa*. Photodynamic antimicrobial chemotherapy with these modified liposomes was highly effective against *S. aureus* and partly effective against *P. aeruginosa*.

Other nanoparticular formulations

The title compound has been used with some other nanoparticular formulations. For example, it has been combined with carbon nanotubes for a synergistic PDT and photothermal approach (173). In this investigation in SKOV3 ovarian cancer cells a synergistic effect was detected based on the induction of different apoptosis signaling pathways by PDT and the photothermal treatment. Nanoparticles of different sizes have also been prepared from neat temoporfin (197). The nanoparticles were produced either by dissolution in an organic solvent (ethanol, DMSO) followed by precipitation with distilled water and ultrasound treatment or by direct ultrasound treatment of temoporfin powder (197). These crystalline temoporfin nanoparticles were more efficiently taken up in macrophages (J774A.1 cells) than in L929 fibroblast cells. Later it was found that PDT with these temoporfin nanoparticles can induce a phenotypic shift in macrophages (163). Dissolution from temoporfin nanocrystals has been analyzed using mathematical models (423). In another combinatorial approach, temoporfin and a nitric oxide photodonor have been incorporated into calix[4]arene nanoassemblies (424). Upon visible light excitation, the nanoconstruct was able to independently release nitric oxide and singlet oxygen. Recently, nanoparticles consisting of supramolecular organic frameworks and temoporfin have been prepared and tested in cell cultures and *in vivo* in mice (99). The nanoparticles showed photocytotoxicity in several cancer cell lines and were able to suppress tumor growth in mice. In a theranostic approach, Sun *et al*. prepared cRGD-modified liposomes encapsulating oxygen-carrying perfluorocarbon and temoporfin, these liposomes then being loaded into living neutrophils (224). These modified neutrophils served as sonosensitizers and effectively suppressed tumor growth in mice. Imaging of the tumors was realized by temoporfin fluorescence detection and perfluorocarbon-microbubble enhanced ultrasound imaging.

CLINICAL EXPERIENCE

Temoporfin is the active substance in the medicinal product Foscan® which is authorized in 2001 in the European Union for the palliative treatment of head and neck cancer. The standard dosage in this treatment is 0.15 mg per kg body weight. Illumination is performed with laser light at 652 nm (425). Temoporfin is one of the few photosensitizers authorized for clinical use in the European Union (245,426,427). Others are padeliporfin (Tookad®) (428), verteporfin (Visudyne®) (429) or ALA (5-aminolevulinic acid hydrochloride, Ameluz®) (430), all of those being authorized via the centralized procedure with the European Medicines Agency (EMA) (431). Padeliporfin is authorized for the treatment of low-risk prostate cancer, verteporfin for the treatment of the so-called 'wet' form of age-related macular degeneration, and ALA for the treatment of actinic keratoses and basal cell carcinoma. A different medicinal product, also containing ALA as the active substance, Gliolan®, is authorized in the European Union for intraoperative fluorescence diagnosis of tumorous tissue in the surgery of malignant glioma (432). The photosensitizer fimaporfin (Amphinex®) has received an orphan drug designation by the EMA (433) for the treatment of cholangiocarcinoma in combination with the chemotherapeutic gemcitabine (434). Fimaporfin (disulfonated tetraphenylchlorin, $TPCS_{2a}$) enhances the effect of gemcitabine *via* photochemical internalization (PCI) (67,435). The well-known photosensitizer porfimer sodium is authorized in some European countries for the treatment of cholangiocarcinoma. Worldwide, numerous other photosensitizers are authorized for clinical use or are under clinical development. Examples are tin ethyl etiopurpurin (Purlytin®), motexafin lutetium (Antrin®), radachlorin, talaporfin (Laserphyrin®) or redaporfin (426,436–438).

During its development temoporfin, like other photosensitizers, has been investigated for the treatment of numerous indications, mainly certain forms of cancer (42,43). This development continues after the marketing authorization. Based on the established level of quality and safety shown in the original marketing authorization new indications can be explored in clinical studies. For example, verteporfin which - being authorized for the treatment of the age-related macular degeneration – has been investigated in the palliative treatment of pancreatic cancer (439). In recent years a number of comprehensive reviews on the role of temoporfin and other photosensitizers in the therapy against cancer and other diseases have appeared paving the way through the ever-expanding field of PDT research (15,19,39,426,427,436,437,440–448). Algorri *et al*. (449) recently undertook the effort to compile all the latest reviews in the area of PDT. This is further amended by reviews on PDT of specific forms of cancer, encompassing the use of temoporfin in the area (42) and among other therapies for brain cancer (450,451), lung cancer (452), prostate cancer (453–455), esophageal cancer (456,457), peritoneal metastasis (458), and recurrent respiratory papillomatosis (459). Table 3 gives an overview of the main fields of clinical applications of temoporfin in roughly the last ten years. These include clinical trials, as well as single-patient treatments (case reports). Most clinical experience has been collected in the field of head and neck cancer and other head and neck malformations, which is not surprising given the authorized indication. Apart from these investigations, considerable clinical experience has also been acquired with gastrointestinal diseases and certain forms of skin cancer.

In addition, recent years have seen single reports on the use of temoporfin for bone cancer (469), primary brain tumors (470), prostate cancer (308,471,472), and *ex-vivo* studies with human retinoblastoma (522).

Skin cancer

Temoporfin has been investigated for its use against non-melanoma skin cancers and a number of clinical studies and case reports have been published (see Table 3) (42,473–481). These non-melanoma skin cancers - the most common malignancy among the Caucasian population – comprise *i.a.* actinic keratoses (pre-cancerous lesions), Bowen's disease (carcinoma *in situ*) and basal cell (BCC) carcinoma as well as squamous cell carcinoma (SCC) (523). Specifically for actinic keratoses, Bowen's disease and BCC PDT has been established as an alternative treatment to surgery, with ALA or MAL (methyl aminolevulinate) being the most widely applied photosensitizer (prodrug) (523,524). The largest study with temoporfin PDT on BCC comprised 117 patients with a total of 460 lesions treated (for these and all other clinical investigations compare Table 3) (477–479). In 2008 Betz *et al*. published the initial study (478,479), which was later followed by the evaluation of the long-term outcomes in 2012 (477). The mean follow-up period was 42 months with a sustained clearance rate of 93.7% and an overall success rate of 90.7%. The authors compared four different dose groups ranging from 0.06 to 0.15 mg kg^{-1} (highest dose group) to 0.03 mg kg^{-1} (lowest dose). They also specifically looked at the effect on 'high-risk lesions' (recurrent lesions, lesions of >3 mm thickness). Overall long-term outcomes for BCC were best for the high-dose (0.06–0.15 mg kg^{-1}) and the reduced dose (0.05 mg kg^{-1}). The authors name the optimized treatment parameters for this reduced dose as 0.05 mg kg^{-1} temoporfin, 24 h DLI, and a light fluence of ≥ 40 J cm^{-2}. For the high-risk lesions, the authors state that the results are favorable compared to conventional treatment or ALA and MAL PDT. The observed side effects of the treatment were more common in patients of the high drug dose group and comprised mostly of pain and phototoxic reactions (479).

In 2017 Jerjes *et al*. (475) published the retrospective evaluation of the treatment of 148 patients with BCC who were treated with MAL PDT or temoporfin PDT, the MAL PDT group comprising 86 patients with 127 thin BCCs and the temoporfin PDT group with 62 patients with 116 thick BCCs. The attribution to the respective patient (and photosensitizer) group was done on the basis of the thickness of the lesions, as local treatment with MAL due to the low treatment depth is only possible for superficial lesions (~1 mm), whereas thicker lesions required systemic administration of the photosensitizer (temoporfin). Treatment with temoporfin was done with a reduced dose (0.05 mg kg^{-1}) and a DLI of 48h. Of the 62 patients treated with temoporfin 60 had a complete response after one PDT treatment. In the temoporfin, PDT group both superficial and nodular types of BCC responded significantly better than invasive BCCs (475). This is in line with other clinical observations (523). The most common side effect for both patient groups (MAL and temoporfin PDT) was hypopigmentation at the treatment site (5 of 148 patients) (475). In 2019 Jerjes *et al*. (474) published a retrospective study on the use of temoporfin PDT for non-metastatic SCC (T1/T2N0), again using a dose of 0.05 mg kg^{-1}, and a DLI of 48 h. Of the 22 patients treated 20 showed complete response after one round of treatment (3-year follow-up). The two patients experiencing recurrence then underwent surgical resection. The same team investigated temoporfin PDT for the treatment of periorbital skin cancers, 14 patients with BCC and four patients with T1N0 SCC (473). Of the BCC group, 12 out of 14 patients showed a complete response after one PDT treatment, the two remaining patients underwent a second PDT treatment which led to a complete response. Complete response was also observed for the four treated patients with SCC. For the treatment of SCC, a higher dose (0.1 mg kg^{-1}) and a longer DLI, 96 h, was employed (473). In an earlier case report, the authors showed that this treatment of SCC can be combined with optical coherence tomography to better assess tumor extent and tumor margins (480).

Motta *et al*. (481) reported on the treatment of different non-melanoma skin cancers in 9 patients with recurrent multiple lesions. In total, 152 lesions were treated achieving complete response for 117 and partial response in 35 cases. In a review combined with case reports Horlings *et al*. (476) summarized the results of temoporfin PDT for non-melanoma skin cancers until 2015. Their clinical experience supports the high response rates found in earlier studies, however, they observed slow healing when applying the PDT to the lower leg area, the facial and head and neck area had fewer problems in this respect and showed good cosmesis, which corresponds to the recent results by Hamdoon *et al*. (473).

Gastrointestinal cancer

Temoporfin has been tested for the treatment of anal cancer (460–462). Anal cancer has a low incidence, with one of the main risk factors being a persistent high-risk human papillomavirus infection (462,525). Originally, the anal intraepithelial neoplasia, grade III, was treated topically with temoporfin in a thermosetting gel formulation. However, this proved to be ineffective, presumably due to the low penetration depth of temoporfin from this formulation into the neoplasia, exemplarily underlining the importance of pharmaceutical formulation development (462). In a second study, the anal neoplasia was treated after intravenous administration of temoporfin (460). For this, a specific light applicator was developed (461). Treatment was performed with different doses of temoporfin (0.075–0.15 mg mL^{-1}) with 48 h DLI and with red and green light illumination. With intravenously injected temoporfin the treatment was partially effective; 4 of 25 patients showed persistent complete response, all of these receiving green light illumination (460). Red light illumination was found to cause more severe side effects (intense pain, bleeding) than green light illumination (460).

Cholangiocarcinoma is a rare form of cancer – <2% of all cancers – of the bile duct with a poor prognosis; hence, there is a high need for additional treatment options (526–531). In 2013, Kniebühler *et al*. (463) published an exploratory study on the treatment of nonresectable cholangiocarcinoma with stenting and PDT. The 13 patients were treated with different doses of temoporfin (0.032–0.063 mg per kg body weight, a lower dose compared to the dose used for head and neck cancer), different DLIs, starting with 20 h later extended to 67–72 h, and different light doses. With these low doses, side effects such as skin phototoxicity and perforations were not observed. The median survival time was 13 months. The temoporfin fluorescence from the tumor tissue could clearly be observed; however, a distinct fluorescence contrast between the tumor and adjacent healthy tissue was not observed (463,464).

In non-resectable bile duct cancer, PDT is an established option for palliative treatment improving cholestasis and survival

thereby improving quality of life and median survival time (532,533). Most often porfimer sodium is used as a photosensitizer (533). However, the lower light absorption at longer wavelengths limits the tumoricidal effect of porfimer sodium compared to chlorin or bacteriochlorin photosensitizers (42,534). In 2013 Wagner *et al*. (468) published the results of the first stage of a phase II clinical trial on temoporfin PDT for the treatment of hilar bile duct cancer in a small group of patients. Looking at the local response and tumoricidal penetration depth, they observed complete local response in 1 out of 10 patients and partial response in 8 patients. In four patients a tumoricidal effect was observed up to a depth of ≥ 7.5 mm which is approximately a doubled tumor-ablative depth compared to porfimer sodium. The overall median survival time was 18 months. The results of the second stage of this trial were published in 2015 this time analyzing the data from 29 patients (466,467). In the patients with occlusion of biliary segments at the start of the study (29), 16 local response was observed, 11 patients stable disease was noted and one case of progressive disease. The overall results of the study were compared to a historical cohort of patients treated with porfimer sodium (466,467). The effect of PDT on biliary cancer has also been studied by the authors at the cellular level. They detected pronounced differences between cell lines and identified possible markers for the prediction of PDT efficiency (203,204). In this comparison the authors note a prolonged time to local tumor progression, the need for fewer PDT treatments and a higher 6-months survival rate. The observed trend for longer overall median survival; however, was not significant compared to treatment with porfimer sodium (466). In 2016, Hauge *et al*. (465) published a report on a randomized trial in patients with nonresectable biliary tract carcinoma about the combination of chemotherapy and stenting with and without temoporfin PDT treatment, with ten patients in each group. The study was primarily concerned with the question of feasibility and safety of this combination. Looking at these endpoints no serious, procedure-related complications due to PDT or the treatment combination were observed. The number of cholangitis was equal in the two treatment groups; however, the progression-free survival was longer in the PDT group.

Head and neck

As mentioned above, temoporfin is authorized in the EU for the palliative treatment of head and neck cancer therefore most of the clinical investigations with temoporfin PDT have been done in this area. A number of reviews have appeared giving of overview on the use of PDT in this indication (535–539). Though the majority of clinical applications of temoporfin PDT in the head and neck area are focused on cancer, it has also been successfully employed for other malformations in this region of the body (Table 3) (497,500,503,504,507,508,515,517,519–521). The predominant number of clinical investigations were performed with a dose of 0.15 mg temoporfin per kg of body weight, a DLI of 96 h, and illumination at 652 nm with 20 J per cm^2; however, there are reports where a different dosage and other DLIs as well as other light dosages have been used (483,498,504,509,510). Head and neck cancer comprises cancers usually starting from the squamous cells that line the mucosal surfaces of the head and neck region, like the oral cavity, the pharynx, the larynx and the nasal cavity. These cancers are referred to as squamous cell carcinomas (SCCs). Head and neck cancers can also originate from the paranasal sinuses as well as the salivary glands. For all of these, temoporfin PDT has been applied (cf. Table 3).

The anatomy of the head and neck area poses specific challenges for light delivery, so for some of these applications, *e.g.* in the nasopharyngeal area specific light applicators needed to be developed (486,499,508). This specific issue with light administration in the nasopharyngeal area was recently investigated in more detail with eleven patients where the fluence and fluence rates at the target location – paranasal sinuses - were detected using *in vivo* light dosimetry during PDT. As the result, major temporal and spatial variations in fluence rate and light exposure time were found (485). The highest measured fluence rate was 328 mW cm^{-2}, in other cases it was below 20 mW cm^{-2}, illustrating how difficult light dosage in certain anatomic areas can be.

Several temoporfin PDT studies with larger patient cohorts have been published, e.g. studies by de Visscher *et al*. (494) on temoporfin PDT for oral SCCs (214 patients), by Karakullukcu *et al*. (496) on early oral cavity carcinoma (98 patients), and on oral and oropharyngeal carcinoma (170 patients) (512), by van Doeveren *et al*. (540) on head and neck cancer (54 patients), and by Jerjes *et al*. on head and neck cancer including vascular anomalies (110 patients) (507), on oral dysplasia (147 patients) (510), and on tumors and malformations in the oropharyngeal region but also including face and limbs (68 patients) (519). Clinical endpoints were mainly local response, progression-free and overall survival (cf. Table 3).

De Visscher *et al*. (494) and Karakullukcu *et al*. (496) compared PDT treatment to surgery for oral SCC and early oral cavity carcinoma. They found similar results for disease control and overall survival, though in the study with oral SCC PDT seemed less effective for larger T2 tumors (tumor size ~2–5 cm) whereas for smaller T1 tumors (tumor size <2 cm) a similar effectivity was found (494). Visible light of 652 nm has only limited penetration depth into the tissue, which in turn limits the PDT effect specifically for larger and thicker tumors. One way to overcome this problem is the use of an interstitial treatment, whereby multiple fibers are introduced into the tumor tissue allowing to treat of the complete tumor mass and improving local tumor control (541). This treatment variant has been applied for many cases in the head and neck area using temoporfin PDT (469,483,489–493,497,501,502,504–507,511,513,514,517,519–521). To achieve complete illumination of the tumor a correct positioning of the fibers is important; this treatment is usually supported using imaging methods like MR, CT or mostly ultrasound (469,491,492,497,500,504–507,511,517,520,521). In addition, fluorescence-based methods like fluorescence differential path length spectroscopy have been used (514,542). Prior to its application in patients, this method was previously developed in animal studies (305,306,543).

Very recently, a study in 38 patients was published analyzing the effect of PDT with temoporfin in the head and neck area on the quality of life of patients (482). In this study, all patients reported an improved quality of life after PDT. The main problem reported by the patients was pain after the PDT treatment. In the 4 weeks after treatment improvement was reported for visual symptoms, breathing, speaking and swallowing and for the following weeks an improvement in daily life activities, social life, mood and anxiety were reported (482).

PDT is primarily a local treatment - though exerting systemic immunological effects which find increasing interest

(253,276,277) – PDT with temoporfin in the head and neck area is usually combined with chemotherapy. Based on the marketing authorization it is specifically used for recurrent tumors which are resistant to other treatments like chemo- or radiotherapy or cannot be treated by surgery (425,486). One application is the adjuvant therapy after chemotherapy or salvage surgery, allowing to treatment of remaining microscopic diseases after tumor resection (484,487,488,540). In this respect, Jerjes *et al*. published a case report, where cutaneous SCCs in the face were treated by PCI with fimaporfin/bleomycin followed by interstitial PDT with temoporfin for deeper tumor areas (484). With PDT, often effective local control of tumor growth can be achieved (483,486,487,489,495,498,499,509,510,512) with extended periods of progression-free disease (487,499,502,508,509). Effective local tumor control was found to correlate positively with survival times (516,518).

Side effects

Concomitant with their desired pharmacological effect all medicinal products can elicit side effects. These side effects differ from substance class to substance class but of course also from drug to drug (544). The side effects of temoporfin and the medicinal product derived therefrom, Foscan®, are reflected in the patient information and the official EMA documents (319). As for many other drug products, the side effects of temoporfin and Foscan® are associated with their intended photodynamic action mechanism. Therefore, the most common side effects apart from pain are phototoxic reactions, e.g. skin photosensitivity, skin burns or phototoxic reactions at the injection site (see also Table 3) (466,467,495,506,520,540). Most of these may be avoided or limited by strictly adhering to the light-protection given in the patient information.

Severe side effects like cholangitis have been observed in biliary tract cancer treatment though those are also observed in the standard chemotherapeutic treatment for this disease (465–467). When the tumor to be treated is near a large blood vessel this poses a risk for PDT treatment. In a publication by Hamdoon *et al*. (513) endoluminal carotid stenting has been reported as a precautionary measure. In PDT treatments in the head and neck area swelling after PDT can lead to complications therefore airway management is important specifically for tongue-based tumors (490,493). An important issue is also the unintended interaction with other drugs. For temoporfin, an interaction with other drugs with photosensitizing potential is a cause for concern (319,545). In a single case in the literature, the authors report on bisphosphonate-related osteonecrosis of the jaw which occurred associated with PDT for the treatment of oral proliferative verrucous leukoplakia (503). An interaction of a drug molecule with others may also be beneficial. In an interesting publication in this respect, Lange and Bednarski investigated the synergistic effects of three platinum-based chemotherapeutics, carboplatin, cisplatin and oxaliplatin in combination with PDT with temoporfin in five cancer cell lines. Depending on the type of cancer cell line pretreatment with PDT sensitized the cells for the treatment with the platinum complexes (131). A similar effect was shown in Hep-2 cells (106).

Veterinary applications

In contrast to clinical use for humans, PDT is much less developed in the veterinary field and progress has been slow. It is mainly used to treat early skin tumors in cats and some studies have reported treating urinary tract neoplasia in dogs and equine sarcoids (546). With regard to temoporfin, a study by Flickinger *et al*. (310) investigated the long-term outcome of using Foslip for systemic treatment of feline squamous cell carcinomas. The study (0.15 mg drug kg^{-1} body weight i.v., 6 h postinjection, illumination with 652 nm diode laser, 0.5 W cm^{-2}) showed a very good response rate of 84% and a mean progression-free interval of 35 months. However, the results were unsatisfactory for invasive tumors and larger lesions.

Using Fospeg®, a case study reported the successful surgical and photodynamic treatment of an equine sarcoid (311). Treatment conditions were similar to those used for cats. The main tumor mass and some lateral tumors showed complete remission while remaining tumors decreased in size or stopped growing.

DOSIMETRY AND DETECTION

PDT faces the issue of dose not only a drug (like in chemotherapy) or radiation (as in radiotherapy) but both. Hence, drug and light dosage, and especially light dosimetry are a constant challenge in PDT (446,547–551). For drug dosage of temoporfin in clinical practice there is a quite clear picture in the literature: In most cases a dosage of 0.15 mg per kg body weight and a DLI of 96 h has been used, corresponding to the marketing authorization (cf. Table 3) (425). In exploratory clinical investigations for anal intraepithelial neoplasia, cholangiocarcinoma and non-melanoma skin cancers lower dosages (down to 0.03 mg kg^{-1}) have been used (cf. Table 3). Treatment dosage variations, *e.g.* compartmental targeting using a fractionated double-injection protocol have been investigated in animals (296).

Dosing of light is a challenge in PDT which is reflected in the general PDT review literature (449,548,550,551) but becomes also apparent from Table 3 listing temoporfin clinical trials which shows a broader variation compared to the drug dosage, though in many cases a fluence of 20 J cm^{-2} has been used. In some cases, lower (461,471) but also much higher fluences have been employed (460,477,478,481). The use of temoporfin with low light doses has been discussed as an option for PDT (136,552). Light dosage in PDT is influenced by the optical properties of the tissue to be treated (549); anatomical factors can influence the light dose that can be administered as well, and sometimes specific light applicators are required (461,485,486,499,508). As mentioned above, in interstitial PDT imaging methods, mostly ultrasound, are employed to assure correct positioning of the light-guiding fibers (469,491,492,497,500,504–507,511,517,519–521). Nevertheless, in some cases pronounced differences in fluence and fluence rate were detected (485).

A laser is the common light source for PDT generally (548), for temoporfin PDT in the clinical environment (cf. Table 3) and in most pre-clinical investigations in animal species. However, with the development of high-power LEDs, irradiation with LEDs has become an alternative that is investigated and has been used with temoporfin (105,206,282). Etcheverry *et al*. (105) performed a comparative *in vitro* investigation on the use of a 637 nm LED and a 654 nm laser light source in PDT with temoporfin on HeLa cells and found the photodynamic efficiency to be similar. Apart from this, other light sources are investigated as well for PDT, *e.g.* implantable ones (446,553).

Due to temoporfin's intense fluorescence, fluorescence methods, e.g. the aforementioned fluorescence differential path length spectroscopy, can be employed to measure its concentration *in vivo* aiding the optimization of PDT treatment parameters (171,293,305,306,463,464,480,514,542,543). Optical methods like optical coherence tomography can also be used to more precisely determine tumor extension margins, e.g. in skin cancer (480). Recently, the combination of Raman spectroscopy and PDT (with ALA, protoporphyrin IX and temoporfin) has been proposed for theranostics (115). Efforts to optimize treatment parameters for PDT with temoporfin are also supported by preclinical testing in animals and modelling approaches (288,293,302–304,307–309,471,472,554,555), e.g. for prostate cancer (308,471,472), liver cancer (300,307,555), esophagus (309), transplanted mammary carcinoma (302,303), and gliosarcoma (288). Axelsson *et al*. (472) described an experimental approach to reconstruct the spatial distribution of temoporfin inside the human prostate. In some of these animal investigations with temoporfin detection *via* fluorescence, the window-chamber tumor model has successfully been used (288,302–304). The detection of temoporfin by fluorescence spectroscopy methods as well as absorption spectroscopy has also proven to be a valuable or perhaps even the standard tool in pharmaceutical formulation development, allowing to follow the active substance molecule when the pharmaceutical formulation interacts with body fluids and is distributed to body compartments (129,171,221,293,365,367,392). Moreover, changes in fluorescence behavior of temoporfin and changes in its absorption spectrum can be used to characterize the immediate surroundings of the photosensitizer (366,368,393,554). Analysis of temoporfin fluorescence in PDT investigations is closely associated with the photobleaching of the photosensitizer, where the photosensitizer is destroyed by photochemical reactions under illumination (42,556–558). Photobleaching of temoporfin has been investigated in detail by Bonnett *et al*. (559,560) and has been reviewed before (42). In a series of publications, Atif reported on photobleaching studies in keratinocytes treated with PDT with temoporfin (554,557,558,561). These investigations found that photobleaching of temoporfin is increasing with the higher local concentrations of the photosensitizer (558).

In general, PDT relies on the local availability of oxygen to achieve its desired effect on the tumor cells (6,245). Thus, the question of the supply of oxygen at the tissue and cellular level is critical for PDT and hence intensely discussed in the PDT literature (6,245,440,442,449). Tumorous tissue is often hypoxic, *i.a*. due to fast tissue growth and insufficiently developed vasculature (6,245,440,442). This is an important medical issue as hypoxic zones in tumors can be more resistant to chemo- and radiotherapy (562). In addition, photosensitization by itself reduces cellular oxygen levels quickly, especially at higher light fluences, not only by oxygen consumption through the PDT process but also by occluding tumor vasculature (6,245,440,442,449). This self-limiting effect of PDT can partly be overcome by optimizing light dose and light fluence, *e.g.* by fractionated light administration or by using hyperbaric oxygen conditions or oxygen carriers (6,438,442,449,563).

Therefore, the detection, measurement and modelling of singlet oxygen luminescence is an important approach to PDT dosimetry (6,564–568). Singlet oxygen monitoring for dose–response studies in PDT is challenging because, as mentioned above, there is oxygen depletion during treatment; additionally, the oxygen concentrations in the tumor differ between different areas, e.g. cellular tissue and vasculature (569,570). However, considerable progress has been made with respect to singlet oxygen measurements (222,568,571), direct and time-resolved measurements of singlet oxygen in living cells and tumor models like the CAM model have been performed (179,222,571). Using the CAM model and a liposomal temoporfin formulation it was possible to deduce the oxygen content during PDT from the singlet oxygen kinetics (222,571). The importance of singlet oxygen kinetics and time-resolved luminescence measurements has already been pointed out by Jarvi *et al*. (107,108) these are critical in using singlet oxygen signal as a dose metric when employing temoporfin as photosensitizer. Wilson *et al*. (288) investigated singlet oxygen luminescence in comparison with bioluminescence from luciferase- and green fluorescent protein-transduced gliosarcoma grown in a dorsal window chamber in mice, finding that tumor response (measured via the bioluminescence signal) correlated well with singlet oxygen luminescence, underlining that singlet oxygen can serve as a dose metric. Zhu *et al*. (285,286,312) looked at determining singlet oxygen threshold doses for PDT for different photosensitizers including temoporfin, also including a comparison to literature data. Not unexpectedly, they found large differences, observing that the experimental *in vivo* singlet oxygen threshold doses for the photosensitizers investigated (porfimer sodium, verteporfin, and temoporfin) were about 20 times lower than those found *in vitro* – underlining, that additional factors to singlet oxygen mediated cell death contribute to the PDT effect observed *in vivo* (286). These PDT threshold investigations should illuminate clinical experiences, where a too low light threshold dose can result in incomplete tumor response (308,471).

The *in vitro* separation and detection of temoporfin, e.g. in biological samples relies on chromatographic methods, with detection *via* absorption or fluorescence (572). These classical chromatographic methods are now amended by newer separation methods, specifically, if particles are involved, like the asymmetrical flow field-flow fractionation which has become a routine technique in nanoparticle separation and characterization. This technique has successfully been applied in the characterization of temoporfin-loaded liposomes and in the investigation of the drug transfer from such liposomes (394,397,398).

With respect to the photophysical properties of temoporfin, it should be noted that also the two-photon cross-section of temoporfin has been investigated experimentally and theoretically (260–262) in the context of two-photon PDT (573). The values found were lower than those for specifically designed two-photon sensitizers (61,573) but higher than expected from theoretical calculations (256).

OTHER APPLICATIONS

Combination of PDT with other therapies

The interest in the combination of PDT with other therapies and treatment modalities mainly comes from two directions: finding synergistic effects of combined treatments could increase effectiveness (446) and, as PDT in nearly all of its medical applications is not a first-line treatment – except, perhaps, for certain forms of skin cancer like actinic keratosis – in investigating compatible pathways for patients already under treatment. In addition, PDT is principally a local treatment thus requiring systemic tumor treatment to prevent metastasis. Tumor therapy with PDT

is therefore in clinical practice mostly combined with other tumor treatments such as chemo- or radiotherapy (574). This is also the case of temoporfin which is authorized for the palliative treatment of head and neck cancer meaning that patients are concomitantly treated with, *e.g.* chemotherapy. Therefore, knowledge about interactions and possible synergism of such combinations is of high medical importance.

Combination with chemotherapeutics

This dual motivation is apparent in the investigations on the interaction of temoporfin PDT with chemotherapeutics. A synergistic effect of temoporfin PDT followed by cisplatin was reported for Hep-2 cells, the combination resulting in increased apoptosis, necrosis, and mitochondrial destruction and reduced autophagy (106). Lange and Bednarski (131) investigated the effect of a combination of temoporfin PDT with carboplatin, cisplatin, or oxaliplatin in five cancer cell lines (A-427, BHY, KYSE-70, RT-4, and SISO cells). The authors identified some synergistic combinations, e.g. for oxaliplatin in three of the cell lines (BHY, RT-4, and SISO cells), however, in some cases even an antagonistic effect was found. In cases of synergy elevated ROS levels were found but these did not necessarily lead to increased apoptosis (131). The same authors analyzed the synergism of a combination of temoporfin PDT with two glutathione peroxidase inhibitors in the five above-mentioned cell-lines (130). Again, a synergistic effect was found for both peroxidase inhibitors but not in all cell lines (130). Also, the combination of PDT with the chemotherapeutics taxotere and doxorubicin has been investigated *in vitro* in A-431 cells (153). Cells were exposed to the taxotere followed by temoporfin PDT or cells were incubated with temoporfin followed by the PDT-treatment and exposure to doxorubicin. The combination treatment was found to increase cytotoxicity at the same time differences in the expression of VEGF and IL-1alpha were detected (153). Doxorubicin has also been combined in a liposomal formulation with temoporfin PDT and magnetic nanoparticles and tested on HeLa cells, the combined treatment being more effective than the separate treatments (104). In another approach temoporfin was combined with doxorubicin, magnetic nanoparticles and second photosensitizer ($TPCS_{2a}$) in extracellular vesicles as the carrier system (180,216). Combinatorial approaches have also been described for temoporfin with the DNA topoisomerase inhibitor β-lapachone (183), Navelbine® (297), and fenretinide (96).

An important issue in cancer therapy is the resistance of certain cancer cell types to common chemotherapeutics (575,576). In this context temoporfin PDT has been tested on 5-fluorouracil-resistant HCT116 (208) and HT29 (209) cancer cells. In both investigations, PDT proved to be effective against these cancer cell lines (208,209).

Antibodies

The efficacy of the combination of the anti-VEGF monoclonal neutralizing antibody bevacizumab and PDT with temoporfin has been evaluated in a mouse colon cancer model (HT29 tumors) (281). PDT followed by administration of the antibody increased the anti-tumor effect. Administration of bevacizumab prior to temoporfin, however, led to a decreased accumulation of temoporfin in tumor tissue at 24 h after photosensitizer administration (281). In another approach involving antibodies, micellar nanoparticles containing temoporfin labelled with llama single-domain antibody fragments for targeting have been prepared (156). In this case, temoporfin served also as a fluorescence label for the carrier systems. On the other hand, bispecific antibody-redirected T lymphocytes have been used as carrier vehicles for *m*THPP (577).

Other photosensitizers

In a few cases, temoporfin has also been combined with other photosensitizers and photoactive compounds, so for example with $TPCS_{2a}$, used for photochemical internalization (216), a nitric oxide photodonor (424), and hypericin (97,98). The latter combination showed a reduced dark toxicity in head and neck squamous carcinoma cells (UMB-SCC 745 and 969) and a combination of apoptotic and necrotic cell death (97,98). See also Table 1.

Quantum and polymer dots

Temoporfin has been incorporated into quantum dots and polymer dots to exploit the resonant energy transfer for and an increased and optimized PDT effect (112,120,121,363,375,578). The respective examples are discussed above under 'Formulation development'.

Hperthermia

Hyperthermia combined with temoporfin PDT was investigated with liposomes and extracellular vesicles carrying the photosensitizer as well as magnetic iron oxide nanoparticles *in vitro* and *in vivo* in mice (see above under 'Formulation development') (164,172,216).

Photothermal treatment

Photothermal treatment was used in a combination of temoporfin and multi-walled carbon nanotube PDT (173). The two treatments were found to induce apoptosis by different cell signaling pathways.

Photoprotection

PDT is associated with side effects like skin photosensitization. In this respect the photoprotective properties of plant extracts have been investigated (176,291,579). In investigations with a plant extract from *P. halepensis* the authors reported that the extract prevented photosensitivity after temoporfin PDT in mice (291) and even increased intracellular ROS levels (176).

PDT-immunotherapy combinations

The immune response to the PDT treatment contributes to the PDT effect *in vivo* as mentioned above. Hence, there are a number of publications investigating these effects for PDT with temoporfin and utilizing this for PDT-immunotherapy combinations. Korbelik *et al.* thoroughly evaluated the role of ceramides and sphingosines in PDT immune response in several *in vitro*

(95,96,169,195,274) and *in vivo* investigations, also aiming at anti-cancer vaccines generated by PDT (273,275,284). They, as others, emphasize the role of neutrophils in the immediate reaction to PDT (201,224,284). It has been reported for the nasopharyngeal KJ-1 cell line that treatment with temoporfin and light is able to inhibit migration and invasion in this cancer cell line (88). In a mouse model, a synergistic antitumor effect could be demonstrated for a combination of PDT with temoporfin, chemotherapy and immune lymphocytes (297). Extracellular vesicles from the mesenchymal stem and stromal cells, respectively, loaded with temoporfin showed increased necrosis and a decrease in intratumoral proliferation in a mouse model of peritoneal metastasis (201). Recently, PDT with temoporfin in a formulation, containing RGD-modified nanoparticles has been combined with a PD-L1 checkpoint inhibitor (PD-L1 blockade antibody) in a mouse model (CT26 tumors) (133). This combination was found to inhibit distant tumor growth and also stimulate immune memory response. In addition, even without the antibody treatment, the RGD-modified nanoparticles were able to inhibit cell proliferation and stimulate an immune response. This is attributed to promotion of dendritic cell maturation (133).

Antimicrobial PDT

Following the general trend in PDT in recent years, which has seen a renewed focus on antimicrobial applications, temoporfin and its formulations are featured in related studies. Target bacterial species were primarily those related to wound healing and dental hygiene. In the former, a study using Foslip® showed that low doses of photosensitizer embedded in collagen matrixes after implantation and illumination did significantly advance wound healing in mice (294). *Staphylococcus* infections are often a complicating factor in wound and skin diseases. Here, both PVP-hypericin and Fospeg® resulted in a 4-5 log reduction in bacterial count (100 nM PS, 5 min incubation, 30 min illumination 75 mW cm^{-2}) (234). This effect could be significantly enhanced by using antimicrobial peptide (AMP) modified liposomal formulations. The use of the AMP WLBU2 for conjugation to temoporfin liposomes resulted in the complete eradication of methicillin-resistant *Staphylococcus aureus* (MRSA). Together with a 3.3 log reduction of *Pseudomonas aeruginosa* this indicates the utility of bacteria-targeted PS delivery to combat both Gram-positive and -negative bacteria (231,233). Likewise, wheat germ agglutinin (WGA) modified liposomes containing temoporfin proved effective with similar results in a related study (232).

Clostridium difficile, the main cause of antibiotic-associated diarrhea, was the target of a comparative investigation using 13 standard photosensitizers (228). In contrast to PSs such as talaporfin or chlorin e_6, which achieved up to 3 log reductions, temoporfin proved to be inactive, most likely due to the formation of turbid suspensions in the medium used.

In dentistry, cariogenic bacteria such as *Streptococcus mutans* and *Streptococcus sobrinus* are potential targets for aPDT. Studies with hypericin and Fospeg® showed that both species could be completely eradicated using short PDT protocols with either PS or a combination of both (235). Another target, esp. in endodontic infections, is *Enterococcus faecalis*. The use of Foslipos (50 mM *m*THPC, illumination with 100 J cm^{-2}) completely eradicated the bacterium, while 10 mM *m*THPC still gave a CFU reduction by 5.8 log units (229). A comparative study of temoporfin incorporated into liposomes and invasomes using freshly extracted human wisdom teeth and inoculated with *E. faecalis* showed a 3.6 log unit reduction directly at the root canal wall with the latter. This was a significant improvement compared to a standard treatment with 1% chlorohexidine gel (reduction by 1.2 log units) (422). Ultrasonic activation can be used to improve the aPDT as it facilitates deeper diffusion into dentinal tubules and biofilms (580).

Eradication of bacteria alone is not enough. In periodontitis treatment often grafting materials are required to support the regeneration of injured periodontium. In an innovative approach, Kranz *et al*. (230) developed antimicrobial photodynamic active biomaterials for periodontal regeneration. For this, curable biomaterials (either urethane dimethacrylate or oligoester urethane methacrylate which contained a mixture of tricalcium phosphate microparticles and temoporfin were prepared). Both materials exhibited suitable mechanical and biocompatible properties and were capable of completely suppressing *P. gingivalis* and significantly reduce *E. faecalis* after illumination.

Antiviral PDT

The Coronavirus pandemic has elicited an increased awareness of the potential of PDT to combat viruses (15,581). In a natural product screening study pheophorbide a (a chlorophyll derivative) showed a light-dependent antiviral activity on SARS-CoV-2 and inhibited virus-cell fusion. A similar mechanism was shown for temoporfin; however, it exhibited only moderate antiviral activity (582). Note, temoporfin has also been suggested in a pre-print as a potential blocker of SARS-CoV-2 E channel based on a docking study (583). A computational study by Absalan *et al*. identified temoporfin as the best candidate for docking with the COVID-19 major protease (6LU7) (584).

A promising development is the identification of temoporfin as a potential drug to inhibit the replication of the Zika virus (585). Initially endemic to Africa Zika infections have now spread and are a global health concern. A broad screening of >2800 existing drugs by Li *et al*. (586) in 2017 identified three lead compounds as flavivirus NS2B-NS3 interaction inhibitors with nanomolar potencies. Among them, the most promising is temoporfin as a cytotoxic compound. Zika virus infection was inhibited in human placental and neural progenitor cells and the virus-induced viremia and mortality could be prevented in mouse models. Docking studies indicate that the chlorin binds to NS3 pockets resulting in non-competitive inhibition of flaviviral polyprotein processing.

Other infectious disease pathogens

A study by Preuß *et al*. (587) investigated the use of temoporfin, a cationic and anionic photosensitizer for Mosquito larvae control. Using *Chaoborus* sp. as a model they showed that all three PSs accumulated in the intestinal tract of larvae, not the tissue. Only the cationic PS (5,10,15,20-tetrakis(1-methylpyridinium-4-yl)porphyrin toluene sulfonate) which is known to be active against Gram-positive bacteria resulted in the photodynamic killing of the larvae, possibly by inactivation of the intestinal flora.

Non-medical applications

Although developed as a drug candidate temoporfin-related compounds are occasionally used for other purposes. One such example relies on the capability of (free base) porphyrins to act as sensors (588) or in CBRN defense and remediation (589). Rout and coworkers showed that changes in the Q-band absorption pattern of temoporfin upon binding of metal ions allow temoporfin to be used as a 'miniaturized unimolecular analytic system' to detect metal ions. Furthermore, considering the resultant absorption intensities at different wavelengths as output signals allowed us to use of temoporfin a logic 4-to-2 encoders and 2-to-3 decoders in logical computing (590,591).

Temoporfin has also been used to modify protonated graphitic carbon nitride (pCN) (592). Compared with unmodified pCN the new material showed stronger absorption in the visible and near-IR regions and higher photocatalytic activity in hydrogen evolution.

CONCLUSIONS

This overview of the literature underlines the continuous scientific and medical interest in the photosensitizer temoporfin. Temoporfin – being on the market since 2001 – is one of the few clinically established photosensitizers. The advances and continuing research outlined herein illustrate the increasing interest in PDT in general, visible from the continuously high number of publications in the field of PDT. Clearly, the field is not standing still. Currently, several clinical studies with different photosensitizers including temoporfin are under way (426,437).

With respect to clinical development, there are diverse fields of application, from human to emerging uses in animal PDT. Clearly, the main clinical application remains in head and neck cancer and malformations, but PDT with temoporfin is now also used in other fields such as skin cancer and gastrointestinal applications like cholangiocarcinoma. Apart from this, temoporfin and its formulations have also found interest for use in antibacterial and antiviral photodynamic treatments. Together with approved photosensitizers such as verteporfin, ALA, or porfimer sodium, temoporfin is one of the gold standards in contemporary PDT. Temoporfin is also – due to the extensive scientific knowledge about this photosensitizer and the fact that it is a well-characterized single small molecule – often used as a comparator to test the PDT efficacy of other new photosensitizers and their formulations.

In the last decade, most medical developments for temoporfin have been in the development of advanced pharmaceutical formulations with a focus and extensive work on liposomal formulations. Here, temoporfin is often used as a model photosensitizer to be incorporated in new formulations as a test case. Increasingly, the available body of information facilitates its use as a general model compound for highly lipophilic drugs benefitting from its easy detectability *via* absorption or fluorescence spectroscopy.

Acknowledgements—This work was prepared with the support of the Technical University of Munich – Institute for Advanced Study through a Hans Fischer Senior Fellowship (MOS). The authors appreciate helpful comments on the manuscript by Dr. C. J. Kingsbury. Open Access funding enabled and organized by Projekt DEAL.

CONFLICT OF INTEREST

A. Wiehe is an employee of the biolitec research GmbH which belongs to the biolitec group. The biolitec Pharma Ltd., which is also part of the biolitec group, is the marketing authorization holder for the medicinal product Foscan® which contains the photosensitizer temoporfin as the active substance.

REFERENCES

1. Raab, O. (1900) Über die Wirkung fluoreszierender Stoffe auf Infusorien. *Z. Biol.* **39**, 524–546.
2. von Tappeiner, H. and A. Jodlbauer (1904) Über die Wirkung der photodynamischen (fluorescierenden) Stoffe auf Protozoen und Enzyme. *Dtsch. Arch. Klin. Med.* **39**, 427–487.
3. Moan, J. and Q. Peng (2003) An outline of the hundred-year history of PDT. *Anticancer Res.* **23**, 3591–3600.
4. Krasnovsky, A. A., Jr. (2007) Photodynamic Therapy at the Cellular Level. In *Singlet oxygen and primary mechanisms of photodynamic therapy and photodynamic diseases* (Edited by A. B. Uzdensky). Research Signpost, Kerala, India.
5. Dougherty, T. J., C. J. Gomer, B. W. Henderson, G. Jori, D. Kessel, M. Korbelik, J. Moan and Q. Peng (1998) Photodynamic therapy. *J. Natl. Cancer Inst.* **90**, 889–905.
6. Callaghan, S. and M. O. Senge (2018) The good, the bad, and the ugly – controlling singlet oxygen through design of photosensitizers and delivery systems for photodynamic therapy. *Photochem. Photobiol. Sci.* **17**, 1490–1514.
7. Castano, A. P., T. N. Demidova and M. R. Hamblin (2005) Mechanisms in photodynamic therapy: Part three- Photosensitizer pharmacokinetics, biodistribution, tumor localization and modes of tumor destruction. *Photodiagn. Photodyn. Ther.* **2**, 91–106.
8. Donohoe, C., M. O. Senge, L. G. Arnaut and L. C. Gomes-da-Silva (2019) Cell death in photodynamic therapy: From oxidative stress to anti-tumor immunity. *Biochim. Biophys. Acta Rev. Cancer* **1872**, 188308.
9. Castano, A. P., P. Mroz and M. R. Hamblin (2006) Photodynamic therapy and anti-tumour immunity. *Nat. Rev. Cancer* **6**, 535–545.
10. Agostinis, P., K. Berg, K. A. Cengel, T. H. Foster, A. W. Girotti, S. O. Gollnick, S. M. Hahn, M. R. Hamblin, A. Juzeniene, D. Kessel, M. Korbelik, J. Moan, P. Mroz, D. Nowis, J. Piette, B. C. Wilson and J. Golab (2011) Photodynamic therapy of cancer: an update. *CA Cancer J. Clin.* **61**, 250–281.
11. Nesi-Reis, V., D. S. S. L. Lera-Nonose, J. Oyama, M. P. P. Silva-Lalucci, I. G. Demarchi, S. M. A. Aristides, J. J. V. Teixeira, T. G. V. Silveira and M. V. C. Lonardoni (2018) Contribution of photodynamic therapy in wound healing: A systematic review. *Photodiagn. Photodyn. Ther.* **21**, 294–305.
12. Babilas, P., S. Schreml, M. Landthaler and R. M. Szeimies (2010) Photodynamic therapy in dermatology: state-of-the-art. *Photodermatol. Photoimmunol. Photomed.* **26**, 118–132.
13. Monfrecola, G., M. Megna, C. Rovati, M. Arisi, M. Rossi, I. Calzavara-Pinton, G. Fabbrocini and P. Calzavara-Pinton (2021) A critical reappraisal of off-label use of photodynamic therapy for the treatment of non-neoplastic skin conditions. *Dermatology* **237**, 262–276.
14. Maisch, T. (2009) A new strategy to destroy antibiotic resistant microorganisms: Antimicrobial photodynamic treatment. *Mini-Rev. Med. Chem.* **9**, 974–983.
15. Wiehe, A., J. M. O'Brien and M. O. Senge (2019) Trends and targets in antiviral phototherapy. *Photochem. Photobiol. Sci.* **18**, 2565–2612.
16. Feng, Y. F., C. C. Tonon, S. Ashraf and T. Hasan (2021) Photodynamic and antibiotic therapy in combination against bacterial infections: efficacy, determinants, mechanisms, and future perspectives. *Adv. Drug Deliv. Rev.* **177**, 113941.
17. Pibiri, I., S. Buscemi, A. P. Piccionello and A. Pace (2018) Photochemically produced singlet oxygen: Applications and perspectives. *ChemPhotoChem* **2**, 535–547.
18. Diamond, I., R. Jaenicke, C. B. Wilson, A. F. McDonagh, S. Nielsen and S. G. Granelli (1972) Photodynamic therapy of malignant tumors. *Lancet* **2**, 1175–1177.

19. Firczuk, M., M. Winiarska, A. Szokalska, M. Jodlowska, M. Swiech, K. Bojarczuk, P. Salwa and D. Nowis (2011) Approaches to improve photodynamic therapy of cancer. *Front. Biosci.* **16**, 208–224.
20. Keum, H., D. Yoo and S. Jon (2022) Photomedicine based on heme-derived compounds. *Adv. Drug Deliv. Rev.* **182**, 114134.
21. Ethirajan, M., Y. H. Chen, P. Joshi and R. K. Pandey (2011) The role of porphyrin chemistry in tumor imaging and photodynamic therapy. *Chem. Soc. Rev.* **40**, 340–362.
22. Abrahamse, H. and M. R. Hamblin (2016) New photosensitizers for photodynamic therapy. *Biochem. J.* **473**, 347–364.
23. Pham, T. C., V.-N. Nguyen, Y. Choi, S. Lee and J. Yoon (2009) Recent Strategies to Develop Innovative Photosensitizers for Enhanced Photodynamic Therapy. *Chem. Rev.* **121**, 13454–13619.
24. Paszko, E., C. Ehrhard, M. O. Senge, D. P. Kelleher and J. V. Reynolds (2011) Nanodrug applications in photodynamic therapy. *Photodiagn. Photodyn. Ther.* **8**, 224–231.
25. Chen, J. M., T. J. Fan, Z. J. Xie, Q. Q. Zeng, P. Xue, T. T. Zheng, Y. Chen, X. L. Luo and H. Zhang (2020) Advances in nanomaterials for photodynamic therapy applications: Status and challenges. *Biomaterials* **237**, 119827.
26. Son, S., J. H. Kim, X. W. Wang, C. L. Zhang, S. A. Yoon, J. Shin, A. Sharma, M. H. Lee, L. Cheng, J. S. Wu and K. S. Kim (2020) Multifunctional sonosensitizers in sonodynamic cancer therapy. *Chem. Sov. Rev.* **49**, 3244–3261.
27. Lin, X. H., J. B. Song, X. Y. Chen and H. H. Yang (2020) Ultrasound-activated sensitizers and applications. *Angew. Chem. Int. Ed.* **59**, 14212–14233.
28. Shah, N., J. Squire, M. Guirguis, D. Saha, K. Hoyt, K. K.-H. Wang, V. Agarwal and G. Obaid (2022) Deep-tissue activation of photonanomedicines: An update and clinical perspectives. *Cancer* **14**, 2004.
29. Laxminarayan, R., A. Duse, C. Wattal, A. K. M. Zaidi, J. F. L. Wertheim, N. Sumpradit, E. Vlieghe, G. L. Hara, I. M. Gould, H. Goossens, C. Greko, A. D. So, M. Bigdeli, G. Tomson, W. Woodhouse, E. Ombaka, A. Q. Peralta, F. N. Qamar, F. Mir, S. Kariuki, Z. A. Bhutta, A. Coates, R. Bergstrom, G. D. Wright, E. D. Brown and O. Cars (2013) Antibiotic resistance-the need for global solutions. *Lancet Infect. Dis.* **13**, 1057–1098.
30. Dhama, K., S. Khan, R. Tiwari, S. Sircar, S. Bhat, Y. S. Malik, K. P. Singh, W. Cahicumpa, D. K. Bonilla-Aldana and A. J. Rodriguez-Morales (2020) Coronavirus disease 2019-COVID-19. *Clin. Microbiol. Rev.* **33**, e00028–e00020.
31. Finsen, N. R. (1896) *Om Anvendelse i Medicinen af Koncentrerede Kemiske Lysstraaler*. Gyldendalske Boghandels Forlag, Copenhagen, Denmark.
32. Møller, K. I., B. Kongshoj, P. A. Philipsen, V. O. Thomsen and H. C. Wulf (2005) How Finsen's light cured lupus vulgaris. *Photodermatol. Photoimmunol. Photomed.* **21**, 118–124.
33. Li, X. S., J. F. Lovell, J. Yoon and X. Y. Chen (2020) Clinical development and potential of photothermal and photodynamic therapies for cancer. *Nat. Rev. Clin. Oncol.* **17**, 657–674.
34. Alsaab, H. O., M. S. Alghamdi, A. S. Alotaibi, R. Alzhrani, F. Alwuthaynani, Y. S. Althobaiti, A. H. Almalki, S. Sau and A. K. Iyer (2020) Progress in clinical trials of photodynamic therapy for solid tumors and the role of nanomedicine. *Cancer* **12**, 2793.
35. Peng, Q., T. Warloe, K. Berg, J. Moan, M. Kongshaug, K. E. Giercksky and J. M. Nesland (1997) 5-Aminolevulinic acid-based photodynamic therapy – Clinical research and future challenges. *Cancer* **79**, 2282–2308.
36. Schmidt-Erfurth, U. and T. Hasan (2000) Mechanisms of action of photodynamic therapy with verteporfin for the treatment of age-related macular degeneration. *Surv. Ophthalmol.* **45**, 195–214.
37. Pathak, M. A. and T. B. Fitzpatrick (1992) The evolution of photochemotherapy with psoralens and UVA (PUVA) – 2000 BC to 1992 AD. *J. Photochem. Photobiol. B Biol.* **14**, 3–22.
38. Bonnett, R. (2000) *Chemical Aspects of Photodynamic Therapy*. Gordon & Breach Publ., Amsterdam, The Netherlands.
39. Allison, R. R., V. S. Bagnato and C. H. Sibata (2010) Future of oncologic photodynamic therapy. *Future Oncol.* **6**, 929–940.
40. Bonnett, R., R. D. White, U. J. Winfield and M. C. Berenbaum (1989) Hydroporphyrins of the *meso*-tetra(hydroxyphenyl)porphyrin series as tumor photosensitizers. *Biochem. J.* **261**, 277–280.
41. Ris, H.-B., H. J. Altermatt, R. Inderbitzi, R. Hess, B. Nachbur, J. C. Stewart, Q. Wang, C. K. Lim, R. Bonnett and M. C. Berenbaum (1991) Photodynamic therapy with chlorins of diffuse malignant mesothelioma: Initial clinical results. *Br. J. Cancer* **64**, 1116–1120.
42. Senge, M. O. and J. C. Brandt (2011) Temoporfin (Foscan®, 5,10,15,20-Tetra(*m*-hydroxyphenyl)chlorin)—A second-generation photosensitizer. *Photochem. Photobiol.* **87**, 1240–1296.
43. Senge, M. O. (2012) *m*THPC – A drug on its way from second to third generation photosensitizer? *Photodiagn. Photodyn. Ther.* **9**, 170–179.
44. Berenbaum, M. C., S. L. Akande, R. Bonnett, H. Kaur, S. Ioannou, R. D. White and U. J. Winfield (1986) meso-Tetra (hydroxyphenyl)porphyrins, a new class of potent tumor photosensitizers with favorable selectivity. *Br. J. Cancer* **54**, 717–725.
45. Nascimento, B. F. O., A. M. d.'. A. Rocha Gonsalves and M. Pineiro (2010) MnO_2 instead of quinones as selective oxidant of tetrapyrrolic macrocycles. *Inorg. Chem. Commun.* **13**, 395–398.
46. Pineiro, M., C. Gomes and M. Peixoto (2021) Mechanochemical in situ generated gas reactant for the solvent-free hydrogenation of porphyrins. *Green Chem. Lett. Rev.* **14**, 339–344.
47. Aicher, D., S. Gräfe, C. B. W. Stark and A. Wiehe (2011) Synthesis of β-functionalized Temoporfin derivatives for an application in photodynamic therapy. *Bioorg. Med. Chem. Lett.* **21**, 5808–5811.
48. Crossley, M. J., P. L. Burn, S. J. Langford, S. M. Pyke and A. G. Stark (1991) A new method for the synthesis of porphyrin-α-diones that is applicable to the synthesis of trans-annular extended porphyrin systems. *J. Chem. Soc., Chem. Commun.*, 1567–1568.
49. Yu, Q., E. M. Rodriguez, R. Naccache, P. Forgione, G. Lamoureux, F. Sanz-Rodriguez, D. Scheglmann and J. A. Capobianco (2014) Chemical modification of temoporfin – a second generation photosensitizer activated using upconverting nanoparticles for singlet oxygen generation. *Chem. Commun.* **50**, 12150–12153.
50. Xi, L. P., L. D. Hong, W. Chuan and C. B. Shou (2019) Design, synthesis, and biological activity of releasable m-THPC-PEGfolate conjugate using a disulfide-containing linker. *Lett. Org. Chem.* **16**, 165–169.
51. Rogers, L., N. N. Sergeeva, E. Paszko and M. O. Senge (2015) Lead structures for applications in photodynamic therapy. 6. Temoporfin anti-inflammatory conjugates to target the tumor microenvironment for in vitro PDT. *PLoS One* **10**, e0125372.
52. Hurtado, C. R., G. R. Hurtado, G. L. D. Cena, R. C. Queiroz, A. V. Silva, M. F. Diniz, V. R. d. Santos, V. Trava-Airoldi, M.d. S. Baptista, N. Tsolekile, O. S. Oluwafemi, K. Conceição and D. B. Tada (2021) Diamond nanoparticles-porphyrin mTHPP conjugate as photosensitizing platform: cytotoxicity and antibacterial activity. *Nano* **11**, 1393.
53. Haimov, E., H. Weitman, S. Polani, H. Schori, D. Zitoun and O. Shefi (2018) meso-Tetrahydroxyphenylchlorin-conjugated gold nanoparticles as a tool to improve photodynamic therapy. *ACS Appl. Mater. Interfaces* **10**, 2319–2327.
54. Rogers, L., E. Burke-Murphy and M. O. Senge (2014) Simple porphyrin desymmetrization: 5,10,15,20-Tetrakis(3-hydroxyphenyl)porphyrin (mTHPP) as a gateway molecule for peripheral functionalization. *Eur. J. Org. Chem.* **2010**, 4283–4294.
55. Rogers, L., F. Majer, N. N. Sergeeva, E. Paszko, J. F. Gilmer and M. O. Senge (2013) Synthesis and biological evaluation of Foscan® bile acid conjugates to target esophageal cancer cells. *Bioorg. Med. Chem. Lett.* **23**, 2495–2499.
56. Moylan, C., A. M. K. Sweed, Y. M. Shaker, E. M. Scanlan and M. O. Senge (2015) Lead structures for applications in photodynamic therapy 7. Efficient synthesis of amphiphilic glycosylated lipid porphyrin derivatives: refining linker conjugation for potential PDT applications. *Tetrahedron* **71**, 4145–4153.
57. Locos, O. B., C. C. Heindl, A. Corral, M. O. Senge and E. M. Scanlan (2010) Efficient synthesis of glycoporphyrins by microwave-mediated "Click" reactions. *Eur. J. Org. Chem.* **2010**, 1026–1028.
58. Daly, R., G. Vaz, A. M. Davies, M. O. Senge and E. M. Scanlan (2012) Synthesis and biological evaluation of a library of glycoporphyrin compounds. *Chem. Eur. J.* **18**, 14671–14679.
59. Moylan, C., E. M. Scanlan and M. O. Senge (2015) Chemical synthesis and medicinal applications of glycoporphyrins. *Curr. Med. Chem.* **22**, 2238–2348.

60. Chen, J., Y. Xu, Y. Gao, D. Yang, F. Wand, L. Zhang, B. Bao and L. Wang (2018) Nanoscale organic−inorganic hybrid photosensitizers for highly effective photodynamic cancer therapy. *ACS Appl. Mater. Interfaces* **10**, 248–255.
61. Gierlich, P., S. G. Mucha, E. Robbins, L. C. Gomes-da-Silva, K. Matczyszyn and M. O. Senge (2022) One-photon and two-photon photophysical properties of tetrafunctionalized 5,10,15,20-tetrakis (mhydroxyphenyl) chlorin (temoporfin) derivatives as potential two-photon-induced photodynamic therapy agents. *ChemPhotoChem* **2022**(6), e202100249.
62. Shaker, Y. M., A. M. K. Sweed, C. Moylan, L. Rogers, A. A. Ryan, R. Petitdemange and M. O. Senge (2016) Current developments in using *MESO*-(TETRA) substituted porphyrins for PDT. In *Handbook of Photodynamic Therapy* (Edited by R. K. Pandey, D. Kessel and T. J. Dougherty), pp. 95–149. World Scientific, Singapore.
63. Staegemann, M. H., S. Gräfe, B. Gitter, K. Achazi, E. Quaas, R. Haag and A. Wiehe (2018) Hyperbranched polyglycerol loaded with (zinc-)porphyrins: Photosensitizer release under reductive and acidic conditions for improved photodynamic therapy. *Biomacromolecules* **19**, 222–238.
64. Lin, Y., T. Zhou, R. Bai and Y. Xie (2020) Chemical approaches for the enhancement of porphyrin skeleton-based photodynamic therapy. *J. Enzyme Inhib. Med. Chem.* **35**, 1080–1099.
65. Gao, Y.-H., M.-Y. Li, F. Sajjad, J.-H. Wang, F. Meharban, M. A. Gadoora, Y.-J. Yan, T. Nyokong and Z.-L. Chen (2020) Synthesis and pharmacological evaluation of chlorin derivatives for photodynamic therapy of cholangiocarcinoma. *Eur. J. Med. Chem.* **189**, 112049.
66. Theodossiou, T. A., A. R. Goncalves, K. Yannakopoulou, E. Skarpen and K. Berg (2015) Photochemical internalization of tamoxifens transported by a "trojan-horse" nanoconjugate into breast-cancer cell lines. *Angew. Chem. Int. Ed.* **54**, 4885–4889.
67. Berg, K., S. Nordstrand, P. K. Selbo, D. T. T. Tran, E. Angell-Petersen and A. Høgset (2011) Disulfonated tetraphenyl chlorin ($TPCS_{2a}$), a novel photosensitizer developed for clinical utilization of photochemical internalization. *Photochem. Photobiol. Sci.* **10**, 1637–1651.
68. Dąbrowski, J. M., L. G. Arnaut, M. M. Pereira, K. Urbańska, S. Simões, G. Stochel and L. Cortes (2012) Combined effects of singlet oxygen and hydroxyl radical in photodynamic therapy with photostable bacteriochlorins: Evidence from intracellular fluorescence and increased photodynamic efficacy in vitro. *Free Radic. Biol. Med.* **52**, 1188–1200.
69. Gomes-da-Silva, L. C., L. Zhao, L. Bezu, H. Zhou, A. Sauvat, P. Liu, S. Durand, M. Leduc, S. Souquere, F. Loos, L. Mondragon, B. Sveinbjørnsson, Ø. Rekdal, G. Boncompain, F. Perez, L. G. Arnaut, O. Keep and G. Kroemer (2018) Photodynamic therapy with redaporfin targets the endoplasmic reticulum and Golgi apparatus. *EMBO J.* **37**, e98354.
70. Donohoe, C., F. A. Schaberle, F. M. S. Rodrigues, N. Gonçalves, C. J. Kingsbury, M. M. Pereira, M. O. Senge, L. C. Gomes-da-Silva and L. G. Arnaut (2022) Unravelling the pivotal role of atropisomerism for cellular internalization. *J. Am. Chem. Soc.* **144**, 15252–15256.
71. Gariboldi, M. B., R. Ravizza, P. Baranyai, E. Caruso, S. Banfi, S. Meschini and E. Monti (2009) Photodynamic effects of novel 5,15-diaryl-tetrapyrrole derivatives on human colon carcinoma cells. *Bioorg. Med. Chem.* **17**, 2009–2016.
72. Marydasan, B., B. Madhuri, S. Cherukommu, J. Jose, M. Viji, S. C. Karunakaran, T. K. Chandrashekar, K. S. Rao, C. M. Rao and D. Ramaiah (2018) In vitro and in vivo demonstration of human-ovarian-cancer necrosis through a water-soluble and near-infrared-absorbing chlorin. *J. Med. Chem.* **61**, 5009–5019.
73. Rojkiewicz, M., P. Kuś, P. Kozub and M. Kempa (2013) The synthesis of new potential photosensitizers. Part 2. Tetrakis-(hydroxyphenyl)porphyrins with long alkyl chain in the molecule. *Dyes Pigments* **99**, 627–635.
74. Costa, L. D., J. d. A. e Silva, S. M. Fonseca, C. T. Arranja, A. M. Urbano and A. J. F. N. Sobral (2016) Photophysical characterization and in vitro phototoxicity evaluation of 5,10,15,20-Tetra (quinolin-2-yl)porphyrin as a potential sensitizer for photodynamic therapy. *Molecules* **21**, 439.
75. Ryan, A. A., M. M. Ebrahim, R. Petitdemange, G. M. Vaz, E. Paszko, N. N. Sergeeva and M. O. Senge (2014) Lead structures for applications in photodynamic therapy. 5. Synthesis and biological evaluation of water soluble phosphorus(V) 5,10,15,20-tetraalkylporphyrins for PDT. *Photodiagn. Photodyn. Ther.* **11**, 510–515.
76. Zhang, Z., H. Yu, S. Wu, H. Huang, L. Si, H. Liu, L. Shi and H. Zhang (2019) Synthesis, characterization, and photodynamic therapy activity of 5,10,15,20-tetrakis(carboxyl)porphyrin. *Bioorg. Med. Chem.* **27**, 2598–2608.
77. Garćıa-Díaz, M., D. Sánchez-García, J. Soriano, M. L. Sagristà, M. Mora, A. Villanueva, J. C. Stockert, M. Cañete and S. Nonell (2011) Temocene: The porphycene analogue of temoporfin (Foscan®). *Med. Chem. Commun.* **2**, 616–619.
78. García-Díaz, M., M. Kawakubo, P. Mroz, M. L. Sagristà, M. Mora, S. Nonell and M. R. Hamblin (2012) Cellular and vascular effects of the photodynamic agent temocene are modulated by the delivery vehicle. *J. Control. Release* **162**, 355–363.
79. Alberto, M. E., T. Marino, A. D. Quartarolo and N. Russo (2013) Photophysical origin of the reduced photodynamic therapy activity of temocene compared to Foscan: insights from theory. *Phys. Chem. Chem. Phys.* **15**, 16167–16171.
80. Mazzone, G., M. E. Alberto, B. C. De Simone, T. Marino and N. Russo (2016) Can expanded bacteriochlorins act as photosensitizers in photodynamic therapy? Good news from density functional theory computations. *Molecules* **21**, 288.
81. Eriksson, E. S. E. and L. A. Eriksson (2011) Computational design of chlorin based photosensitizers with enhanced absorption properties. *Phys. Chem. Chem. Phys.* **13**, 11590–11596.
82. Eriksson, E. S. E. and L. A. Eriksson (2011) Predictive power of long-range corrected functionals on the spectroscopic properties of tetrapyrrole derivatives for photodynamic therapy. *Phys. Chem. Chem. Phys.* **13**, 7207–7217.
83. Cardenas-Jiron, G. I., M. Santander-Nelli, R. Lopez and M. I. Menendez (2011) Quantitative structure property relationships to evaluate the photosensitizing capability in porphyrins and chlorins. *Int. J. Quantum Chem.* **111**, 1570–1582.
84. de Oliveira, O. V. and J. M. Pires (2014) Quantum chemistry studies of meta-tetra(hydroxyphenyl)chlorin (mTHPC) and its isomers. *J. Porphyrins Phthalocyanines* **18**, 465–470.
85. Friaa, O., P. Maillard and D. Brault (2012) Reaction of the m-THPC triplet state with the antioxidant Trolox and the anesthetic Propofol: Modulation of photosensitization mechanisms relevant to photodynamic therapy? *Photochem. Photobiol. Sci.* **11**, 703–714.
86. Kapałczyńska, M., T. Kolenda, W. Przybyła, M. Zajączkowska, A. Teresiak, V. Filas, M. Ibbs, R. Bliźniak, Ł. Łuczewski and K. Lamperska (2018) 2D and 3D cell cultures – A comparison of different types of cancer cell cultures. *Arch. Med. Sci.* **14**, 910–919.
87. Jensen, C. and Y. Teng (2020) Is it time to start transitioning from 2D to 3D cell culture? *Front. Mol. Biosci.* **7**, 33.
88. Wang, C.-P., P.-J. Lou, F.-Y. Lo and M.-J. Shieh (2014) Meta-tetrahydroxyphenyl chlorine mediated photodynamic therapy inhibits the migration and invasion of a nasopharyngeal carcinoma KJ-1 cell line. *J. Formosan Med. Assoc.* **113**, 173–178.
89. Senge, M. O. and M. W. Radomski (2013) Platelets, photosensitizers, and PDT. *Photodiagn. Photodyn. Ther.* **10**, 1–16.
90. Lange, C., C. Lehmann, M. Mahler and P. J. Bednarski (2019) Comparison of cellular death pathways after mTHPC-mediated photodynamic therapy (PDT) in five human cancer cell lines. *Cancer* **2019**(11), 702.
91. Ziegler, V., T. Kiesslich, B. Krammer and K. Plaetzer (2013) Photosensitizer adhered to cell culture microplates induces phototoxicity in carcinoma cells. *BioMed Res. Int*. **2013**, 549498.
92. Engelhardt, V., T. Kiesslich, J. Berlanda, S. Hofbauer, B. Krammer and K. Plaetzer (2011) Lipophilic rather than hydrophilic photosensitizers show strong adherence to standard cell culture microplates under cell-free conditions. *J. Photochem. Photobiol. B Biol.* **103**, 222–229.
93. Olivier, D., S. Douillard, I. Lhommeau and T. Patrice (2009) Photodynamic treatment of culture medium containing serum induces long-lasting toxicity in vitro. *Radiat. Res.* **172**, 451–462.
94. Syu, W.-J., H.-P. Yu, C.-Y. Hsu, Y. C. Rajan, Y.-H. Hsu, Y.-C. Chang, W.-Y. Hsieh, C.-H. Wang and P.-S. Lai (2012) Improved photodynamic cancer treatment by folate-conjugated polymeric micelles in a KB xenografted animal model. *Small* **8**, 2060–2069.

95. Boppana, N. B., J. S. DeLor, E. Van Buren, A. Bielawska, J. Bielawski, J. S. Pierce, M. Korbelik and D. Separovic (2016) Enhanced apoptotic cancer cell killing after Foscan photodynamic therapy combined with fenretinide via de novo sphingolipid biosynthesis pathway. *J. Photochem. Photobiol. B Biol.* **159**, 191–195.
96. Boppana, N. B., J. M. Kraveka, M. Rahmaniyan, L. Li, A. Bielawska, J. Bielawski, J. S. Pierce, J. S. Delor, K. Zhang, M. Korbelik and D. Separovic (2017) Fumonisin B1 inhibits endoplasmic reticulum stress associated-apoptosis after foscan PDT combined with C6-pyridinium ceramide or fenretinide. *Anticancer Res.* **37**, 455–464.
97. Besic Gyenge, E., D. Lüscher, P. Forny, M. Antoniol, G. Geisberger, H. Walt, G. Patzke and C. Maake (2013) Photodynamic mechanisms induced by a combination of hypericin and a chlorin based-photosensitizer in head and neck squamous cell carcinoma cells. *Photochem. Photobiol.* **89**, 150–162.
98. Besic Gyenge, E., P. Forny, D. Lüscher, A. Laass, H. Walt and C. Maake (2012) Effects of hypericin and a chlorin based photosensitizer alone or in combination in squamous cell carcinoma cells in the dark. *Photodiagn. Photodyn. Ther.* **9**, 321–331.
99. Xu, Z.-Y., W. Mao, Z. Zhao, Z.-K. Wang, Y.-Y. Liu, Y. Wu, H. Wang, D.-W. Zhang, Z.-T. Li and D. Ma (2022) Self-assembled nanoparticles based on supramolecular-organic frameworks and temoporfin for an enhanced photodynamic therapy *in vitro* and *in vivo*. *J. Mater. Chem. B* **10**, 899–908.
100. Machacek, M., J. Demuth, P. Cermak, M. Vavreckova, L. Hruba, A. Jedlickova, P. Kubat, T. Simunek, V. Novakova and P. Zimcik (2016) Tetra(3,4-pyrido)porphyrazines caught in the cationic cage: Toward nanomolar active photosensitizers. *J. Med. Chem.* **59**, 9443–9456.
101. Liu, Y., M. H. A. M. Fens, B. Lou, N. C. H. van Kronenburg, R. F. M. Maas-Bakker, R. J. Kok, S. Oliveira, W. E. Hennink and C. F. van Nostrum (2020) π-π-stacked poly(ε-caprolactone)-*b*-poly (ethyleneglycol) micelles loaded with a photosensitizer for photodynamic therapy. *Pharmaceutics* **12**, 338.
102. Liu, Y., L. Scrivano, J. D. Peterson, M. H. A. M. Fens, I. B. Hernández, B. Mesquita, J. S. Toraño, W. E. Hennink, C. F. van Nostrum and S. Oliveira (2020) EGFR-targeted nanobody functionalized polymeric micelles loaded with mTHPC for selective photodynamic therapy. *Mol. Pharm.* **17**, 1276–1292.
103. Ahmadi, V., F. Zabihi, A. Rancan, A. Staszak, C. Nie, M. Dimde, K. Achazi, A. Wiehe, A. Vogt and R. Haag (2021) Amphiphilic co-polypeptides self-assembled into spherical nanoparticles for dermal drug delivery. *ACS Appl. Nano Mater.* **4**, 6709–6721.
104. Shah, S. A., M. U. A. Khan, M. Arshadd, S. U. Awane, M. U. Hashmi and N. Ahmad (2016) Doxorubicin-loaded photosensitive magnetic liposomes for multi-modal cancer therapy. *Colloids Surf. B Biointerfaces* **148**, 157–164.
105. Etcheverry, M. E., M. A. Pasquale and M. Garavaglia (2016) Photodynamic therapy of HeLa cell cultures by using LED or laser sources. *J. Photochem. Photobiol. B Biol.* **160**, 271–277.
106. Xue, K., Y.-N. Wang, X. Zhao, H.-X. Zhang, D. Yu and C.-S. Jin (2019) Synergistic effect of meta-tetra(hydroxyphenyl) chlorin-based photodynamic therapy followed by cisplatin on malignant Hep-2 cells. *Onco. Targets. Ther.* **12**, 5525–5536.
107. Jarvi, M. T., M. J. Niedre, M. S. Patterson and B. C. Wilson (2011) The influence of oxygen depletion and photosensitizer triplet-state dynamics during photodynamic therapy on accurate singlet oxygen luminescence monitoring and analysis of treatment dose response. *Photochem. Photobiol.* **87**, 223–234.
108. Jarvi, M. T., M. S. Patterson and B. C. Wilson (2012) Insights into photodynamic therapy dosimetry: Simultaneous singlet oxygen luminescence and photosensitizer photobleaching measurements. *Biophys. J.* **102**, 661–671.
109. Soares, H. T., J. R. S. Campos, L. C. Gomes-da-Silva, F. A. Schaberle, J. M. Dabrowski and L. G. Arnaut (2016) Pro-oxidant and antioxidant effects in photodynamic therapy: Cells recognise that not all exogenous ROS are alike. *Chembiochem* **17**, 836–842.
110. Kessel, D. (2021) Paraptosis after ER photodamage initiated by m-tetra(hydroxyphenyl) chlorin. *Photochem. Photobiol.* **97**, 1097–1100.
111. Rojnik, M., P. Kocbek, F. Moret, C. Compagnin, L. Celotti, M. J. Bovis, J. H. Woodhams, A. MacRobert, D. Scheglmann, W. Helfrich, M. J. Verkaik, E. Papini, E. Reddi and J. Kos (2012) In vitro and in vivo characterization of temoporfin-loaded PEGylated PLGA nanoparticles for use in photodynamic therapy. *Nanomedicine* **7**, 663–677.
112. Hsu, C.-Y., C.-W. Chen, H.-P. Yu, Y.-F. Lin and P.-S. Lai (2013) Bioluminescence resonance energy transfer using luciferase-immobilized quantum dots for self-illuminated photodynamic therapy. *Biomaterials* **34**, 1204–1212.
113. Compagnin, C., F. Moret, L. Celotti, G. Miotto, J. H. Woodhams, A. J. MacRobert, D. Scheglmann, S. Iratni and E. Reddi (2011) Meta-tetra(hydroxyphenyl)chlorin-loaded liposomes sterically stabilised with poly(ethylene glycol) of different length and density: Characterisation, in vitro cellular uptake and phototoxicity. *Photochem. Photobiol. Sci.* **10**, 1751–1759.
114. Moret, F., D. Scheglmann and E. Reddi (2013) Folate-targeted PEGylated liposomes improve the selectivity of PDT with meta-tetra(hydroxyphenyl)chlorin (m-THPC). *Photochem. Photobiol. Sci.* **12**, 823–834.
115. Horgan, C. C., M. S. Bergholt, A. Nagelkerke, M. Z. Thin, I. J. Pence, U. Kauscher, T. L. Kalber, D. J. Stucke and M. M. Stevens (2021) Integrated photodynamic Raman theranostic system for cancer diagnosis, treatment, and post-treatment molecular monitoring. *Theranostics* **11**, 2006–2019.
116. François, A., S. Marchal, F. Guillemin and L. Bezdetnaya (2011) mTHPC-based photodynamic therapy induction of autophagy and apoptosis in cultured cells in relation to mitochondria and endoplasmic reticulum stress. *Int. J. Oncol.* **39**, 1537–1543.
117. Teiten, M.-H., S. Marchal, M. A. D'Hallewin, F. Guillemin and L. Bezdetnaya (2003) Primary photodamage sites and mitochondrial events after Foscan® photosensitization of MCF-7 human breast cancer cells. *Photochem. Photobiol.* **78**, 9–14.
118. Lin, S., L. Zhang, K. Lei, A. Zhang, P. Liu and J. Liu (2014) Development of a multifunctional luciferase reporters (sic!) system for assessing endoplasmic reticulum-targeting photosensitive compounds. *Cell Stress Chaperones* **19**, 927–937.
119. Caruso, E., M. Cerbara, M. C. Malacarne, E. Marras, E. Monti and M. B. Gariboldi (2019) Synthesis and photodynamic activity of novel non-symmetrical diaryl porphyrins against cancer cell lines. *J. Photochem. Photobiol. B Biol.* **195**, 39–50.
120. Zhang, Y., L. Pang, C. Ma, Q. Tu, R. Zhang, E. Saeed, A. E. Mahmoud and J. Wang (2014) Small molecule-initiated light-activated semiconducting polymer dots: An integrated nanoplatform for targeted photodynamic therapy and imaging of cancer cells. *Anal. Chem.* **86**, 3092–3099.
121. Haupt, S. I., H. W. Lazar, Y. Shav-Tal and B. Ehrenberg (2016) FRET energy transfer via Pdots improves the efficiency of photodynamic therapy and leads to rapid cell death. *J. Photochem. Photobiol. B Biol.* **164**, 123–131.
122. Navarro, F. P., D. Bechet, T. Delmas, P. Couleaud, C. Frochot, M. Verhille, E. Kamarulzaman, R. Vanderesse, P. Boisseau, I. Texier, J. Gravier, F. Vinet, M. Barberi-Heyob and A. C. Couffin (2011) Preparation, characterization and cellular studies of photosensitizer-loaded lipid nanoparticles for photodynamic therapy. *Proc. SPIE* **2011**(7886), 78860Y.
123. Navarro, F. P., G. Creusat, C. Frochot, A. Moussaron, M. Verhille, R. Vanderesse, J.-S. Thomann, P. Boisseau, I. Texier, A.-C. Couffin and M. Barberi-Heyob (2014) Preparation and characterization of mTHPC-loaded solid lipid nanoparticles for photodynamic therapy. *J. Photochem. Photobiol. B Biol.* **130**, 161–169.
124. Bressenot, A., S. Marchal, L. Bezdetnaya, J. Garrier, F. Guillemin and F. Plénat (2009) Assessment of apoptosis by immunohistochemistry to active caspase-3, active caspase-7, or cleaved PARP in monolayer cells and spheroid and subcutaneous xenografts of human carcinoma. *J. Histochem. Cytochem.* **57**, 289–300.
125. Sun, Y.-M., X. Jiang, Z.-Y. Liu, L.-G. Liu, Y.-H. Liao, L. Zeng, Y. Ye and H.-Y. Liu (2020) Hydroxy-corrole and its gallium(III) complex as new photosensitizer for photodynamic therapy against breast carcinoma. *Eur. J. Med. Chem.* **208**, 112794.
126. Malarvizhi, G. L., P. Chandran, A. P. Retnakumari, R. Ramachandran, N. Gupta, S. Nair and M. Koyakutty (2014) A rationally designed photo-chemo core-shell nanomedicine for inhibiting the migration of metastatic breast cancer cells followed by photodynamic killing. *Nanomed.: Nanotechnol. Biol. Med.* **10**, 579–587.

127. Brezaniova, I., M. Hruby, J. Kralova, V. Kral, Z. Cernochova, M. Peter Cernoch, J. K. Slouf and P. Stepanek (2016) Temoporfin-loaded 1-tetradecanol-based thermoresponsive solid lipid nanoparticles for photodynamic therapy. *J. Control. Release* **241**, 34–44.
128. Haimov-Talmoud, E., Y. Harel, H. Schori, M. Motiei, A. Atkins, R. Popovtzer, J.-P. Lellouche and O. Shefi (2019) Magnetic targeting of mTHPC to improve the selectivity and efficiency of photodynamic therapy. *ACS Appl. Mater. Interfaces* **11**, 45368–45380.
129. Yakavets, I., I. Yankovsky, T. Zorina, M. Belevtsev, L. Bezdetnaya and V. Zorin (2021) Modulation of temoporfin distribution in blood by β-cyclodextrin nanoshuttles. *Pharmaceutics* **13**, 1054.
130. Lange, C. and P. J. Bednarski (2021) In vitro assessment of synergistic effects in combinations of a temoporfin-based photodynamic therapy with glutathione peroxidase 1 inhibitors. *Photodiagn. Photodyn. Ther.* **36**, 102478.
131. Lange, C. and P. J. Bednarski (2018) Evaluation for synergistic effects by combinations of photodynamic therapy (PDT) with temoporfin (mTHPC) and Pt(II) complexes carboplatin, cisplatin or oxaliplatin in a set of five human cancer cell lines. *Int. J. Mol. Sci.* **19**, 3183.
132. Stein, N. C., D. Mulac, J. Fabian, F. C. Herrmann and K. Langer (2020) Nanoparticle albumin-bound mTHPC for photodynamic therapy: Preparation and comprehensive characterization of a promising drug delivery system. *Int. J. Pharm.* **582**, 119347.
133. Yuan, Z., G. Fan, H. Wu, C. Liu, Y. Zhan, Y. Qiu, C. Shou, F. Gao, J. Zhang, P. Yin and K. Xu (2021) Photodynamic therapy synergizes with PD-L1 checkpoint blockade for immunotherapy of CRC by multifunctional nanoparticles. *Mol. Ther.* **29**, 2931–2948.
134. Szurko, A., M. Rams-Baron, F.-P. Montforts, D. Bauer, P. Kozub, J. Gubernator, S. Altmann, A. Stanek, A. Sieroń and A. Ratuszna (2020) Photodynamic performance of amphiphilic chlorin e6 derivatives with appropriate properties: A comparison between different-type liposomes as delivery systems. *Photodiagn. Photodyn. Ther.* **30**, 101799.
135. Song, C., W. Xu, H. Wu, X. Wang, Q. Gong, C. Liu, J. Liu and L. Zhou (2020) Photodynamic therapy induces autophagy-mediated cell death in human colorectal cancer cells via activation of the ROS/JNK signaling pathway. *Cell Death Dis.* **11**, 938.
136. Rodrigues, J. A., R. Amorim, M. F. Silva, F. Baltazar, R. F. Wolffenbuttel and J. H. Correia (2019) Photodynamic therapy at low-light fluence rate: in vitro assays on colon cancer cells. *IEEE J. Sel. Topics Quant. Electr.* **25**, 7202506.
137. Löw, K., T. Knobloch, S. Wagner, A. Wiehe, A. Engel, K. Langer and H. von Briesen (2011) Comparison of intracellular accumulation and cytotoxicity of free mTHPC and mTHPC-loaded PLGA nanoparticles in human colon carcinoma cells. *Nanotechnology* **22**, 245102.
138. Villa Nova, M., C. Janas, M. Schmidt, T. Ulshoefer, S. Gräfe, S. Schiffmann, N. de Bruin, A. Wiehe, V. Albrecht, M. J. Parnham, M. L. Bruschi and M. G. Wacker (2015) Nanocarriers for photodynamic therapy—rational formulation design and medium-scale manufacture. *Int. J. Pharm.* **491**, 250–260.
139. Peng, C.-L., L.-Y. Yang, T.-Y. Luo, P.-S. Lai, S.-J. Yang, W.-J. Lin and M.-J. Shieh (2010) Development of pH sensitive 2-(diisopropylamino)ethyl methacrylate based nanoparticles for photodynamic therapy. *Nanotechnology* **21**, 155103.
140. Schoppa, T., D. Jung, T. Rust, D. Mulac, D. Kuckling and K. Langer (2021) Light-responsive polymeric nanoparticles based on a novel nitropiperonal based polyester as drug delivery systems for photosensitizers in PDT. *Int. J. Pharm.* **597**, 120326.
141. Shieh, M.-J., C.-L. Peng, W.-L. Chiang, C.-H. Wang, C.-Y. Hsu, S.-J. J. Wang and P.-S. Lai (2010) Reduced skin photosensitivity with meta-tetra(hydroxyphenyl)chlorin-loaded micelles based on a poly(2-ethyl-2-oxazoline)-b-poly(D,L-lactide) diblock copolymer in vivo. *Mol. Pharm.* **7**, 1244–1253.
142. Dragicevic-Curic, N., S. Gräfe, B. Gitter and A. Fahr (2010) Efficacy of temoporfin-loaded invasomes in the photodynamic therapy in human epidermoid and colorectal tumour cell lines. *J. Photochem. Photobiol. B Biol.* **101**, 238–250.
143. Liu, Y., J. W. de Vries, Q. Liu, A. M. Hartman, G. D. Wieland, S. Wieczorek, H. G. Börner, A. Wiehe, E. Buhler, M. C. A. Stuart, W. R. Browne, A. Herrmann and A. K. H. Hirsch (2018) Lipid-DNAs as solubilizers of mTHPC. *Chem. Eur. J.* **24**, 798–802.
144. Yankovsky, I., E. Bastien, I. Yakavets, I. Khludeyev, H.-P. Lassalle, S. Gräfe, L. Bezdetnaya and V. Zorin (2016) Inclusion complexation with β-cyclodextrin derivatives alters photodynamic activity and biodistribution of meta-tetra(hydroxyphenyl)chlorin. *Eur. J. Pharm. Sci.* **91**, 172–182.
145. Yakavets, I., M. Millard, L. Lamy, A. Francois, D. Scheglmann, A. Wiehe, H.-P. Lassalle, V. Zorin and L. Bezdetnaya (2019) Matryoshka-type liposomes offer the improved delivery of temoporfin to tumor spheroids. *Cancer* **11**, 1366.
146. Wu, R. W. K., E. S. M. Chu, Z. Huang, M. C. Olivo, D. C. W. Ip and C. M. N. Yow (2015) An in vitro investigation of photodynamic efficacy of FosPeg® on human colon cancer cells. *J. Innov. Opt. Health. Sci.* **8**, 15500273.
147. Mahlert, L., J. Anderski, T. Schoppa, D. Mulac, J. Sun, D. Kuckling and K. Langer (2019) In vitro evaluation of innovative light-responsive nanoparticles for controlled drug release in intestinal PDT. *Int. J. Pharm.* **565**, 199–208.
148. Anderski, J., L. Mahlert, J. Sun, W. Birnbaum, D. Mulac, S. Schreiber, F. Herrmann, D. Kuckling and K. Langer (2019) Light-responsive nanoparticles based on new polycarbonate polymers as innovative drug delivery systems for photosensitizers in PDT. *Int. J. Pharm.* **557**, 182–191.
149. Yang, K., M. Luo, H. Li, G. Abdulrehman and L. Kang (2021) Effects of jasplakinolide on cytotoxicity, cytoskeleton and apoptosis in two different colon cancer cell lines treated with m-THPC-PDT. *Photodiagn. Photodyn. Ther.* **35**, 102425.
150. Abdulrehman, G., K. Xv, Y. Li and L. Kang (2018) Effects of meta-tetrahydroxyphenylchlorin photodynamic therapy on isogenic colorectal cancer SW480 and SW620 cells with different metastatic potentials. *Lasers Med. Sci.* **33**, 1581–1590.
151. Berlanda, J., T. Kiesslich, V. Engelhardt, B. Krammer and K. Plaetzer (2010) Comparative in vitro study on the characteristics of different photosensitizers employed in PDT. *J. Photochem. Photobiol. B Biol.* **100**, 173–180.
152. Sasnauskiene, A., J. Kadziauskas, N. Vezelyte, V. Jonusiene and V. Kirveliene (2009) Apoptosis, autophagy and cell cycle arrest following photodamage to mitochondrial interior. *Apoptosis* **14**, 276–286.
153. Dabkeviciene, D., A. Sasnauskiene, R. Kvietkauskaite, V. Kirveliene and E. Leman (2014) Differential expression of VEGF and IL-1alpha after photodynamic treatment in combination with doxorubicin or taxotere. *Anticancer Res.* **34**, 5295–5302.
154. Dabkeviciene, D., A. Sasnauskiene, E. Leman, R. Kvietkauskaite, N. Daugelaviciene, V. Stankevicius, V. Jurgelevicius, B. Juodka and V. Kirveliene (2012) mTHPC-mediated photodynamic treatment up-regulates the cytokines VEGF and IL-1alpha. *Photochem. Photobiol.* **88**, 432–439.
155. Gao, Y.-H., V. Lovreković, A. Kussayeva, D.-Y. Chen, D. Margetić and Z.-L. Chen (2019) The photodynamic activities of dimethyl 13^1-[2-(guanidinyl)ethylamino] chlorin e6 photosensitizers in A549 tumor. *Eur. J. Med. Chem.* **177**, 144–152.
156. van Lith, S. A. M., S. M. J. van Duijnhoven, A. C. Navis, W. P. J. Leenders, E. Dolk, J. W. H. Wennink, C. van Nostrum and J. C. M. van Hest (2017) Legomedicine – A versatile chemo-enzymatic approach for the preparation of targeted dual-labeled llama antibody−nanoparticle conjugates. *Bioconjug. Chem.* **28**, 539–548.
157. Compagnin, C., L. Baù, M. Mognato, L. Celotti, G. Miotto, M. Arduini, F. Moret, C. Fede, F. Selvestrel, I. M. R. Echevarria, F. Mancin and E. Reddi (2009) The cellular uptake of meta-tetra (hydroxyphenyl)chlorin entrapped in organically modified silica nanoparticles is mediated by serum proteins. *Nanotechnology* **20**, 345101.
158. Paszko, E., G. M. F. Vaz, C. Ehrhardt and M. O. Senge (2013) Transferrin conjugation does not increase the efficiency of liposomal Foscan during in vitro photodynamic therapy of oesophageal cancer. *Eur. J. Pharm. Sci.* **48**, 202–210.
159. Peng, W., D. F. Samplonius, S. de Visscher, J. L. N. Roodenburg, W. Helfrich and M. J. H. Witjes (2014) Photochemical internalization (PCI)-mediated enhancement of bleomycin cytotoxicity by liposomal mTHPC formulations in human head and neck cancer cells. *Lasers Surg. Med.* **46**, 650–658.
160. Sherifa, G., M. A. Saad Zaghloul, O. F. Elsayed, A. Rueck, R. Steiner, A. I. Abdelaziz and M. H. Abdel-Kader (2013) Functional characterization of Fospeg, and its impact on cell cycle upon PDT

of Huh7 hepatocellular carcinoma cell model. *Photodiagn. Photodyn. Ther.* **10**, 87–94.
161. Mitra, S., B. R. Giesselman, F. J. De Jesús-Andino and T. H. Foster (2011) Tumor response to mTHPC-mediated photodynamic therapy exhibits strong correlation with extracellular release of HSP70. *Lasers Surg. Med.* **43**, 632–643.
162. Calvo, G., D. Sáenz, M. Simian, R. Sampayo, L. Mamone, P. Vallecorsa, A. Batlle, A. Casas and G. Di Venosa (2017) Reversal of the migratory and invasive phenotype of ras-transfected mammary cells by photodynamic therapy treatment. *J. Cell. Biochem.* **118**, 464–477.
163. Zhua, Z., C. Scalfi-Happ, A. Ryabova, S. Gräfe, A. Wiehe, R.-U. Peter, V. Loschenov, R. Steinera and R. Wittig (2018) Photodynamic activity of Temoporfin nanoparticles induces a shift to the M1-like phenotype in M2-polarized macrophages. *J. Photochem. Photobiol. B Biol.* **185**, 215–222.
164. Silva, A. K. A., J. Kolosnjaj-Tabi, S. Bonneau, I. Marangon, N. Boggetto, K. Aubertin, O. Clément, M. F. Bureau, N. Luciani, F. Gazeau and C. Wilhelm (2013) Magnetic and photoresponsive theranosomes: Translating cell-released vesicles into smart nanovectors for cancer therapy. *ACS Nano* **7**, 4954–4966.
165. Wu, R. W. K., E. S. M. Chu, Z. Huang, C. S. Xu, C. W. Ip and C. M. N. Yow (2015) Effect of FosPeg® mediated photoactivation on *P-gp*/ABCB1 protein expression in human nasopharyngeal carcinoma cells. *J. Photochem. Photobiol. B Biol.* **148**, 82–87.
166. Wu, R. W. K., E. S. M. Chu, Z. Huang, C. S. Xu, C. W. Ip and C. M. N. Yow (2013) FosPeg® PDT alters the EBV miRNAs and LMP1 protein expression in EBV positive nasopharyngeal carcinoma cells. *J. Photochem. Photobiol. B Biol.* **127**, 114–122.
167. Wu, R. W. K., E. S. M. Chu, J. W. M. Yuen and Z. Huang (2020) Comparative study of FosPeg® photodynamic effect on nasopharyngeal carcinoma cells in 2D and 3D models. *J. Photochem. Photobiol. B Biol.* **210**, 111987.
168. Yow, C. M. N., N. K. Mak, A. W. N. Leung and Z. Huang (2009) Induction of early apoptosis in human nasopharyngeal carcinoma cells by mTHPC-mediated photocytotoxicity. *Photodiagn. Photodyn. Ther.* **6**, 122–127.
169. Korbelik, M., J. Banáth, J. Sun, D. Canals, Y. A. Hannun and D. Separovic (2014) Ceramide and sphingosine-1-phosphate act as photodynamic therapy-elicited damage-associated molecular patterns: Cell surface exposure. *Int. Immunopharmacol.* **20**, 359–365.
170. Haedicke, K., D. Kozlova, S. Gräfe, U. Teichgräber, M. Epple and I. Hilger (2015) Multifunctional calcium phosphate nanoparticles for combining near-infrared fluorescence imaging and photodynamic therapy. *Acta Biomater.* **14**, 197–207.
171. Haedicke, K., S. Gräfe, F. Lehmann and I. Hilger (2013) Multiplexed in vivo fluorescence optical imaging of the therapeutic efficacy of photodynamic therapy. *Biomaterials* **34**, 10075–10083.
172. Di Corato, R., G. Béalle, J. Kolosnjaj-Tabi, A. Espinosa, O. Clément, A. K. A. Silva, C. Ménager and C. Wilhelm (2015) Combining magnetic hyperthermia and photodynamic therapy for tumor ablation with photoresponsive magnetic liposomes. *ACS Nano* **9**, 2904–2916.
173. Marangon, I., C. Ménard-Moyon, A. K. A. Silva, A. Bianco, N. Luciani and F. Gazeau (2016) Synergic mechanisms of photothermal and photodynamic therapies mediated by photosensitizer/carbon nanotube complexes. *Carbon* **97**, 110–123.
174. Ali, S., M. U. Amin, M. Y. Ali, I. Tariq, S. R. Pinnapireddy, L. Duse, N. Goergen, C. Wölk, G. Hause, J. Jedelská, J. Schäfer and U. Bakowsky (2020) Wavelength dependent photo-cytotoxicity to ovarian carcinoma cells using temoporfin loaded tetraether liposomes as efficient drug delivery system. *Eur. J. Pharm. Biopharm.* **150**, 50–65.
175. Ali, S., M. U. Amin, I. Tariq, M. F. Sohail, M. Y. Ali, E. Preis, G. Ambreen, S. R. Pinnapireddy, J. Jedelská, J. Schäfer and U. Bakowsky (2021) Lipoparticles for synergistic chemo-photodynamic therapy to ovarian carcinoma cells: in vitro and in vivo assessments. *Int. J. Nanomed.* **16**, 951–976.
176. Petri, A., E. Alexandratou and D. Yova (2022) Assessment of natural antioxidants' effect on PDT cytotoxicity through fluorescence microscopy image analysis. *Lasers Surg. Med.* **54**, 311–319.
177. Petri, A., M. Kyriazi, E. Alexandratou, M. Rallis, S. Grafe and D. Yova (2009) Evaluation of the PDT effect of Foscan® and Fospeg® in the LNCaP human prostate cancer cell line. *Proc. SPIE* **7373**, 73731I.
178. Petri, A., D. Yova, E. Alexandratou, M. Kyriazi and M. Rallis (2012) Comparative characterization of the cellular uptake and photodynamic efficiency of Foscan® and Fospeg in a human prostate cancer cell line. *Photodiagn. Photodyn. Ther.* **9**, 344–354.
179. Hackbarth, S., J. Schlothauer, A. Preuß, C. Ludwig and B. Röder (2012) Time resolved sub-cellular singlet oxygen detection – ensemble measurements versus single cell experiments. *Laser Phys. Lett.* **9**, 474–480.
180. Aubertin, K., A. K. A. Silva, N. Luciani, A. Espinosa, A. Djemat, D. Charue, F. Gallet, O. Blanc-Brude and C. Wilhelm (2016) Massive release of extracellular vesicles from cancer cells after photodynamic treatment or chemotherapy. *Sci. Rep.* **6**, 35376.
181. Aubertin, K., S. Bonneau, A. K. A. Silva, J.-C. Bacri, F. Gallet and C. Wilhelm (2013) Impact of photosensitizers activation on intracellular trafficking and viscosity. *PLoS One* **8**, e84850.
182. Besic Gyenge, E., S. Hiestand, S. Graefe, H. Walt and C. Maake (2011) Cellular and molecular effects of the liposomal mTHPC derivative Foslipos in prostate carcinoma cells in vitro. *Photodiagn. Photodyn. Ther.* **8**, 86–96.
183. N'Diaye, M., J. Vergnaud-Gauduchon, V. Nicolas, V. Faure, S. Denis, S. Abreu, P. Chaminade and V. Rosilio (2019) Hybrid lipid polymer nanoparticles for combined chemo- and photodynamic therapy. *Mol. Pharm.* **16**, 4045–4058.
184. Saboktakin, M. R., R. M. Tabatabaie, A. Maharramov and M. A. Ramazanov (2011) Synthesis and in vitro studies of biodegradable modified chitosan nanoparticles for photodynamic treatment of cancer. *Int. J. Biol. Macromol.* **49**, 1059–1065.
185. Beyer, S., L. Xie, S. Gräfe, V. Vogel, K. Dietrich, A. Wiehe, V. Albrecht, W. Mäntele and M. G. Wacker (2015) Bridging laboratory and large scale production: Preparation and in vitro-evaluation of photosensitizer-loaded nanocarrier devices for targeted drug delivery. *Pharm. Res.* **32**, 1714–1726.
186. Piffoux, M., A. K. A. Silva, J.-B. Lugagne, P. Hersen, C. Wilhelm and F. Gazeau (2017) Extracellular vesicle production loaded with nanoparticles and drugs in a trade-off between loading, yield and purity: towards a personalized drug delivery system. *Adv. Biosys.* **1**, 1700044.
187. Piffoux, M., A. K. A. Silva, C. Wilhelm, F. Gazeau and D. Tareste (2018) Modification of extracellular vesicles by fusion with liposomes for the design of personalized biogenic drug delivery systems. *ACS Nano* **12**, 6830–6842.
188. Chen, K., M. Wacker, S. Hackbarth, C. Ludwig, K. Langer and B. Röder (2010) Photophysical evaluation of mTHPC-loaded HSA nanoparticles as novel PDT delivery systems. *J. Photochem. Photobiol. B Biol.* **101**, 340–347.
189. Wacker, M., K. Chen, A. Preuss, K. Possemeyer, B. Roeder and K. Langer (2010) Photosensitizer loaded HSA nanoparticles. I: Preparation and photophysical properties. *Int. J. Pharm.* **393**, 253–262.
190. Preuß, A., K. Chen, S. Hackbarth, M. Wacker, K. Langer and B. Röder (2011) Photosensitizer loaded HSA nanoparticles II: In vitro investigations. *Int. J. Pharm.* **404**, 308–316.
191. Rad, A. T., C.-W. Chen, W. Aresh, Y. Xia, P.-S. Lai and M.-P. Nieh (2019) Combinational effects of active targeting, shape, and enhanced permeability and retention for cancer theranostic nanocarriers. *ACS Appl. Mater. Interfaces* **11**, 10505–10519.
192. Fang, J., S. Gao, R. Islam, H. Nema, R. Yanagibashi, N. Yoneda, N. Watanabe, Y. Yasuda, N. Nuita, J.-R. Zhou and K. Yokomizo (2021) Styrene maleic acid copolymer-based micellar formation of temoporfin (SMA@ mTHPC) behaves as a nanoprobe for tumor-targeted photodynamic therapy with a superior safety. *Biomedicine* **9**, 1493.
193. Kralova, J., M. Kolar, M. Kahle, J. Truksa, S. Lettlova, K. Balusikova and P. Bartunek (2017) Glycol porphyrin derivatives and temoporfin elicit resistance to photodynamic therapy by different mechanisms. *Sci. Rep.* **7**, 44497.
194. Brezániová, I., K. Záruba, J. Králová, A. Sinica, H. Adámková, P. Ulbrich, P. Poučková, M. Hrubý, P. Štěpánek and V. Král (2018) Silica-based nanoparticles are efficient delivery system for temoporfin. *Photodiagn. Photodyn. Ther.* **21**, 275–284.
195. Korbelik, M., J. Zhao, H. Zeng, A. Bielawska and Z. M. Szulc (2020) Mechanistic insights into ceramidase inhibitor LCL521-

enhanced tumor cell killing by photodynamic and thermal ablation therapies. *Photochem. Photobiol. Sci.* **19**, 1145–1151.
196. Wennink, J. W. H., Y. Liu, P. I. Mäkinen, F. Setaro, A. de la Escosura, M. Bourajjaj, J. P. Lappalainen, L. P. Holappa, J. B. van den Dikkenberg, M. Al Fartousia, P. N. Trohopoulos, S. Ylä-Herttuala, T. Torres, W. E. Hennink and C. F. van Nostrum (2017) Macrophage selective photodynamic therapy by meta-tetra (hydroxyphenyl) chlorin loaded polymeric micelles: A possible treatment for cardiovascular diseases. *Eur. J. Pharm. Sci.* **107**, 112–125.
197. Scalfi-Happ, C., Z. Zhu, S. Graefe, A. Wiehe, A. Ryabova, V. Loschenov, R. Wittig and R. W. Steiner (2018) Chlorin nanoparticles for tissue diagnostics and photodynamic therapy. *Photodiagn. Photodyn. Ther.* **22**, 106–114.
198. Boeuf-Muraille, G., G. Rigaux, M. Callewaert, N. Zambrano, L. Van Gulick, V. G. Roullin, C. Terryn, M.-C. Andry, F. Chuburu, S. Dukic and M. Molinari (2019) Evaluation of mTHPC-loaded PLGA nanoparticles for in vitro photodynamic therapy on C6 glioma cell line. *Photodiagn. Photodyn. Ther.* **25**, 448–455.
199. Sasnauskiene, A., J. Kadziauskas, D. Labeikyte and V. Kirveliene (2009) Rhodamine 123-mediated photodamage to mitochondrial interior does not develop hallmarks of apoptosis in MH22 cells. *Biol. Ther. Dent.* **55**, 51–56.
200. Dabkevičienė, D., V. Stankevičius, G. Graželienė, A. Markuckas, J. Didžiapetrienė and V. Kirvelienė (2010) mTHPC-mediated photodynamic treatment of Lewis lung carcinoma in vitro and in vivo. *Medicina (Kaunas)* **46**, 345–350.
201. Pinto, A., I. Marangon, J. Méreaux, A. Nicolás-Boluda, G. Lavieu, C. Wilhelm, L. Sarda-Mantel, A. K. A. Silva, M. Pocard and F. Gazeau (2021) Immune reprogramming precision photodynamic therapy of peritoneal metastasis by scalable stem-cell-derived extracellular vesicles. *ACS Nano* **15**, 3251–3263.
202. Kv, R., T.-I. Liu, I.-L. Lu, C.-C. Liu, H.-H. Chen, T.-Y. Lu, W.-H. Chiang and H.-C. Chiu (2020) Tumor microenvironment-responsive and oxygen self-sufficient oil droplet nanoparticles for enhanced photothermal/photodynamic combination therapy against hypoxic tumors. *J. Control. Release* **328**, 87–99.
203. Wagner, A., C. Mayr, D. Bach, R. Illig, K. Plaetzer, F. Berr, M. Pichler, D. Neureiter and T. Kiesslich (2014) MicroRNAs associated with the efficacy of photodynamic therapy in biliary tract cancer cell lines. *Int. J. Mol. Sci.* **15**, 20134–20157.
204. Kiesslich, T., D. Neureiter, B. Alinger, G. L. Jansky, J. Berlanda, V. Mkrtchyan, M. Ocker, K. Plaetzer and F. Berr (2010) Uptake and phototoxicity of meso-tetrahydroxyphenyl chlorine are highly variable in human biliary tract cancer cell lines and correlate with markers of differentiation and proliferation. *Photochem. Photobiol. Sci.* **9**, 734–743.
205. Gaio, E., D. Scheglmann, E. Reddi and F. Moret (2016) Uptake and photo-toxicity of Foscan®, Foslip® and Fospeg® in multicellular tumor spheroids. *J. Photochem. Photobiol. B Biol.* **161**, 244–252.
206. Etcheverry, M. E., M. A. Pasquale, C. Bergna, C. Ponzinibbio and M. Garavaglia (2020) Photodynamic therapy in 2D and 3D human cervical carcinoma cell cultures employing LED light sources emitting at different wavelengths. *Phys. Med. Biol.* **65**, 015017.
207. Wright, K. E., E. Liniker, M. Loizidou, C. Moore, A. J. MacRobert and J. B. Phillips (2009) Peripheral neural cell sensitivity to mTHPC-mediated photodynamic therapy in a 3D *in vitro* model. *Br. J. Cancer* **101**, 658–665.
208. Kukcinaviciute, E., A. Sasnauskiene, D. Dabkeviciene, V. Kirveliene and V. Jonusiene (2017) Effect of mTHPC-mediated photodynamic therapy on 5-fluorouracil resistant human colorectal cancer cells. *Photochem. Photobiol. Sci.* **16**, 1063–1070.
209. Wu, R. W. K., C. M. N. Yow, E. Law, E. S. M. Chu and Z. Huang (2020) Effect of Foslip® mediated photodynamic therapy on 5-fluorouracil resistant human colorectal cancer cells. *Photodiagn. Photodyn. Ther.* **31**, 101945.
210. Yakavets, I., I. Yankovsky, M. Millard, L. Lamy, H.-P. Lassalle, A. Wiehe, V. Zorin and L. Bezdetnaya (2017) The alteration of temoporfin distribution in multicellular tumor spheroids by β-cyclodextrins. *Int. J. Pharm.* **529**, 568–575.
211. Millard, M., I. Yakavets, M. Piffoux, A. Brun, F. Gazeau, J.-M. Guigner, J. Jasniewski, H.-P. Lassalle, C. Wilhelm and L. Bezdetnaya (2018) mTHPC-loaded extracellular vesicles outperform liposomal and free mTHPC formulations by an increased stability, drug delivery efficiency and cytotoxic effect in tridimensional model of tumors. *Drug Deliv.* **25**, 1790–1801.
212. Millard, M., S. Posty, M. Pioux, J. Jasniewski, H.-P. Lassalle, I. Yakavets, F. Gazeau, C. Wilhelm, A. K. A. Silva and L. Bezdetnaya (2020) mTHPC-loaded extracellular vesicles significantly improve mTHPC diffusion and photodynamic activity in preclinical models. *Pharmaceutics* **12**, 676.
213. Srdanović, S. Y.-H., D.-Y. Gao, Y.-J. Chen, D. M. Yan and Z.-L. Chen (2018) The photodynamic activity of 13^1-[2′-(2-pyridyl) ethylamine] chlorin e_6 photosensitizer in human esophageal cancer. *Bioorg. Med. Chem. Lett.* **28**, 1785–1791.
214. Wu, J., S. Feng, W. Liu, F. Gao and Y. Chen (2017) Targeting integrin-rich tumors with temoporfin-loaded vitamin-E-succinate-grafted chitosan oligosaccharide/D-α-tocopheryl polyethylene glycol 1000 succinate nanoparticles to enhance photodynamic therapy efficiency. *Int. J. Pharm.* **528**, 287–298.
215. Bombelli, C., A. Stringaro, S. Borocci, G. Bozzuto, M. Colone, L. Giansanti, R. Sgambato, L. Toccaceli, G. Mancini and A. Molinari (2010) Efficiency of liposomes in the delivery of a photosensitizer controlled by the stereochemistry of a gemini surfactant component. *Mol. Pharm.* **7**, 130–137.
216. Silva, A. K. A., N. Luciani, F. Gazeau, K. Aubertin, S. Bonneau, C. Chauvierre, D. Letourneur and C. Wilhelm (2015) Combining magnetic nanoparticles with cell derived microvesicles for drug loading and targeting. *Nanomed: Nanotechnol. Biol. Med.* **11**, 645–655.
217. Meier, D., S. M. Botter, C. Campanile, B. Robl, S. Gräfe, G. Pellegrini, W. Born and B. Fuchs (2017) Foscan and foslip based photodynamic therapy in osteosarcoma in vitro and in intratibial mouse models. *Int. J. Cancer* **140**, 1680–1692.
218. Reidy, K., C. Campanile, R. Muff, W. Born and B. Fuchs (2012) mTHPC-mediated photodynamic therapy is effective in the metastatic human 143B osteosarcoma cells. *Photochem. Photobiol.* **88**, 721–727.
219. Yakavets, I., A. Francois, L. Lamy, M. Piffoux, F. Gazeau, C. Wilhelm, V. Zorin, A. K. A. Silva and L. Bezdetnaya (2021) Effect of stroma on the behavior of temoporfin-loaded lipid nanovesicles inside the stroma-rich head and neck carcinoma spheroids. *NanoBiotechnology* **19**, 3.
220. Yakavets, I., S. Jenard, A. Francois, Y. Maklygina, V. Loschenov, H.-P. Lassalle, G. Dolivet and L. Bezdetnaya (2019) Stroma-rich co-culture multicellular tumor spheroids as a tool for photoactive drugs screening. *J. Clin. Med.* **8**, 1686.
221. Yakavets, I., C. Guereschi, L. Lamy, I. Kravchenko, H.-P. Lassalle, V. Zorinc and L. Bezdetnayaa (2020) Cyclodextrin nanosponge as a temoporfin nanocarrier: Balancing between accumulation and penetration in 3D tumor spheroids. *Eur. J. Pharm. Biopharm.* **154**, 33–42.
222. Pfitzner, M., A. Preuß and B. Röder (2020) A new level of in vivo singlet molecular oxygen luminescence measurements. *Photodiagn. Photodyn. Ther.* **29**, 101613.
223. Hinger, D., F. Navarro, A. Käch, J.-S. Thomann, F. Mittler, A.-C. Couffin and C. Maake (2016) Photoinduced effects of m-tetrahydroxyphenylchlorin loaded lipid nanoemulsions on multicellular tumor spheroids. *J. Nanobiotechnol.* **14**, 68.
224. Sun, L., J.-e. Zhou, T. Luo, J. Wang, L. Kang, Y. Wang, S. Luo, Z. Wang, Z. Zhou, J. Zhu, J. Yu, L. Yu and Z. Yan (2022) Nano-engineered neutrophils as cellular sonosensitizer for visual sonodynamic therapy of malignant tumors. *Adv. Mater.* **34**, e2109969.
225. Wright, K. E., A. J. MacRobert and J. B. Phillips (2012) Inhibition of specific cellular antioxidant pathways increases the sensitivity of neurons to meta-tetrahydroxyphenyl chlorin-mediated photodynamic therapy in a 3D co-culture model. *Photochem. Photobiol.* **88**, 1539–1545.
226. Elberskirch, L., R. Le Harzic, D. Scheglmann, G. Wieland, A. Wiehe, M. Mathieu-Gaedke, H. R. A. Golf, H. von Briesen and S. Wagner (2022) A HET-CAM based vascularized intestine tumor model as a screening platform for nano-formulated photosensitizers. *Eur. J. Pharm. Sci.* **168**, 106046.
227. Hasanin, M. S., M. Abdelraof, M. Fikry, Y. M. Shaker, A. M. K. Sweed and Senge (2021) Development of antimicrobial laser-induced photodynamic therapy based on ethylcellulose/chitosan nanocomposite with 5,10,15,20-Tetrakis(*m*-Hydroxyphenyl)porphyrin. *Molecules* **26**, 3551.

228. De Sordi, L., M. A. Butt, H. Pye, D. Kohoutova, C. A. Mosse, G. Yahioglu, I. Stamati, M. Deonarain, S. Battah, D. Ready, E. Allan, P. Mullany and L. B. Lovat (2015) Development of photodynamic antimicrobial chemotherapy (PACT) for clostridium difficile. *PLoS One* **10**, e0135039.
229. Kranz, S., A. Guellmar, A. Völpel, B. Gitter, V. Albrecht and B. W. Sigusch (2011) Photodynamic suppression of *Enterococcus faecalis* using the photosensitizer mTHPC. *Lasers Surg. Med.* **43**, 241–248.
230. Sigusch, B. W., S. Dietsch, A. Berg, A. Voelpel, A. Guellmar, U. Rabe, M. Schnabelrauch, D. Steen, B. Gitter, V. Albrecht, D. C. Watts and S. Kranz (2018) Antimicrobial photodynamic active biomaterials for periodontal regeneration. *Dental Mater.* **34**, 1542–1554.
231. Yang, K., B. Gitter, R. Rüger, G. D. Wieland, M. Chen, X. Liu, V. Albrecht and A. Fahr (2011) Antimicrobial peptide-modified liposomes for bacteria targeted delivery of temoporfin in photodynamic antimicrobial chemotherapy. *Photochem. Photobiol. Sci.* **10**, 1593–1601.
232. Yang, K., B. Gitter, R. Rüger, V. Albrecht, G. D. Wieland and A. Fahr (2012) Wheat germ agglutinin modified liposomes for the photodynamic inactivation of bacteria. *Photochem. Photobiol.* **88**, 548–556.
233. Hampden-Martin, A., J. Fothergill, M. El Mohtadi, L. Chambers, A. J. Slate, K. A. Whitehead and K. Shokrollahi (2021) Photodynamic antimicrobial chemotherapy coupled with the use of the photosensitizers methylene blue and temoporfin as a potential novel treatment for *Staphylococcus aureus* in burn infections. *Access Microbiol.* **3**, 000273.
234. Engelhardt, V., B. Krammer and K. Plaetzer (2010) Antibacterial photodynamic therapy using water-soluble formulations of hypericin or mTHPC is effective in inactivation of *Staphylococcus aureus*. *Photochem. Photobiol. Sci.* **9**, 365–369.
235. Lüthi, M., E. Besic Gyenge, M. Engström, M. Bredell, K. Grätz, H. Walt, R. Gmür and C. Maake (2009) Hypericin- and mTHPC-mediated photodynamic therapy for the treatment of cariogenic bacteria. *Med. Laser Appl.* **24**, 227–236.
236. Ryan, S.-L., A.-M. Baird, G. Vaz, A. J. Urquhart, M. O. Senge, D. J. Richard, K. J. O'Byrne and A. M. Davies (2016) Drug discovery approaches utilizing three-dimensional cell culture. *Assay Drug Dev. Technol.* **14**, 19–28.
237. Ravi, M., V. Paramesh, S. R. Kaviya, E. Anuradha and F. D. P. Solomon (2015) 3D cell culture systems: Advantages and applications. *J. Cell. Physiol.* **230**, 16–26.
238. Niehoff, C., J. Grünebaum, A. Moosmann, D. Mulac, J. Söbbing, R. Niehaus, R. Buchholz, S. Kröger, A. Wiehe, S. Wagner, M. Sperling, H. von Briesen, K. Langer and U. Karst (2016) Quantitative bioimaging of platinum group elements in tumor spheroids. *Anal. Chim. Acta* **938**, 106–113.
239. Boutros, M., F. Heigwer and C. Laufer (2015) Microscopy-based high-content screening. *Cell* **163**, 1314–1325.
240. Vaz, G. M. F., E. Paszko, A. M. Davies and M. O. Senge (2013) High content screening as high quality assay for biological evaluation of photosensitizers in vitro. *PLoS One* **8**, e70653.
241. Lai, Y.-C., S.-Y. Su and C.-C. Chang (2013) Special reactive oxygen species generation by a highly photostable BODIPY-based photosensitizer for selective photodynamic therapy. *ACS Appl. Mater. Interfaces* **5**, 12935–12943.
242. Gariboldi, M. B., E. Marras, I. Vaghi, A. Margheritis, M. C. Malacarne and E. Caruso (2021) Phototoxicity of two positive-charged diaryl porphyrins in multicellular tumor spheroids. *J. Photochem. Photobiol. B Biol.* **225**, 112353.
243. Marydasan, B., R. R. Nair, P. S. S. Babu, D. Ramaiah and S. A. Nair (2019) Picolyl porphyrin nanostructures as a functional drug entrant for photodynamic therapy in human breast cancers. *ACS Omega* **4**, 12808–12816.
244. Ghazal, B., M. Machacek, M. A. Shalaby, V. Novakova, P. Zimcik and S. Makhseed (2017) Phthalocyanines and tetrapyrazinoporphyrazines with two cationic donuts: high photodynamic activity as a result of rigid spatial arrangement of peripheral substituents. *J. Med. Chem.* **60**, 6060–6076.
245. Gunaydin, G., M. E. Gedik and S. Aylan (2021) Photodynamic therapy – current limitations and novel approaches. *Front. Chem.* **9**, 691697.
246. Kessel, D. (2020) Photodynamic therapy: apoptosis, paraptosis and beyond. *Apoptosis* **25**, 611–615.
247. Kessel, D. (2020) Paraptosis and photodynamic therapy: A progress report. *Photochem. Photobiol.* **96**, 1096–1100.
248. Kessel, D. and N. L. Oleinick (2018) Cell death pathways associated with photodynamic therapy: An update. *Photochem. Photobiol.* **94**, 213–218.
249. Mishchenko, T., I. Balalaeva, A. Gorokhova, M. Vedunova and D. V. Krysko (2022) Which cell death modality wins the contest for photodynamic therapy of cancer? *Cell Death Dis.* **13**, 455.
250. Mokoena, D. R., B. P. George and H. Abrahamse (2021) Photodynamic therapy induced cell death mechanisms in breast cancer. *Int. J. Mol. Sci.* **22**, 10506.
251. Castano, A. P., T. N. Demidova and M. R. Hamblin (2005) Mechanisms in photodynamic therapy: Part three – Photosensitizer pharmacokinetics, biodistribution, tumor localization and modes of tumor destruction. *Photodiagn. Photodyn. Ther.* **2**, 91–106.
252. Castano, A. P., P. Mroz and M. R. Hamblin (2006) Photodynamic therapy and anti-tumour immunity. *Nat. Rev. Cancer* **6**, 535–545.
253. Wachowska, M., A. Muchowicz and U. Demkow (2015) Immunological aspects of antitumor photodynamic therapy outcome. *Centr. Eur. J. Immunol.* **40**, 481–485.
254. Theodoraki, M. N., K. Lorenz, R. Lotfi, D. Fürst, C. Tsamadou, S. Jaekle, J. Mytilineos, C. Brunner, J. Theodorakis, T. K. Hoffmann, S. Laban and P. J. Schuler (2017) Influence of photodynamic therapy on peripheral immune cell populations and cytokine concentrations in head and neck cancer. *Photodiagn. Photodyn. Ther.* **19**, 194–201.
255. Dabrowski, J. M. and L. G. Arnaut (2015) Photodynamic therapy (PDT) of cancer: From local to systemic treatment. *Photochem. Photobiol. Sci.* **14**, 1765–1780.
256. Nath, S., G. Obaid and T. Hasan (2019) The course of immune stimulation by photodynamic therapy: Bridging fundamentals of photochemically induced immunogenic cell death to the enrichment of T-cell repertoire. *Photochem. Photobiol.* **95**, 1288–1305.
257. Tan, L., X. Shen, Z. He and Y. Lu (2022) The role of photodynamic therapy in triggering cell death and facilitating antitumor immunology. *Front. Oncol.* **12**, 863107.
258. De Vetta, M., O. Baig, D. Steen, J. J. Nogueira and L. González (2018) Assessing configurational sampling in the quantum mechanics/molecular mechanics calculation of temoporfin absorption spectrum and triplet density of states. *Molecules* **23**, 2932.
259. De Vetta, M., L. Gonzalez and J. J. Nogueira (2018) Hydrogen bonding regulates the rigidity of liposome-encapsulated chlorin photosensitizers. *ChemistryOpen* **7**, 475–483.
260. Araujo, V. d. J., H. J. Soscún and L. J. Rodríguez (2009) Theoretical study of the linear and nonlinear optical properties of the Photosensibilizer molecules: Photofrin and foscan in gas phase. *J. Computat. Methods Sci. Eng.* **9**, 313–322.
261. Atif, M. (2012) Two-photon cross-section measurement of meso-tetra-hydroxyphenyl-chlorin using femtosecond laser pulses. *Opt. Spectrosc.* **112**, 763–766.
262. Hamed, B., T. V. Haimberger, V. Kozich, A. Wiehe and K. Heyne (2014) Two-photon cross-sections of the photosensitizers m-THPC and m-THPP in the 1.05–1.45 μm range. *J. Photochem. Photobiol. A Chem.* **295**, 53–56.
263. Ferreira, J., P. F. C. Menezes, C. H. Sibata, R. R. Allison, S. Zucoloto, O. CastroeSilva and V. S. Bagnato (2009) Can efficiency of the photosensitizer be predicted by its photostability in solution? *Laser Phys.* **19**, 1932–1938.
264. Mitra, S. and T. H. Foster (2005) Photophysical parameters, photosensitizer retention and tissue optical properties completely account for the higher photodynamic efficacy of meso-tetrahydroxyphenylchlorin vs. *Photofrin. Photochem. Photobiol.* **81**, 849–859.
265. Mojzisova, H., S. Bonneau, P. Maillard, K. Berg and D. Brault (2009) Photosensitizing properties of chlorins in solution and in membrane-mimicking systems. *Photochem. Photobiol. Sci.* **8**, 778–787.
266. Mu, C., J. Wang, K. M. Barraza, X. Zhang and J. L. Beauchamp (2019) Mass spectrometric study of acoustically levitated droplets illuminates molecular-level mechanism of photodynamic therapy for cancer involving lipid oxidation. Angew. Chem. 131, 8166–8170. *Angew. Chem. Int. Ed.* **58**, 8028–8086.
267. Mu, C., W. Wang, J. Wang, C. Gong, D. Zhang and X. Zhang (2020) Probe-free direct identification of type I and type II

photosensitized oxidation using field-induced droplet ionization mass spectrometry. Angew. Chem. 132, 21699–21703. *Angew. Chem. Int. Ed.* **59**, 21515–21519.
268. Geng, W.-C., D. Zhang, C. Gong, Z. Li, K. M. Barraza, J. L. Beauchamp, D.-S. Guo and X. Zhang (2020) Host–guest complexation of amphiphilic molecules at the air–water interface prevents oxidation by hydroxyl radicals and singlet oxygen. Angew. Chem. 132, 12784-12788. *Angew. Chem. Int. Ed.* **59**, 12684–12688.
269. Teiten, M.-H., L. Bezdetnaya, P. Morliere, R. Santus and F. Guillemin (2003) Endoplasmatic reticulum and Golgi apparatus are the preferential sites of Foscan® localisation in cultured tumour cells. *Br. J. Cancer* **88**, 146–152.
270. Kessel, D. (2011) Inhibition of endocytic processes by photodynamic therapy. *Lasers Surg. Med.* **43**, 542–547.
271. Kessel, D. (1999) Transport and localization of m-THPC in vitro. *Int. J. Clin. Pract.* **53**, 263–267.
272. Kaneko, K., T. Osada, M. A. Morse, W. R. Gwin, J. D. Ginzel, J. C. Snyder, X.-Y. Yang, C.-X. Liu, M. A. Diniz, K. Bodoor, P. F. Hughes, T. A. J. Haystead and H. K. Lyerly (2020) Heat shock protein 90-targeted photodynamic therapy enables treatment of subcutaneous and visceral tumors. *Commun. Biol.* **3**, 226.
273. Korbelik, M., W. Zhang and D. Separovic (2011) Amplification of cancer cell apoptosis in photodynamic therapy-treated tumors by adjuvant ceramide analog LCL29. *Lasers Surg. Med.* **43**, 614–620.
274. Korbelik, M., W. Zhang and D. Separovic (2012) Monitoring ceramide and sphingosine-1-phosphate levels in cancer cells and macrophages from tumours treated by photodynamic therapy. *Photochem. Photobiol. Sci.* **11**, 779–784.
275. Separovic, D., J. Bielawski, J. S. Pierce, S. Merchant, A. L. Tarca, G. Bhatti, B. Ogretmen and M. Korbelik (2011) Enhanced tumor cures after Foscan photodynamic therapy combined with the ceramide analog LCL29. Evidence from mouse squamous cell carcinomas for sphingolipids as biomarkers of treatment response. *Int. J. Oncol.* **38**, 521–527.
276. Falk-Mahapatra, R. and S. O. Golnick (2020) Photodynamic therapy and immunity: An update. *Photochem. Photobiol.* **96**, 550–559.
277. Gellén, E., E. Fidrus, M. Péter, A. Szegedi, G. Emri and E. Remenyik (2018) Immunological effects of photodynamic therapy in the treatment of actinic keratosis and squamous cell carcinoma. *Photodiagn. Photodyn. Ther.* **24**, 342–348.
278. Aniogo, E. C., B. P. George and H. Abrahamse (2021) Molecular Effectors of Photodynamic Therapy-Mediated Resistance to Cancer Cells. *Int. J. Mol. Sci.* **22**, 13182.
279. Information about replacement, reduction and refinement in animal experimentation on the EU level: Animals used for scientific purposes. Available at: https://ec.europa.eu/environment/chemicals/lab_animals/3r/alternative_en.htm. Retrieved May 2022.
280. Liu, Y., M. H. A. M. Fens, R. B. Capomaccio, D. Mehn, L. Scrivano, R. J. Kok, S. Oliveira, W. E. Hennink and C. F. van Nostrum (2020) Correlation between in vitro stability and pharmacokinetics of poly (ε-caprolactone)-based micelles loaded with a photosensitizer. *J. Control. Release* **328**, 942–951.
281. Peng, C.-L., H.-C. Lin, W.-L. Chiang, Y.-H. Shih, P.-F. Chiang, T.-Y. Luo, C.-C. Cheng and M.-J. Shieh (2018) Anti-angiogenic treatment (Bevacizumab) improves the responsiveness of photodynamic therapy in colorectal cancer. *Photodiagn. Photodyn. Ther.* **23**, 111–118.
282. Etcheverry, M. E., A. Pasquale Miguel, A. Gutiérrez, S. Bibé, C. Ponzinibbio, H. Poteca and M. Garavaglia (2018) Photodynamic therapy in fibrosarcoma BALB/c animal model: Observation of the rebound effect. *Photodiagn. Photodyn. Ther.* **21**, 98–107.
283. Hinger, D., S. Gräfe, F. Navarro, B. Spingler, D. Pandiarajan, H. Walt, A.-C. Couffin and C. Maake (2016) Lipid nanoemulsions and liposomes improve photodynamic treatment efficacy and tolerance in CAL-33 tumor bearing nude mice. *J. Nanobiotechnol.* **14**, 71.
284. Korbelik, M., J. Banáth and W. Zhang (2016) Mreg activity in tumor response to photodynamic therapy and photodynamic therapy-generated cancer vaccines. *Cancer* **8**, 94.
285. Zhu, T. C., B. Liu, M. M. Kim, D. McMillan, X. Liang, J. C. Finlay and T. M. Busch (2014) Comparison of singlet oxygen threshold dose for PDT. *Proc. SPIE* **8391**, 89310I.
286. Zhu, T. C., M. M. Kim, X. Liang, J. C. Finlay and T. M. Busch (2015) *In-vivo* singlet oxygen threshold doses for PDT. *Photon. Lasers Med* **4**, 59–71.
287. Xie, H., P. Svenmarker, J. Axelsson, S. Gräfe, M. Kyriazi, N. Bendsoe, S. Andersson-Engels and K. Svanberg (2015) Pharmacokinetic and biodistribution study following systemic administration of Fospeg® – A Pegylated liposomal mTHPC formulation in a murine model. *J. Biophotonics* **8**, 142–152.
288. Wilson, B. C., M. S. Patterson, B. Li and M. T. Jarvi (2015) Correlation of *in vivo* tumor response and singlet oxygen luminescence detection in mTHPC-mediated photodynamic therapy. *J. Innovat. Opt. Health Sci.* **8**, 1540006.
289. Reinhard, A., A. Bressenot, R. Dassonneville, A. Loywick, D. Hot, C. Audebert, S. Marchal, F. Guillemin, M. Chamaillard, L. Peyrin-Biroulet and L. Bezdetnaya (2015) Photodynamic therapy relieves colitis and prevents colitis-associated carcinogenesis in mice. *Inflamm. Bowel Dis.* **21**, 985–995.
290. Reshetov, V., H.-P. Lassalle, A. François, D. Dumas, S. Hupont, S. Gräfe, V. Filipe, W. Jiskoot, F. Guillemin, V. Zorin and L. Bezdetnaya (2013) Photodynamic therapy with conventional and PEGylated liposomal formulations of mTHPC (temoporfin): comparison of treatment efficacy and distribution characteristics in vivo. *Int. J. Nanomedicine* **8**, 3817–3831.
291. Petri, A., E. Alexandratou, M. Kyriazi, M. Rallis, V. Roussis and D. Yova (2012) Combination of Fospeg-IPDT and a natural antioxidant compound prevents photosensitivity in a murine prostate cancer tumour model. *Photodiagn. Photodyn. Ther.* **9**, 100–108.
292. Kroeze, S. G. C., M. C. M. Grimbergen, H. Rehmann, J. L. H. R. Bosch and J. J. M. Jans (2012) Photodynamic therapy as novel nephron sparing treatment option for small renal masses. *J. Urol.* **187**, 289–295.
293. Xie, H., H. Liu, P. Svenmarker, J. Axelsson, C. T. Xu, S. Gräfe, J. H. Lundeman, H. P. H. Cheng, S. Svanberg, N. Bendsoe, P. E. Andersen, K. Svanberg and S. Andersson-Engels (2011) Drug quantification in turbid media by fluorescence imaging combined with light-absorption correction using white Monte Carlo simulations. *J. Biomed. Opt.* **16**, 066002.
294. Garrier, J., L. Bezdetnaya, C. Barlier, S. Gräfe, F. Guillemin and M.-A. D'Hallewin (2011) Foslip®-based photodynamic therapy as a means to improve wound healing. *Photodiagn. Photodyn. Ther.* **8**, 321–327.
295. Aerts, I., P. Leuraud, J. Blais, A.-l. Pouliquen, P. Maillard, C. Houdayer, J. Couturier, X. Sastre-Garau, D. Grierson, F. Doza and M. F. Poupon (2010) In vivo efficacy of photodynamic therapy in three new xenograft models of human retinoblastoma. *Photodiagn. Photodyn. Ther.* **7**, 275–283.
296. Garrier, J., A. Bressenot, S. Gräfe, S. Marchal, S. Mitra, T. H. Foster, F. Guillemin and L. Bezdetnaya (2010) Compartmental targeting for mTHPC-based photodynamic treatment in vivo: Correlation of efficiency, pharmacokinetics, and regional distribution of apoptosis. *Int. J. Radiat. Oncol. Biol. Phys.* **78**, 563–571.
297. Canti, G., A. Calastretti, A. Bevilacqua, E. Reddi, G. Palumbo and A. Nicolin (2010) Combination of photodynamic therapy + immunotherapy + chemotherapy in murine leukiemia. *Neoplasma* **57**, 184–188.
298. Lassalle, H.-P., D. Dumas, S. Gräfe, M.-A. D'Hallewin, F. Guillemin and L. Bezdetnaya (2009) Correlation between in vivo pharmacokinetics, intratumoral distribution and photodynamic efficiency of liposomal mTHPC. *J. Control. Rel.* **134**, 118–124.
299. de Visscher, S. A. H. J., M. J. H. Witjes, B. van der Vegt, H. S. de Bruijn, A. van der Ploeg – van den Heuvel, A. Amelink, H. J. C. M. Sterenborg, J. L. N. Roodenburg and D. J. Robinson (2013) Localization of liposomal mTHPC formulations within normal epithelium, dysplastic tissue, and carcinoma of oral epithelium in the 4NQO-carcinogenesis rat model. *Lasers Surg. Med.* **45**, 668-678.
300. Wang, J.-d., J. Shen, X.-p. Zhou, W.-b. Shi, J.-h. Yan, F.-h. Luo and Z.-w. Quan (2013) Optimal treatment opportunity for mTHPC-mediated photodynamic therapy of liver cancer. *Lasers Med. Sci.* **28**, 1541-1548.
301. Bovis, M. J., J. H. Woodhams, M. Loizidou, D. Scheglmann, S. G. Bown and A. J. MacRobert (2012) Improved *in vivo* delivery of m-THPC via pegylated liposomes for use in photodynamic therapy. *J. Control. Release* **157**, 196–205.
302. de Visscher, S. A. H. J., S. Kaščáková, H. S. de Bruijn, A. van der Ploeg, A. Amelink, H. J. C. M. Sterenborg, D. J. Robinson, J. L. N. Roodenburg and M. J. H. Witjes (2011) Fluorescence

localization and kinetics of mTHPC and liposomal formulations of mTHPC in the window-chamber tumor model. *Lasers Surg. Med.* **43**, 528–536.
303. Kaščáková, S., S. de Visscher, B. Kruijt, H. S. de Bruijn, A. van der Ploeg-van, H. J. C. M. den Heuvel, M. J. H. Sterenborg, A. A. Witjes and D. J. Robinson (2011) In vivo quantification of photosensitizer fluorescence in the skin-fold observation chamber using dual-wavelength excitation and NIR imaging. *Lasers Med. Sci.* **26**, 789–801.
304. Kaščáková, S., S. de Visscher, B. Kruijt, H. S. de Bruijn, A. van der Ploeg, H. J. C. M. Sterenborg, M. J. H. Witjes, A. Amelink and D. J. Robinson (2009) In vivo quantification of mTHPC fluorescence in skinfold observation chamber using excitation and detection towards the near infrared region. *Proc. SPIE* **7380**, 738063.
305. Kruijt, B., S. Kascakova, H. S. de Bruijn, A. van der Ploeg-van den Heuvel, H. J. C. M. Sterenborg, D. J. Robinson and A. Amelink (2009) In vivo quantification of chromophore concentration using fluorescence differential path length spectroscopy. *J. Biomed. Opt.* **14**, 034022.
306. Kruijt, B., A. van der Ploeg-van den Heuvel, H. S. de Bruijn, H. J. C. M. Sterenborg, A. Amelink and D. J. Robinson (2009) Monitoring interstitial m-THPC-PDT in vivo using fluorescence and reflectance spectroscopy. *Lasers Surg. Med.* **41**, 653–664.
307. Ferraz, R. C. M. C., J. Ferreira, P. F. C. Menezes, C. H. Sibata, O. Castro e Silva and V. S. Bagnato (2009) Determination of threshold dose of photodynamic therapy to measure superficial necrosis. *Photomed. Laser Surg.* **27**, 93–99.
308. Swartling, J., O. V. Höglund, K. Hansson, F. Södersten, J. Axelsson and A.-S. Lagerstedt (2016) Online dosimetry for temoporfin-mediated interstitial photodynamic therapy using the canine prostate as model. *J. Biomed. Opt.* **21**, 28002.
309. Glanzmann, T. M., M. P. E. Zellweger, F. Borle, R. Conde, A. Radu, J.-P. Ballini, Y. Jaquet, R. Pilloud, H. van den Bergh, P. Monnier, S. Andrejevic-Blant and G. A. Wagnières (2009) Assessment of a sheep animal model to optimize photodynamic therapy in the oesophagus. *Lasers Surg. Med.* **41**, 643–652.
310. Flickinger, I., E. Gasymova, S. Dietiker-Moretti, A. Tichy and C. Rohrer Bley (2018) Evaluation of long-term outcome and prognostic factors of feline squamous cell carcinomas treated with photodynamic therapy using liposomal phosphorylated metatetra (hydroxylphenyl)chlorine. *J. Feline Med. Surg.* **20**, 1100–1104.
311. Reschke, C. (2012) Erfolgreiche Behandlung eines rezidivierenden equinen Sarkoids. Fallbericht einer kombinierten chirurgischen und photodynamischen Therapie. *Tierarztl. Prax.* **40**, 309–313.
312. Wang, K. K.-H., J. C. Finlay, T. M. Busch, S. M. Hahn and T. C. Zhu (2010) Explicit dosimetry for photodynamic therapy: macroscopic singlet oxygen modelling. *J. Biophotonics* **3**, 304–318.
313. Kępczyński, M., R. P. Pandian, K. M. Smith and B. Ehrenberg (2002) Do liposome-binding constants of porphyrins correlate with their measured and predicted partitioning between octanol and water? *Photochem. Photobiol.* **76**, 127–134.
314. Chauvin, B., B. I. Iorga, P. Chaminade, J.-L. Paul, P. Maillard, P. Prognon and A. Kasselouri (2013) Plasma distribution of tetraphenylporphyrin derivatives relevant for Photodynamic Therapy: Importance and limits of hydrophobicity. *Eur. J. Pharm. Biopharm.* **83**, 244–252.
315. Lucky, S. S., K. C. Soo and Y. Zhang (2015) Nanoparticles in photodynamic therapy. *Chem. Rev.* **115**, 1990–2042.
316. Mesquita, M. Q., C. J. Dias, S. Gamelas, M. Fardilha, M. G. M. S. Neves and M. A. F. Faustino (2018) An insight on the role of photosensitizer nanocarriers for Photodynamic Therapy. *Ann. Braz. Acad. Sci.* **90**, 1101–1130.
317. Douroumis, D. and A. Fahr (eds) (2012) *Drug Delivery Strategies for Poorly Water-Soluble Drugs*. Wiley, Weinheim, Germany.
318. Savjani, K. T., A. K. Gajjar and J. K. Savjani (2012) Drug solubility: Importance and enhancement techniques. *ISRN Pharm.* 195727.
319. Information about Foscan® on the EMA homepage: European Medicines Agency (2016). Foscan (temoporfin) (EMEA/H/C/000318). Available at: https://www.ema.europa.eu/en/documents/product-information/foscan-epar-product-information_en.pdf. Retrieved June 2022.
320. Yakavets, I., M. Millard, V. Zorin, H.-P. Lassalle and L. Bezdetnaya (2019) Current state of the nanoscale delivery systems for temoporfin-based photodynamic therapy: Advanced delivery strategies. *J. Control. Release* **304**, 268–287.
321. Jeon, G. and Y. T. Ko (2019) Enhanced photodyamic therapy via photosensitizer-loaded nanoparticles for cancer treatment. *J. Pharm. Investig.* **49**, 1–8.
322. Wicki, A., D. Witzigmann, V. Balasubramanian and J. Huwyler (2015) Nanomedicine in cancer therapy: Challenges, opportunities, and clinical applications. *J. Control. Rel.* **200**, 138–157.
323. Lee, D., S. Kwon, S.-y. Jang, E. Park, Y. Lee and H. Koo (2022) Overcoming the obstacles of current photodynamic therapy in tumors using nanoparticles. *Bioact. Mater.* **8**, 20–34.
324. Matsumura, Y. and H. Maeda (1986) A new concept for macromolecular therapeutics in cancer chemotherapy: mechanism of tumoritropic accumulation of proteins and the antitumor agent smancs. *Cancer Res.* **46**, 6387–6392.
325. Nasseri, B., E. Alizadeh, F. Bani, S. Davaran, A. Akbarzadeh, N. Rabiee, A. Bahadori, M. Ziaei, M. Bagherzadeh, M. R. Saeb, M. Mozafari and M. R. Hamblin (2022) Nanomaterials for photothermal and photodynamic cancer therapy. *Appl. Phys. Rev.* **9**, 11317.
326. Pivetta, T. P., C. E. A. Botteon, P. A. Ribeiro, P. D. Marcato and M. Raposo (2021) Nanoparticle systems for cancer phototherapy: An overview. *Nano* **11**, 3132.
327. Kumar, S. S. D. and H. Abrahamse (2021) Biocompatible nanocarriers for enhanced cancer photodynamic therapy applications. *Pharmaceutics* **13**, 1933.
328. Escudero, A., C. Carrillo-Carrión, M. C. Castillejos, E. Romero-Ben, C. Rosales-Barrios and N. Kiar (2021) Photodynamic therapy: Photosensitizers and nanostructures. *Mater. Chem. Front.* **5**, 3788.
329. Alsaab, H. O., M. S. Alghamdi, A. S. Alotaibi, R. Alzhrani, F. Alwuthaynani, Y. S. Althobaiti, A. H. Almaki, S. Sau and A. K. Iyer (2020) Progress in clinical trials of photodynamic therapy for solid tumors and the role of nanomedicine. *Cancer* **12**, 2793.
330. Qidwai, A. A., B. Nabi, S. Kotta, J. K. Narang, S. Baboota and J. Ali (2020) Role of nanocarriers in photodynamic therapy. *Photodiagn. Photodyn. Ther.* **30**, 101782.
331. Sztandera, K., M. Gorzkiewicz and B. Klajnert-Maculewicz (2019) Nanocarriers in photodynamic therapy—in vitro and in vivo studies. *WIREs Nanomed. Nanobiotechnol.* **12**, 1509.
332. Yaraki, M. T., B. Liu and Y. N. Tan (2022) Emerging strategies in enhancing singlet oxygen generation of nano-photosensitizers toward advanced phototherapy. *Nano-Micro Lett.* **14**, 123.
333. Ding, H., H. Yu, Y. Dong, R. Tian, G. Huang, D. A. Boothman, B. S. Sumer and J. Gao (2011) Photoactivation switch from type II to type I reactions by electron-rich micelles for improved photodynamic therapy of cancer cells under hypoxia. *J. Control. Release* **156**, 276–280.
334. Wieczorek, S., S. Vigne, T. Masini, D. Ponader, L. Hartmann, A. K. H. Hirsch and H. G. Börner (2015) Combinatorial screening for specific drug solubilizers with switchable release profiles. *Macromol. Biosci.* **15**, 82–89.
335. Wieczorek, S., T. Schwaar, M. O. Senge and H. G. Börner (2015) Specific drug formulation additives: revealing the impact of architecture and block length ratio. *Biomacromolecules* **16**, 3308–3312.
336. Khurana, B., P. Gierlich, A. Meindl, L. C. Gomes-da-Silva and M. O. Senge (2019) Hydrogels: Soft matters in photomedicine. *Photochem. Photobiol. Sci.* **18**, 2613–1656.
337. Saboktakin, M. R., R. M. Tabatabaie, P. Ostovarazar, A. Maharramov and M. A. Ramazanov (2012) Synthesis and characterization of modified starch hydrogels for photodynamic treatment of cancer. *Int. J. Biol. Macromol.* **51**, 544–549.
338. Belali, S., H. Savoie, J. M. O'Brien, A. A. Cafolla, B. O'Connell, A. R. Karimi, R. W. Boyle and M. O. Senge (2018) Synthesis and characterization of temperature-sensitive and chemically cross-linked poly(*N*-isopropylacrylamide)/Photosensitizer hydrogels for applications in photodynamic therapy. *Biomacromolecules* **19**, 1592–1601.
339. Brezaniova, I., J. Trousil, Z. Cernochova, V. Kral, M. Hruby, P. Stepanek and M. Slouf (2017) Self-assembled chitosan-alginate polyplex nanoparticles containing temoporfin. *Colloid Polym. Sci.* **295**, 1259–1270.
340. Sannikova, N. E., I. O. Timofeev, A. S. Chubarov, N. S. Lebedeva, A. S. Semeikin, I. A. Kirilyuk, Y. P. Tsentalovich, M. V. Fedin, E. G. Bagryanskaya and O. A. Krumkacheva (2020) Application of

EPR to porphyrin-protein agents for photodynamic therapy. *J. Photochem. Photobiol. B:Biol.* **211**, 112008.
341. Preuß, A., S. Hackbarth, M. Wacker, T. Knobloch, K. Langer and B. Röder (2010) Comprehensive in vitro investigations on biodegradable photosensitizer-nanoparticle delivery systems. *J. Control. Release* **148**, e117–e118.
342. Ramachandran, R., G. L. Malarvizhi, P. Chandran, N. Gupta, D. Menon, D. Panikar, S. Nair and M. Koyakutty (2014) A polymer-protein core-shell nanomedicine for inhibiting cancer migration followed by photo-triggered killing. *J. Biomed. Nanotechnol.* **10**, 1401–1415.
343. Li, L. and K. M. Huh (2014) Polymeric nanocarrier systems for photodynamic therapy. *Biomater. Res.* **18**, 19.
344. Cohen, E. M., H. Ding, C. W. Kessinger, C. Khemtong, J. Gao and B. D. Sumer (2010) Polymeric micelle nanoparticles for photodynamic treatment of head and neck cancer cells. *Otolaryngol. Head Neck Surg.* **143**, 109–115.
345. Xie, L., S. Beyer, V. Vogel, M. G. Wacker and W. Mäntele (2015) Assessing the drug release from nanoparticles: Overcoming the shortcomings of dialysis by using novel optical techniques and a mathematical model. *Int. J. Pharm.* **488**, 108–119.
346. Li, T. and L. Yan (2018) Functional polymer nanocarriers for photodynamic therapy. *Pharmaceuticals* **11**, 133.
347. Zabihi, F., H. Koeppe, K. Achazi, S. Hedtrich and R. Haag (2019) One-pot synthesis of poly(glycerol-co-succinic acid) nanogels for dermal delivery. *Biomacromolecules* **20**, 1867–1875.
348. Zhang, P., T. Han, H. Xia, L. Dong, L. Chen and L. Lei (2022) Advances in photodynamic therapy based on nanotechnology and its application in skin cancer. *Front. Oncol.* **12**, 836397.
349. Saneja, A., R. Kumar, D. Arora, S. Kumar, A. K. Panda and S. Jaglan (2018) Recent advances in near-infrared light-repsonsive nanocarriers for cancer therapy. *Drug Discov. Today* **23**, 1115–1125.
350. Sun, J., W. Birnbaum, J. Anderski, M.-T. Picker, D. Mulac, K. Langer and D. Kuckling (2018) Use of light-degradable aliphatic polycarbonate nanoparticles as drug carrier for photosensitizer. *Biomacromolecules* **19**, 4677–4690.
351. Anderski, J., L. Mahler, D. Mulac and K. Langer (2018) Mucus-penetrating nanoparticles: Promising drug delivery systems for the photodynamic therapy of intestinal cancer. *Eur. J. Pharm. Biopharm.* **129**, 1–9.
352. Mahlert, L., J. Anderski, D. Mulac and K. Langer (2019) The impact of gastrointestinal mucus on nanoparticle penetration – in vitro evaluation of mucus-penetrating nanoparticles for photodynamic therapy. *Eur. J. Pharm. Sci.* **133**, 28–39.
353. Dhaini, B., B. Kenzhebayeva, A. Ben-Mihoub, M. Gries, S. Acherar, F. Baros, N. Thomas, J. Daouk, H. Schohn, T. Hamieh and C. Frochot (2021) Peptide-conjugated nanoparticles for targeted photodynamic therapy. *Nano* **10**, 3089–3134.
354. Wieczorek, S., A. Dallmann, Z. Kochovski and H. G. Börner (2016) Advancing drug formulation additives toward precision additives with release mediating peptide interlayer. *J. Am. Chem. Soc.* **138**, 9349–9352.
355. Wieczorek, S., E. Krause, S. Hackbarth, B. Röder, A. K. H. Hirsch and H. G. Börner (2013) Exploiting specific interactions toward next-generation polymeric drug transporters. *J. Am. Chem. Soc.* **135**, 1711–1714.
356. Zabihi, F., S. Wieczorek, M. Dimde, S. Hedtrich, H. G. Börner and R. Haag (2016) Intradermal drug delivery by nanogel-peptide conjugates; specific and efficient transport of temoporfin. *J. Control. Release* **242**, 35–41.
357. Wieczorek, S., D. Remmler, T. Masini, Z. Kochovski, A. K. H. Hirsch and H. G. Börner (2017) Fine-tuning nanocarriers specifically toward cargo: A competitive study on solubilizing related photosensitizers for photodynamic therapy. *Bioconjug. Chem.* **28**, 760–767.
358. Celasun, S., D. Remmler, T. Schwaar, M. G. Weller, F. Du Prez and H. G. Börner (2019) Digging into the sequential space of thiolactone precision polymers: A combinatorial strategy to identify functional domains. Angew. Chem. 131, 1980-1984. *Angew. Chem. Int. Ed.* **58**, 1960–1964.
359. Maron, E., Z. Kochovski, R. N. Zuckermann and H. G. Börner (2020) Peptide-assisted design of peptoid sequences: One small step in structure and distinct leaps in functions. *ACS Macro Lett.* **9**, 233–237.
360. Arias, S., E. Maron and H. G. Börner (2021) Information-based design of polymeric drug formulation additives. *Biomacromolecules* **22**, 213–221.
361. Tsolekile, N., S. Nahle, N. Zikalala, S. Parani, E. H. M. Sakho, O. Joubert, M. C. Matoetoe, S. P. Songca and O. S. Oluwafemi (2020) Cytotoxicity, fluorescence tagging and gene-expression study of CuInS/ZnS QDS – meso (hydroxyphenyl) porphyrin conjugate against human monocytic leukemia cells. *Sci. Rep.* **10**, 4936.
362. Tsolekile, N., S. Parani, R. Maluleke, O. Joubert, M. C. Matoetoe, S. P. Songca and O. S. Oluwafemi (2021) Green synthesis of amino acid functionalized CuInS/ZnS-mTHPP conjugate for biolabeling application. *Dyes Pigments* **185B**, 108960.
363. Haupt, S., I. Lazar, H. Weitman, M. O. Senge and B. Ehrenberg (2015) Pdots, a new type of nanoparticle, bind to mTHPC via their lipid modified surface and exhibit very high FRET efficiency between the core and the sensitizer. *Phys. Chem. Chem. Phys.* **17**, 11412–11422.
364. Herrmann, I. K., M. J. A. Wood and G. Fuhrmann (2021) Extracellular vesicles as a next-generation drug delivery platform. *Nat. Nanotechnol.* **16**, 748–759.
365. Yakavets, I., H.-P. Lassalle, I. Yankovsky, F. Ingrosso, A. Monari, L. Bezdetnaya and V. Zorin (2018) Evaluation of temoporfin affinity to β-cyclodextrins assuming self-aggregation. *J. Photochem. Photobiol. A Chem.* **367**, 13–21.
366. Yakavets, I., I. Yankovsky, L. Bezdetnaya and V. Zorin (2017) Soret band shape indicates mTHPC distribution between β-cyclodextrins and serum proteins. *Dyes Pigments* **137**, 299–306.
367. Yakavets, I. V., I. V. Yankovsky, I. I. Khludeyev, H. P. Lassalle, L. N. Bezdetnaya and V. P. Zorin (2018) Optical methods for the analysis of the temoprofin (sic!) photosensitizer distribution between serum proteins and methyl-β-cyclodextrin nanocarriers in blood serum. *J. Appl. Spectrosc.* **84**, 1030–1036.
368. Aslanoglu, B., I. Yakavets, V. Zorin, H.-P. Lassalle, F. Ingrosso, A. Monari and S. Catak (2020) Optical properties of photodynamic therapy drugs in different environments: the paradigmatic case of temoporfin. *Phys. Chem. Chem. Phys.* **22**, 16956–16964.
369. Mihoub, A. B., Z. Youssef, L. Colombeau, V. Jouan-Hureaux, P. Arnoux, C. Frochot, R. Vanderesse and S. Acherar (2020) Inclusion complex *vs*. conjugation of hydrophobic photosensitizers with β-cyclodextrin: Improved disaggregation and photodynamic therapy efficacy against glioblastoma cells. *Mater. Sci. Eng.* **C 109**, 110604.
370. Yakavets, I., H.-P. Lassalle, D. Scheglmann, A. Wiehe, V. Zorin and L. Bezdetnaya (2018) Temoporfin-in-cyclodextrin-in-liposome—a new approach for anticancer drug delivery: The optimization of composition. *Nano* **2018**(8), 847.
371. Md, S., S. Haque, T. Madheswaran, F. Zeeshan, V. S. Meka, A. K. Radhakrishnan and P. Kesharwani (2017) Lipid based nanocarriers system for topical delivery of photosensitizers. *Drug Discov. Today* **22**, 1274–1283.
372. Petersen, S., A. Fahr and H. Bunjes (2010) Flow cytometry as a new approach to investigate drug transfer between lipid particles. *Mol. Pharm.* **7**, 350–363.
373. Dawoud, M. and F. M. Hashem (2014) Comparative study on the suitability of two techniques for measuring the transfer of lipophilic drug models from lipid nanoparticles to lipophilic acceptors. *AAPS Pharm. Sci. Tech.* **15**, 1551–1561.
374. Afonso, D., S. Valetti, A. Fraix, C. Bascetta, S. Petralia, S. Conoci, A. Feiler and S. Sortino (2017) Multivalent mesoporous silica nanoparticles photo-delivering nitric oxide with carbon dots as fluorescence reporters. *Nanoscale* **9**, 13404–13408.
375. Timor, R., H. Weitman, N. Waiskopf, U. Banin and B. Ehrenberg (2015) PEG-phospholipids coated quantum rods as amplifiers of the photosensitization process by FRET. *ACS Appl. Mater. Interfaces* **7**, 21107–21114.
376. Slingerland, M. H.-J. and H. Gelderbloom (2012) Liposomal drug formulations in cancer therapy: 15 years along the road. *Drug Discov. Today* **17**, 160–166.
377. Liu, P. G. and J. Zhang (2022) A review of liposomes as a drug delivery system: Current status of approved products, regulatory environments, and future perspectives. *Molecules* **27**, 1372.

378. Pattni, B. S., V. V. Chupin and V. P. Torchilin (2015) New developments in liposomal drug delivery. *Chem. Rev.* **115**, 10938–10966.
379. Weijer, R., M. Broekgaarden, M. Kos, R. van Vught, E. A. J. Rauws, E. Breukink, T. M. van Gulik, G. Storm and M. Heger (2015) Enhancing photodynamic therapy of refractory solid cancers: Combining second-generation photosensitizers with multi-targeted liposomal delivery. *J Photochem Photobiol C: Photochem Rev* **23**, 103–131.
380. Moghassemi, S., A. Dadashzadeh, R. B. Azevedo, O. Feron and C. A. Amorim (2021) Photodynamic cancer therapy using liposomes as an advanced vesicular photosensitizer delivery system. *J. Control. Release* **339**, 75–90.
381. Fahmy, S. A., H. M. E.-S. Azzazy and J. Schaefer (2021) Liposome photosensitizer formulations for effective cancer photodynamic therapy. *Pharmaceutics* **13**, 1345.
382. Sadasivam, M., P. Avci, G. K. Gupta, S. Lakshmanan, R. Chandran, Y.-Y. Huang, R. Kumar and M. R. Hamblin (2013) Self-assembled liposomal nanoparticles in photodynamic therapy. *Eur. J. Nanomed.* **5**, 115–129.
383. Skupin-Mrugalska, P., J. Piskorz, T. Goslinski, J. Mielcarek, K. Konopka and N. Düzgüneş (2013) Current status of liposomal porphyrinoid photosensitizers. *Drug Discov. Today* **18**, 776–784.
384. Dragicevic-Curic, N. and A. Fahr (2012) Liposomes in topical photodynamic therapy. *Expert Opin. Drug Deliv.* **9**, 1015–1032.
385. Paszko, E. and M. O. Senge (2012) Immunoliposomes. *Curr. Med. Chem.* **19**, 5239–5277.
386. Cheng, X., J. Gao, Y. Ding, Y. Lu, Q. Wei, D. Cui, J. Fan, X. Li, E. Zhu, Y. Lu, Q. Wu, L. Li and W. Huang (2021) Multifunctional liposome: a powerful theranostic nano-platform enhancing photodynamic therapy. *Adv. Sci.* **8**, 2100876.
387. Information about Visudyne® on the EMA homepage: European Medicines Agency (2020). Visudyne (verteporfin) (EMEA/H/C/000305). Available at: https://www.ema.europa.eu/en/documents/product-information/visudyne-epar-product-information_en.pdf. Retrieved June 2022.
388. Dragicevic-Curic, N., D. Scheglmann, V. Albrecht and A. Fahr (2009) Development of liposomes containing ethanol for skin delivery of temoporfin: Characterization and in vitro penetration studies. *Colloids Surf. B Biointerfaces* **74**, 114–122.
389. Castro, D., M. Castro, M. Villafane, R. M. Gobbi and P. Cazzola (2009) Temoporfin liposomal formulation: a medical device to improve skin structure. *J. Plastic Dermatol.* **5**, 169–176.
390. Kuntsche, J., I. Freisleben, F. Steiniger and A. Fahr (2010) Temoporfin-loaded liposomes: Physicochemical characterization. *Eur. J. Pharm. Sci.* **40**, 305–315.
391. Decker, C., A. Fahr, J. Kuntsche and S. May (2012) Selective partitioning of cholesterol and a model drug into liposomes of varying size. *Chem. Phys. Lipids* **165**, 520–529.
392. Reshetov, V. A., T. E. Zorina, M.-A. D'Hallewin, L. N. Bolotina and V. P. Zorin (2011) Fluorescence methods for detecting the kinetics of photosensitizer release from nanosized carriers. *J. Appl. Spectrosc.* **78**, 103–109.
393. Kachatkou, D., S. Sasnouski, V. Zorin, T. Zorina, M.-A. D'Hallewin, F. Guillemin and L. Bezdetnaya (2009) Unusual photoinduced response of mTHPC liposomal formulation (Foslip). *Photochem. Photobiol.* **85**, 719–724.
394. Holzschuh, S., K. Kaeß, A. Fahr and C. Decker (2016) Quantitative in vitro assessment of liposome stability and drug transfer employing asymmetrical flow field-flow fractionation (AF4). *Pharm. Res.* **33**, 842–855.
395. Kaess, K. and A. Fahr (2014) Liposomes as solubilizers for lipophilic parenteral drugs: Transfer of drug and lipid marker to plasma proteins. *Eur. J. Lipid Sci. Technol.* **116**, 1137–1144.
396. Decker, C., F. Steiniger and A. Fahr (2013) Transfer of a lipophilic drug (temoporfin) between small unilamellar liposomes and human plasma proteins: Influence of membrane composition on vesicle integrity and release characteristics. *J. Liposome Res.* **23**, 154–165.
397. Kuntsche, J., C. Decker and A. Fahr (2012) Analysis of liposomes using asymmetrical flow field-flow fractionation: Separation conditions and drug/lipid recovery. *J. Sep. Sci.* **35**, 1993–2001.
398. Holzschuh, S., K. Kaeß, G. V. Bossa, C. Decker, A. Fahr and S. May (2018) Investigations of the influence of liposome composition on vesicle stability and drug transfer in human plasma: a transfer study. *J. Liposome Res.* **28**, 22–34.
399. Hinna, A., F. Steiniger, S. Hupfeld, M. Brandl and J. Kuntsche (2014) Asymmetrical flow field-flow fractionation with on-line detection for drug transfer studies: A feasibility study. *Anal. Bioanal. Chem.* **406**, 7827–7839.
400. Hinna, A. H., S. Hupfeld, J. Kuntsche, A. Bauer-Brandl and M. Brandl (2016) Mechanism and kinetics of the loss of poorly soluble drugs from liposomal carriers studied by a novel flow field-flow fractionation-based drug release−/transfer-assay. *J. Control. Release* **232**, 228–237.
401. Hinna, A. H., S. Hupfeld, J. Kuntsche and M. Brandl (2016) The use of asymmetrical flow field-flow fractionation with on-line detection in the study of drug retention within liposomal nanocarriers and drug transfer kinetics. *J. Pharm. Biomed. Anal.* **124**, 157–163.
402. Yang, K., J. T. Delaney, U. S. Schubert and A. Fahr (2011) Fast high-throughput screening of temoporfin-loaded liposomal formulations prepared by ethanol injection method. *J. Liposome Res.* **22**, 31–41.
403. Chen, M., X. Liu and A. Fahr (2011) Skin penetration and deposition of carboxyfluorescein and temoporfin from different lipid vesicular systems: In vitro study with finite and infinite dosage application. *Int. J. Pharm.* **408**, 223–234.
404. Hefesha, H., S. Loew, X. Liu, S. May and A. Fahr (2011) Transfer mechanism of temoporfin between liposomal membranes. *J. Control. Release* **150**, 279–286.
405. Loew, S., A. Fahr and S. May (2011) Modeling the release kinetics of poorly water-soluble drug molecules from liposomal nanocarriers. *J. Drug Deliv*. 376548.
406. Reshetov, V., D. Kachatkou, T. Shmigol, V. Zorin, M.-A. D'Hallewin, F. Guillemin and L. Bezdetnaya (2011) Redistribution of meta-tetra(hydroxyphenyl)chlorin (m-THPC) from conventional and PEGylated liposomes to biological substrates. *Photochem. Photobiol. Sci.* **10**, 911–919.
407. Reshetov, V., V. Zorin, A. Siupa, M.-A. D'Hallewin, F. Guillemin and L. Bezdetnaya (2012) Interaction of liposomal formulations of meta-tetra(hydroxyphenyl)chlorin (Temoporfin) with serum proteins: protein binding and liposome destruction. *Photochem. Photobiol.* **88**, 1256–1264.
408. Wallenwein, C. M., M. Villa Nov, C. Janas, L. Jablonka, G. F. Gao, M. Thurn, V. Albrecht, A. Wiehe and M. G. Wacker (2019) A dialysis-based in vitro drug release assay to study dynamics of the drug-protein transfer of temoporfin liposomes. *Eur. J. Pharm. Biopharm.* **143**, 44–50.
409. Decker, C., H. Schubert, S. May and A. Fahr (2013) Pharmacokinetics of temoporfin-loaded liposome formulations: Correlation of liposome and temoporfin blood concentration. *J. Control. Release* **166**, 277–285.
410. Park, K. (2013) Not all liposomes are created equal. *J. Control. Release* **166**, 316.
411. Jablonka, L., M. Ashtikar, G. F. Gao, M. Thurn, H. Modh, J.-W. Wang, A. Preuß, D. Scheglmann, V. Albrecht, B. Röder and M. G. Wacker (2020) Predicting human pharmacokinetics of liposomal temoporfin using a hybrid in silico model. *Eur. J. Pharm. Biopharm.* **149**, 121–134.
412. Nagpal, S., S. Branera, H. Modh, A. X. X. Tan, M.-P. Mast, K. Chichakly, V. Albrecht and M. G. Wacker (2020) A physiologically-based nanocarrier biopharmaceutics model to reverse-engineer the in vivo drug release. *Eur. J. Pharm. Biopharm.* **153**, 257–272.
413. Garrier, J., V. Reshetov, S. Gräfe, F. Guillemin, V. Zorin and L. Bezdetnaya (2014) Factors affecting the selectivity of nanoparticle-based photoinduced damage in free and xenografted chorioallantoïc membrane model. *J. Drug Target.* **22**, 220–231.
414. Gravier, J., B. Korchowiec, R. Schneider and E. Rogalska (2009) Interaction of amphiphilic chlorin-based photosensitizers with 1,2-dipalmitoyl-sn-glycero-3-phosphocholine monolayers. *Chem. Phys. Lipids* **158**, 102–109.
415. Massiot, J., A. Makky, F. Di Meo, D. Chapron, P. Trouillas and V. Rosilio (2017) Impact of lipid composition and photosensitizer hydrophobicity on the efficiency of light-triggered liposomal release. *Phys. Chem. Chem. Phys.* **19**, 11460–11473.

416. Dragicevic-Curic, N., S. Gräfe, B. Gitter, S. Winter and A. Fahr (2010) Surface charged temoporfin-loaded flexible vesicles: *In vitro* skin penetration studies and stability. *Int. J. Pharm.* **384**, 100–108.
417. Dragicevic-Curic, N., S. Winter, M. Stupar, J. Milic, D. Krajišnik, B. Gitter and A. Fahr (2009) Temoporfin-loaded liposomal gels: Viscoelastic properties and in vitro skin penetration. *Int. J. Pharm.* **373**, 77–84.
418. Dragicevic-Curic, N., S. Winter, D. Krajisnik, M. Stupar, J. Milic, S. Graefe and A. Fahr (2010) Stability evaluation of temoporfin-loaded liposomal gels for topical application. *J. Liposome Res.* **20**, 38–48.
419. Pathak, K., A. Vaidya and V. Sharma (2018) Confronting penetration threshold via fluidic terpenoid nanovesicles. *Curr. Drug Deliv.* **15**, 765–776.
420. Dragicevic-Curic, N., D. Scheglmann, V. Albrecht and A. Fahr (2009) Development of different temoporfin-loaded invasomes—novel nanocarriers of temoporfin: Characterization, stability and in vitro skin penetration studies. *Colloids Surf. B Biointerfaces* **70**, 198–206.
421. Dragicevic-Curic, N., M. Friedrich, S. Petersen, D. Scheglmann, D. Douroumis, W. Plass and A. Fahr (2011) Assessment of fluidity of different invasomes by electron spin resonance and differential scanning calorimetry. *Int. J. Pharm.* **412**, 85–94.
422. Ossmann, A., S. Kranz, G. Andre, A. Völpel, V. Albrecht, A. Fahr and B. W. Sigusch (2015) Photodynamic killing of *Enterococcus faecalis* in dentinal tubules using mTHPC incorporated in liposomes and invasomes. *Clin. Oral Investig.* **19**, 373–384.
423. Jablonka, L., M. Ashtikar, G. Gao, F. Jung, M. Thurn, A. Preuß, D. Scheglmann, V. Albrecht, B. Röder and M. G. Wacker (2019) Advanced in silico modeling explains pharmacokinetics and biodistribution of temoporfin nanocrystals in humans. *J. Control. Release* **308**, 57–70.
424. Di Bari, I., G. Granata, G. M. L. Consoli and S. Sortino (2018) Simultaneous supramolecular activation of NO photodonor/photosensitizer ensembles by a calix[4]arene nanoreactor. *New J. Chem.* **42**, 18096–18101.
425. Information about Foscan® on the EMA homepage: European Medicines Agency (2016). Foscan (temoporfin) (Pub. No. EMA/235463/2016). Available at: https://www.ema.europa.eu/en/documents/overview/foscan-epar-summary-public_en.pdf. Retrieved May 2022.
426. Gunaydin, G., M. E. Gedik and S. Ayan (2021) Photodynamic therapy for the treatment and diagnosis of cancer–A review of the current clinical status. *Front. Chem.* **9**, 686303.
427. van Straten, D., V. Mashayekhi, H. S. de Bruijn, S. Oliveira and D. J. Robinson (2017) Oncologic photodynamic therapy: Basic principles, current clinical status and future directions. *Cancer* **9**, 19.
428. Lebdai, S., P. Bigot, P.-A. Leroux, L.-P. Berthelot, P. Maulaz and A.-R. Azzouzi (2017) Vascular targeted photodynamic therapy with padeliporfin for low risk prostate cancer treatment: Midterm oncologic outcomes. *J. Urol.* **198**, 335–344.
429. Cruess, A. F., G. Zlateva, A. M. Pleil and B. Wirostko (2009) Photodynamic therapy with verteporfin in age-related macular degeneration: a systematic review of efficacy, safety, treatment modifications and pharmacoeconomic properties. *Acta Ophthalmol.* **87**, 118–132 Information about Visudyne® on the EMA homepage: European Medicines Agency (2016). Visudyne (verteporfin) (Pub. No. EMA/31239/2016). Available at: https://www.ema.europa.eu/en/documents/overview/visudyne-epar-summary-public_en.pdf. Retrieved May 2022
430. Morton, C. A., R.-M. Szeimies, N. Basset-Seguin, P. Calzavara-Pinton, Y. Gilberte, M. Haedersal, G. F. L. Hofbauer, R. E. hunger, S. Karrer, S. Piaserico, C. Ulrich, A.-M. Wennberg and L. R. Braathen (2019) European Dermatology Forum guidelines on topical photodynamic therapy 2019 Part 1: Treatment delivery and established indications – actinic keratoses, Bowen's disease and basal cell carcinomas. *J. Eur. Acad. Dermatol. Venereol.* **33**, 2225–2238 Information about Ameluz® on the EMA homepage: European Medicines Agency (2020). Ameluz (5-aminolevulinic acid hydrochloride), (Pub. No. EMA/80110/2020). https://www.ema.europa.eu/en/documents/overview/ameluz-epar-medicine-overview_en.pdf. Retrieved May 2022
431. Information about the marketing authorization procedures with the EMA: EMA – Human Regulatory – Marketing Authorization. https://www.ema.europa.eu/en/human-regulatory/marketing-authorisation. Retrieved May 2022.
432. Broekx, S., F. Weyns and S. De Vleeschouwer (2020) 5-Aminolevulinic acid for recurrent malignant gliomas: A systematic review. *Clin. Neurol. Neurosurg.* **195**, 105913 Information about Gliolan® on the EMA homepage: European Medicines Agency (2007). Ameluz (5-aminolevulinic acid hydrochloride), (EMEA/H/C/744). Available at: https://www.ema.europa.eu/en/documents/overview/gliolan-epar-summary-public_en.pdf. Retrieved May 2022
433. Information about orphan drugs in the EU: EMA – Human Regulatory – Orphan Designation: Overview. Available at: https://www.ema.europa.eu/en/human-regulatory/overview/orphan-designation-overview. Retrieved May 2022.
434. de Pinillos Bayona, A. M., C. M. Moore, M. Loizidou, A. J. MacRobert and J. H. Woodhams (2016) Enhancing the efficacy of cytotoxic agents for cancer therapy using photochemical internalization. *Int. J. Cancer* **138**, 1049–1057 Information about Amphinex® on the EMA homepage: European Medicines Agency (2016). Fimaporfin, (EU/3/16/1720). Available at: https://www.ema.europa.eu/en/documents/orphan-designation/eu/3/16/1720-public-summary-opinion-orphan-designation-fimaporfin-treatment-cholangiocarcinoma_en.pdf. Retrieved May 2022.
435. Trojan, J., A. Hoffmeister, B. Neu, S. Kasper, A. Dechene, C. Jürgensen, J. Schirra, R. Jakobs, D. Palmer, P. Selbo, H. Olivecrona, L. Finnesand, A. Hogset, P. Walday and R. Sturgess (2022) Photochemical internalization of gemcitabine is safe and effective in locally advanced inoperable cholangiocarcinoma. *Oncologist* **27**, 430–433.
436. Baskaran, R., J. Lee and S.-G. Yang (2018) Clinical development of photodynamic agents and therapeutic applications. *Biomater. Res.* **22**, 303–310.
437. dos Santos, F. A., D. R. Queiroz de Almeida, L. F. Terra, M. S. Baptista and L. Labriola (2019) Photodynamic therapy in cancer treatment – An update review. *J. Cancer Metastasis Treat.* **5**, 25.
438. Lobo, A. C. S., L. C. Gomes-da-Silva, P. Rodrigues-Santos, A. Cabrita, M. Santos-Rosa and L. G. Arnaut (2020) Immune responses after vascular photodynamic therapy with redaporfin. *J. Clin. Med.* **9**, 104.
439. Huggett, M. T., M. Jermyn, A. Gillams, R. Illing, S. Mosse, M. Novelli, E. Kent, S. G. Bown, T. Hasan, B. W. Pogue and S. P. Pereira (2014) Phase I/II study of verteporfin photodynamic therapy in locally advanced pancreatic cancer. *Br. J. Cancer* **110**, 1698–1704.
440. Correia, J. H., J. A. Rodrigues, S. Pimenta, T. Dong and Z. Yang (2021) Photodynamic therapy review: principles, photosensitizers, applications, and future directions. *Pharmaceutics* **13**, 1332.
441. Benov, L. (2015) Photodynamic therapy: Current status and future directions. *Med. Princ. Pract.* **24**(suppl 1), 14–28.
442. Yanovsky, R. L., D. W. Bartenstein, G. S. Rogers, S. J. Isakoff and S. T. Chen (2019) Photodynamic therapy for solid tumors: A review of the literature. *Photodermatol. Photoimmunol. Photomed.* **35**, 295–303.
443. Shi, X., C. Y. Zhang, J. Gao and Z. Wang (2019) Recent advances in photodynamic therapy for cancer and infectious diseases. *WIREs Nanomed. Nanobiotechnol.* **11**, e1560.
444. O'Connor, A. E., W. M. Gallagher and A. T. Byrne (2009) Porphyrin and nonporphyrin photosensitizers in oncology: Preclinical and clinical advances in photodynamic therapy. *Photochem. Photobiol.* **85**, 1053–1074.
445. Niculescu, A.-G. and A. M. Grumezescu (2021) Photodynamic therapy – An up-to-date review. *Appl. Sci.* **2021**(11), 3626.
446. Yang, M., T. Yang and C. Mao (2019) Enhancement of photodynamic cancer therapy by physical and chemical factors. Angew. Chem. 131, 14204-14219. *Angew. Chem. Int. Ed.* **58**, 14066–14080.
447. Mashayekhi, V., C. O.'t. Hoog and S. Oliveira (2019) Vascular targeted photodynamic therapy: A review of the efforts towards molecular targeting of tumor vasculature. *J. Porphyrins Phthalocyanines* **23**, 1229–1240.
448. Hessling, M., B. Lau and P. Vatter (2022) Review of virus inactivation by visible light. *Photo-Dermatology* **9**, 113.
449. Algorri, J. F., M. Ochoa, P. Roldán-Varona, L. Rodríguez-Cobo and J. M. López-Higuera (2021) Photodynamic therapy: A compendium of latest reviews. *Cancer* **13**, 04447.

450. Quirk, B. J., G. Brandal, S. Donlon, J. C. Vera, T. S. Mang, A. B. Foy, S. M. Lew, A. W. Girotti, S. Jogal, P. S. LaViolette, J. M. Connelly and H. T. Whelan (2015) Photodynamic therapy (PDT) for malignant brain tumors—Where do we stand? *Photodiagn. Photodyn. Ther.* **12**, 530–544.
451. Uzdensky, A. B., E. Berezhnaya, V. Kovaleva, M. Neginskaya, M. Rudkovskii and S. Sharifulina (2015) Photodynamic therapy: a review of applications in neurooncology and neuropathology. *J. Biomed. Opt.* **20**, 061108.
452. Wang, K., B. Yu and J. L. Pathak (2021) An update in clinical utilization of photodynamic therapy for lung cancer. *J. Cancer* **12**, 1154–1160.
453. Osuchowski, M., D. Bartusik-Aebisher, F. Osuchowski and D. Aebisher (2021) Photodynamic therapy for prostate cancer – A narrative review. *Photodiagn. Photodyn. Ther.* **33**, 102158.
454. Gheewala, T., T. Skwor and G. Munirathinam (2017) Photosensitizers in prostate cancer therapy. *Oncotarget* **8**, 30524–30538.
455. Moore, C. M., D. Pendse and M. Emberton (2009) Photodynamic therapy for prostate cancer – A review of current status and future promise. *Nat. Clin. Pract. Urol.* **6**, 18–30.
456. Davila, M. L. (2011) Photodynamic Therapy. *Gastrointest. Endosc. Clin. North. Am.* **21**, 67–79.
457. Gross, S. A. and H. C. Wolfsen (2010) The role of photodynamic therapy in the esophagus. *Gastrointest. Endosc. Clin. North. Am.* **20**, 35–53.
458. Pinto, A. and M. Pocard (2018) Photodynamic therapy and photothermal therapy for the treatment of peritoneal metastasis: A systematic review. *Pleura Peritoneum*, **3**, 20180124.
459. Lieder, A., M. K. Khan and B. M. Lippert (2014) Photodynamic therapy for recurrent respiratory papillomatosis. *Cochrane Database Syst. Rev.*, CD009810.
460. van der Snoek, E. M., J. C. den Hollander, J. B. Aans, H. J. C. M. Sterenborg, M. E. van der Ende and D. J. Robinson (2012) Photodynamic therapy with systemic meta-tetrahydroxyphenylchlorin in the treatment of anal intraepithelial neoplasia, grade 3. *Lasers Surg. Med.* **44**, 637–644.
461. Kruijt, B., E. M. van der Snoek, H. J. C. M. Sterenborg, A. Amelink and D. J. Robinson (2010) A dedicated applicator for light delivery and monitoring of PDT of intra-anal intraepithelial neoplasia. *Photodiagn. Photodyn. Ther.* **7**, 3–9.
462. van der Snoek, E. M., A. Amelink, M. E. van der Ende, J. C. den Hollander, J. G. den Hollander, F. P. Kroon, R. Vriesendorp, H. A. M. Neumann and D. J. Robinson (2009) Photodynamic therapy with topical metatetrahydroxychlorin (Fosgel) is ineffective for the treatment of anal intraepithelial neoplasia, grade III. *J. Acquir. Immune Defic. Syndr.* **52**, 141–143.
463. Kniebühler, G., T. Pongratz, C. S. Betz, B. Göke, R. Sroka, H. Stepp and J. Schirra (2013) Photodynamic therapy for cholangiocarcinoma using low dose mTHPC (Foscan®). *Photodiagn. Photodyn. Ther.* **10**, 220–228.
464. Stepp, H., G. Kniebühler, T. Pongratz, C. S. Betz, B. Göke, R. Sroka and J. Schirra (2013) Low dose mTHPC photodynamic therapy for cholangiocarcinoma. *Proc. SPIE* **8803**, 88030M.
465. Hauge, T., P. W. Hauge, T. Warloe, A. Drolsum, C. Johansen, E. Viktil, L. Aabakken, T. Buanes and Z. Konopski (2016) Randomised controlled trial of temoporfin photodynamic therapy plus chemotherapy in nonresectable biliary carcinoma – PCS Nordic study. *Photodiagn. Photodyn. Ther.* **13**, 330–333.
466. Wagner, A., U. W. Denzer, D. Neureiter, T. Kiesslich, A. Puespoeck, E. A. J. Rauws, K. Emmanuel, N. Degenhardt, U. Frick, U. Beuers, A. W. Lohse, F. Berr and G. W. Wolkersdörfer (2015) Temoporfin improves efficacy of photodynamic therapy in advanced biliary tract carcinoma: A multicenter prospective phase II study. *Hepatology* **62**, 1456–1465.
467. Kumta, N. A., K. DeRoche and M. Kahaleh (2015) Temoporfin photodynamic therapy in advanced hilar ductal carcinoma: A promising endoscopic modality. *Hepatology* **62**, 1342–1343.
468. Wagner, A., T. Kiesslich, D. Neureiter, P. Friesenbichler, A. Puespoek, U. W. Denzer, G. W. Wolkersdörfer, K. Emmanuel, A. W. Lohse and F. Berr (2013) Photodynamic therapy for hilar bile duct cancer: Clinical evidence for improved tumoricidal tissue penetration by temoporfin. *Photochem. Photobiol. Sci.* **12**, 1065–1073.
469. Nhembe, F., W. Jerjes, T. Upile, Z. Hamdoon and C. Hopper (2009) Chondrosarcoma of the hyoid treated with interstitial photodynamic therapy: Case study. *Photodiagn. Photodyn. Ther.* **6**, 235–237.
470. Vanaclocha, V., M. Sureda, I. Azinovic, J. Rebollo, R. Cañón, N. S. Sapena, F. G. Cases and A. Brugarolas (2015) Photodynamic therapy in the treatment of brain tumours. A feasibility study. *Photodiagn. Photodyn. Ther.* **12**, 422–427.
471. Swartling, J., J. Axelsson, G. Ahlgren, K. M. Kalkner, S. Nilsson, S. Svanberg, K. Svanberg and S. Andersson-Engels (2010) System for interstitial photodynamic therapy with online dosimetry: first clinical experiences of prostate cancer. *J. Biomed. Opt.* **15**, 058003.
472. Axelsson, J., J. Swartling and S. Andersson-Engels (2009) *In vivo* photosensitizer tomography inside the human prostate. *Opt. Lett.* **34**, 232–234.
473. Hamdoon, Z., W. Jerjes and C. Hopper (2020) Periorbital skin cancers subjected to mTHPC-photodynamic therapy: A prospective study. *Skin Res. Technol.* **26**, 338–342.
474. Jerjes, W., A. A. Yousif, Z. Hamdoon and C. Hopper (2019) Non-metastatic cutaneous squamous cell carcinoma treated with photodynamic therapy using intravenous mTHPC. *Photodiagn. Photodyn. Ther.* **28**, 172–176.
475. Jerjes, W., Z. Hamdoon and C. Hopper (2017) Photodynamic therapy in the management of basal cell carcinoma: Retrospective evaluation of outcome. *Photodiagn. Photodyn. Ther.* **19**, 22–27.
476. Horlings, R. K., J. B. Terra and M. J. H. Witjes (2015) mTHPC mediated, systemic photodynamic therapy (PDT) for nonmelanoma skin cancers: Case and literature review. *Lasers Surg. Med.* **47**, 779–787.
477. Betz, C. S., W. Rauschning, E. P. Stranadko, M. V. Riabov, V. N. Volgin, V. Albrecht, N. E. Nifantiev and C. Hopper (2012) Long-term outcomes following Foscan®-PDT of basal cell carcinomas. *Lasers Surg. Med.* **44**, 533–540.
478. Betz, C. S., W. Rauschning, E. P. Stranadko, M. V. Riabov, V. Albrecht, N. E. Nifantiev and C. Hopper (2009) Efficacy of low-dose mTHPC-PDT for the treatment of basal cell carcinomas. *Proc. SPIE* **7380**, 73800P.
479. Betz, C. S., W. Rauschning, E. P. Stranadko, M. V. Riabov, V. Albrecht, N. E. Nifantiev and C. Hopper (2008) Optimization of treatment parameters for Foscan-PDT of basal cell carcinomas. *Lasers Surg. Med.* **40**, 300–311.
480. Hamdoon, Z., W. Jerjes, T. Upile and C. Hopper (2011) Optical coherence tomography-guided photodynamic therapy for skin cancer: Case study. *Photodiagn. Photodyn. Ther.* **8**, 49–52.
481. Motta, S., L. Paravisi and M. Monti (2011) Italian dermatological experience on non-melanoma skin cancers (nmscs) with temoporfin-pdt. In *13th IPA World Congress Int. Proceedings, Medomond, Monduzzi Editore* (Edited by H. Kostron), pp. 135–138. 13th IPA World Congress, Innsbruck, Austria.
482. Jerjes, W., H. Stevenson, D. Ramsay, Z. Hamdoon and C. Hopper (2022) Quality of life following photodynamic therapy for head and neck pathologies: An exploratory study. *Photodiagn. Photodyn. Ther.* **38**, 102800.
483. Lambert, A., L. Nees, S. Nuyts, P. Clement, J. Meulemans, P. Delaere and V. Vander Poorten (2021) Photodynamic therapy as an alternative therapeutic tool in functionally inoperable oral and oropharyngeal carcinoma: A single tertiary center retrospective cohort analysis. *Front. Oncol.* **11**, 626394.
484. Jerjes, W., Z. Hamdoon, K. Berg, A. Høgset and C. Hopper (2020) Apparent complete response of a treatment refractory and recurrent squamous cell carcinoma lesion to photochemical internalization: A clinical case study. *Photochem. Photobiol.* **96**, 680–683.
485. van Doeveren, T. E. M., R. L. P. van Veen, F. van den Boom, I. B. Tan, W. H. Schreuder and M. B. Karakullukçu (2020) Intracavity Photodynamic Therapy for malignant tumors of the paranasal sinuses: An *in vivo* light dosimetry study. *Photodiagn. Photodyn. Ther.* **32**, 101972.
486. Stoker, S. D., S. R. Indrasari, C. Herdini, B. Hariwiyanto, B. Karakullukcu, W. Dhamiyati, K. Widayati, A. C. Romdhoni, R. Fles, S. M. Haryana, M. A. M. Wildeman and I. B. Tan (2015) Photodynamic therapy as salvage therapy for patients with nasopharyngeal carcinoma experiencing local failures following definitive radiotherapy. *Photodiagn. Photodyn. Ther.* **12**, 519–525.

487. Vander Poorten, V., J. Meulemans, S. Nuyts, P. Clement, R. Hermans, E. Hauben and P. Delaere (2015) Postoperative photodynamic therapy as a new adjuvant treatment after robot-assisted salvage surgery of recurrent squamous cell carcinoma of the base of tongue. *World J. Surg. Oncol.* **13**, 214–217.
488. Caesar, L., T. E. M. van Doeveren, I. B. Tan, A. Dilci, R. L. P. van Veen and B. Karakullukcu (2015) The use of Photodynamic Therapy as adjuvant therapy to surgery in recurrent malignant tumors of the paranasal sinuses. *Photodiagn. Photodyn. Ther.* **12**, 414–421.
489. von Beckerath, M. P., J. A. Reizenstein, A. L. Berner, K. W. O. Nordqvist, F. J. Landström, A. L. Löfgren and C. G. Möller (2014) Outcome of primary treatment of early laryngeal malignancies using photodynamic therapy. *Acta Otolaryngol.* **134**, 852–858.
490. Algharib, A. M. A., A. Sultana, J. Parekh, F. Vaz and C. Hopper (2014) Endoluminal tracheal stenting prior to head and neck PDT. *Photodiagn. Photodyn. Ther.* **11**, 444–446.
491. Succo, G., S. Rosso, G. L. Fadda, M. Fantini and E. Crosetti (2014) Salvage photodynamic therapy for recurrent nasopharyngeal carcinoma. *Photodiagn. Photodyn. Ther.* **11**, 63–70.
492. Karakullukcu, B., R. L. P. van Veen, J. B. Aans, O. Hamming-Vrieze, A. Navran, H. J. Teertstra, F. van den Boom, Y. Niatsetski, H. J. C. M. Sterenborg and I. B. Tan (2013) MR and CT based treatment planning for mTHPC mediated interstitial photodynamic therapy of head and neck cancer: Description of the method. *Lasers Surg. Med.* **45**, 517–523.
493. Story, W., A. A. Sultan, G. Bottini, F. Vaz, G. Lee and C. Hopper (2013) Strategies of airway management for head and neck photodynamic therapy. *Lasers Surg. Med.* **45**, 370–376.
494. de Visscher, S. A. H. J., L. J. Melchers, P. U. Dijkstra, B. Karakullukcu, I. B. Tan, C. Hopper, J. L. N. Roodenburg and M. J. H. Witjes (2013) mTHPC-mediated photodynamic therapy of early stage oral squamous cell carcinoma: A comparison to surgical treatment. *Ann. Surg. Oncol.* **20**, 3076–3082.
495. Durbec, M., A. Cosmidis, C. Fuchsmann, A. Ramade and P. Céruse (2013) Efficacy and safety of photodynamic therapy with temoporfin in curative treatment of recurrent carcinoma of the oral cavity and oropharynx. *Eur. Arch. Otorhinolaryngol.* **270**, 1433–1439.
496. Karakullukcu, B., S. D. Stoker, A. P. E. Wildeman, M. P. Copper, M. A. Wildeman and I. Bing Tan (2013) A matched cohort comparison of mTHPC-mediated photodynamic therapy and trans-oral surgery of early stage oral cavity squamous cell cancer. *Eur. Arch. Otorhinolaryngol.* **270**, 1093–1097.
497. Abbas, S., W. Jerjes, T. Upile, A. Vincent and C. Hopper (2012) Treatment of Kimura disease with photodynamic therapy: A case study. *Photodiagn. Photodyn. Ther.* **9**, 83–86.
498. Nyst, H. J., M. A. Wildeman, S. R. Indrasari, B. Karakullukcu, R. L. P. van Veen, M. Adham, F. A. Stewart, P. C. Levendag, H. J. C. M. Sterenborg and I. B. Tan (2012) Temoporfin mediated photodynamic therapy in patients with local persistent and recurrent nasopharyngeal carcinoma after curative radiotherapy: A feasibility study. *Photodiagn. Photodyn. Ther.* **9**, 274–281.
499. Indrasari, S. R., A. J. Timmermans, M. A. Wildeman, M. B. Karakullukcu, C. Herdini, B. Hariwiyanto and I. B. Tan (2012) Remarkable response to photodynamic therapy in residual T4N0M0 nasopharyngeal carcinoma: A case report. *Photodiagn. Photodyn. Ther.* **9**, 319–320.
500. Hamdoon, Z., W. Jerjes, R. Al-Delayme and C. Hopper (2012) Solitary giant neurofibroma of the neck subjected to photodynamic therapy: Case study. *Head Neck Oncol.* **4**, 30.
501. Abbas, S., W. Jerjes, T. Upile, F. Vaz and C. Hopper (2012) The palliative role of PDT in recurrent advanced nasopharyngeal carcinoma: Case series. *Photodiagn. Photodyn. Ther.* **9**, 142–147.
502. Karakullukcu, B., H. J. Nyst, R. L. van Veen, F. J. P. Hoebers, O. Hamming-Vrieze, M. J. H. Witjes, S. A. H. J. de Visscher, F. R. Burlage, P. C. Levendag, H. J. C. M. Sterenborg and I. B. Tan (2012) mTHPC mediated interstitial photodynamic therapy of recurrent nonmetastatic base of tongue cancers: Development of a new method. *Head Neck* **34**, 1597–1606.
503. Sardella, A., A. Carrassi, M. Tarozzi and G. Lodi (2011) Bisphosphonate-related osteonecrosis of the jaws associated with photodynamic therapy. *J. Oral Maxillofac. Surg.* **69**, e314–e316.
504. Jerjes, W., T. Upile, Z. Hamdoon, C. A. Mosse, S. Akram, S. Morley and C. Hopper (2011) Interstitial PDT for vascular anomalies. *Lasers Surg. Med.* **43**, 357–365.
505. Jerjes, W., T. Upile, H. Radhi and C. Hopper (2011) Photodynamic therapy and end-stage tongue base cancer: Short communication. *Head Neck Oncol.* **3**, 49.
506. Jerjes, W., T. Upile, Z. Hamdoon, S. Abbas, S. Akram, C. A. Mosse, S. Morley and C. Hopper (2011) Photodynamic therapy: The minimally invasive surgical intervention for advanced and/or recurrent tongue base carcinoma. *Lasers Surg. Med.* **43**, 283–292.
507. Jerjes, W., T. Upile, C. A. Mosse, Z. Hamdoon, M. Morcos, S. Morley and C. Hopper (2011) Prospective evaluation of 110 patients following ultrasound-guided photodynamic therapy for deep seated pathologies. *Photodiagn. Photodyn. Ther.* **8**, 297–306.
508. Karakullukcu, B., J. P. De Boer, R. Van Veen, J. Wegman and B. Tan (2011) Surgical debulking combined with photodynamic therapy to manage residual extramedullary plasmacytoma of the nasopharynx. *Photodiagn. Photodyn. Ther.* **8**, 264–266.
509. Jerjes, W., T. Upile, Z. Hamdoon, C. A. Mosse, M. Morcos and C. Hopper (2011) Photodynamic therapy outcome for T1/T2 N0 oral squamous cell carcinoma. *Lasers Surg. Med.* **43**, 463–469.
510. Jerjes, W., T. Upile, Z. Hamdoon, C. A. Mosse, S. Akram and C. Hopper (2011) Photodynamic therapy outcome for oral dysplasia. *Lasers Surg. Med.* **43**, 192–199.
511. Osher, J., W. Jerjes, T. Upile, Z. Hamdoon, S. Morley and C. Hopper (2011) Adenoid cystic carcinoma of the tongue base treated with ultrasound-guided interstitial photodynamic therapy: A case study. *Photodiagn. Photodyn. Ther.* **8**, 68–71.
512. Karakullukcu, B., K. van Oudenaarde, M. P. Copper, W. M. C. Klop, R. van Veen, M. Wildeman and I. B. Tan (2011) Photodynamic therapy of early stage oral cavity and oropharynx neoplasms: an outcome analysis of 170 patients. *Eur. Arch. Otorhinolaryngol.* **268**, 281–288.
513. Hamdoon, Z., W. Jerjes, T. Upile, P. Hoonjan and C. Hopper (2010) Endoluminal carotid stenting prior to photodynamic therapy to pericarotid malignant disease: Technical advance. *Photodiagn. Photodyn. Ther.* **7**, 126–128.
514. Robinson, D. J., B. Karakullukçu, B. Kruijt, S. C. Kanick, R. P. L. van Veen, A. Amelink, H. J. C. M. Sterenborg, M. J. Witjes and I. B. Tan (2010) Optical spectroscopy to guide photodynamic therapy of head and neck tumors. *IEEE J. Sel. Top. Quantum Electron.* **16**, 854–862.
515. Nhembe, F., W. Jerjes, T. Upile, Z. Hamdoon, F. Vaz and C. Hopper (2010) Subglottic carcinoma treated with surgery and adjuvant photodynamic therapy. *Photodiagn. Photodyn. Ther.* **7**, 284–287.
516. Tan, I. B., G. Dolivet, P. Ceruse, V. Vander Poorten, G. Roest and W. Rauschning (2010) Temoporfin-mediated photodynamic therapy in patients with advanced, incurable head and neck cancer: A multicenter study. *Head Neck* **32**, 1597–1604.
517. Hamdoon, Z., W. Jerjes, T. Upile, S. Akram and C. Hopper (2010) Cystic hygroma treated with ultrasound guided interstitial photodynamic therapy: Case study. *Photodiagn. Photodyn. Ther.* **7**, 179–182.
518. Lorenz, K. J. and H. Maier (2009) Photodynamic therapy with meta-tetrahydroxyphenylchlorin (Foscan®) in the management of squamous cell carcinoma of the head and neck: experience with 35 patients. *Eur. Arch. Otorhinolaryngol.* **266**, 1937–1944.
519. Jerjes, W., T. Upile, Z. Hamdoon, F. Nhembe, R. Bhandari, S. Mackay, P. Shah, C. A. Mosse, J. A. S. Brookes, S. Morley and C. Hopper (2009) Ultrasound-guided photodynamic therapy for deep seated pathologies: Prospective study. *Lasers Surg. Med.* **41**, 612–621.
520. Shah, P., W. Jerjes, T. Upile and C. Hopper (2010) The effective management of a leg hemangioma using ultrasound-guided interstitial photodynamic therapy. *Photodiagn. Photodyn. Ther.* **7**, 201–203.
521. Jerjes, W., T. Upile, A. Vincent, S. Abbas, P. Shah, C. A. Mosse, E. McCarthy, M. El-Maaytah, W. Topping, S. Morley and C. Hopper (2009) Management of deep-seated malformations with photodynamic therapy: A new guiding imaging modality. *Lasers Med. Sci.* **24**, 769–775.
522. Maillard, P., M. Lupu, C. D. Thomas and J. Mispelter (2010) Vers un nouveau traitement du rétinoblastome ? *Ann. Pharm. Fr.* **68**, 195–202.

523. Griffin, L. L. and J. T. Lear (2016) Photodynamic therapy and non-melanoma skin cancer. *Cancer* **8**, 98.
524. Wan, M. T. and J. Y. Lin (2014) Current evidence and applications of photodynamic therapy in dermatology. *Clinical Cosm. Invest. Dermatol.* **7**, 145–163.
525. Pessia, B., L. Romano, A. Giuliani, G. Lazzarin, F. Carlei and M. Schietroma (2020) Squamous cell anal cancer: Management and therapeutic options. *Ann. Med. Surg.* **55**, 36–46.
526. Moole, H., H. Tathireddy, S. Dharmapuri, V. Moole, R. Boddireddy, P. Yedama, S. Dharmapuri, A. Uppu, N. Bondalapati and A. Duvvuri (2017) Success of photodynamic therapy in palliating patients with nonresectable cholangiocarcinoma: A systematic review and meta-analysis. *World J. Gastroenterol.* **23**, 1278–1288.
527. Ortner, M.-A. (2011) Photodynamic therapy for cholangiocarcinoma. *Lasers Surg. Med.* **43**, 776–780.
528. Tomizawa, Y. and J. Tian (2012) Photodynamic therapy for unresectable cholangiocarcinoma. *Dig. Dis. Sci.* **57**, 274–283.
529. Shishkova, N., O. Kuznetsova and T. Berezov (2013) Photodynamic therapy in gastroenterology. *J. Gastrointest. Cancer* **44**, 251–259.
530. Ortner, M.-A. (2009) Photodynamic therapy for cholangiocarcinoma: Overview and new developments. *Curr. Opin. Gastroenterol.* **25**, 472–476.
531. Kiesslich, T., G. Wolkersdörfer, D. Neureiter, H. Salmhofer and F. Berr (2009) Photodynamic therapy for non-resectable perihilar cholangiocarcinoma. *Photochem. Photobiol. Sci.* **8**, 23–30.
532. Lee, T. Y., Y. K. Cheon and C. S. Shim (2013) Current status of photodynamic therapy for bile duct cancer. *Clin. Endosc.* **46**, 38–44.
533. Cheon, Y. K. (2021) Recent advances of photodynamic therapy for biliary tract cancer. *Int. J. Gastrointest. Interv.* **10**, 96–100.
534. Lange, C. and P. J. Bednarski (2016) Photosensitizers for photodynamic therapy: Photochemistry in the service of oncology. *Curr. Pharm. Design* **22**, 6956–6974.
535. Ibarra, A. M. C., R. B. Cecatto, L. J. Motta, A. L. dos Santos Franco, D. de F. Teixeira da Silva, F. D. Nunes, M. R. Hamblin and M. F. S. D. Rodrigues (2022) Photodynamic therapy for squamous cell carcinoma of the head and neck: Narrative review focusing on photosensitizers. *Lasers Med. Sci.* **37**, 1441-1470.
536. Lin, J., G. Ni, T. Ding, S. Lei, L. Zhong, N. Liu, K. Pan, T. Chen, X. Zeng, H. Xu, T. Li and H. Dan (2021) Photodynamic therapy for oral squamous cell carcinoma: A systematic review and meta-analysis. *Int. J. Photoenergy* **2021**, 6641358.
537. Biel, M. A. (2010) Photodynamic therapy of head and neck cancers. In *Methods in Molecular Biology*, Vol. **635** (Edited by C. J. Gomer), pp. 281–293. Springer, Clifton.
538. Gondivkar, S. M., A. R. Gadbail, M. G. Choudhary, P. R. Vedpathak and M. S. Likhitkar (2018) Photodynamic treatment outcomes of potentially-malignant lesions and malignancies of the head and neck region: A systematic review. *Invest. Clin. Dent.* **9**, e12270.
539. de Visscher, S. A. H. J., P. U. Dijkstra, I. B. Tan, J. L. N. Roodenburg and M. J. H. Witjes (2013) mTHPC mediated photodynamic therapy (PDT) of squamous cell carcinoma in the head and neck: A systematic review. *Oral Oncol.* **49**, 192–210.
540. van Doeveren, T. E. M., M. B. Karakullukçu, R. L. P. van Veen, M. Lopez-Yurda, W. H. Schreuder and I. B. Tan (2018) Adjuvant photodynamic therapy in head and neck cancer after tumor-positive resection margins. *Laryngoscope* **128**, 657–663.
541. Shafirstein, G., D. Bellnier, E. Oakley, S. Hamilton, M. Potasek, K. Besson and E. Parilov (2017) Interstitial photodynamic therapy – a focused review. *Cancer* **9**, 12.
542. Karakullukcu, B., S. C. Kanick, J. B. Aans, H. J. C. M. Sterenborg, I. B. Tan, A. Amelink and D. J. Robinson (2011) Clinical feasibility of monitoring m-THPC mediated photodynamic therapy by means of fluorescence differential path-length spectroscopy. *J. Biophotonics* **4**, 740–751.
543. de Visscher, S. A. H. J., M. J. H. Witjes, S. Kascakova, H. J. C. M. Sterenborg, D. J. Robinson, J. L. N. Roodenburg and A. Amelink (2012) In vivo quantification of photosensitizer concentration using fluorescence differential path-length spectroscopy: influence of photosensitizer formulation and tissue location. *J. Biomed. Opt.* **17**, 067001.
544. Ebbers, H. C., E. Al-Temimi, E. H. M. Moors, A. K. Mantel-Teeuwisse, H. Schellekens and H. G. M. Leufkens (2013) Differences between post-authorization adverse drug reactions of biopharmaceuticals and small molecules. *BioDrugs* **27**, 167–174.
545. Hofmann, G. A. and B. Weber (2021) Drug-induced photosensitivity: Culprit drugs, potential mechanisms and clinical consequences. *J. Dtsch. Dermatol. Ges.* **19**, 19–29.
546. Buchholz, J. and H. Walt (2013) Veterinary photodynamic therapy: A review. *Photodiagn. Photodyn. Ther.* **10**, 342–347.
547. Wilson, B. C., M. S. Patterson and L. Lilge (1997) Implicit and explicit dosimetry in photodynamic therapy: a new paradigm. *Lasers Med. Sci.* **12**, 182–199.
548. Kim, M. M. and A. Darafsheh (2020) Light sources and dosimetry techniques for photodynamic therapy. *Photochem. Photobiol.* **96**, 280–294.
549. Jacques, S. L. (2010) How tissue optics affect dosimetry of photodynamic therapy. *J. Biomed. Opt.* **15**, 051608.
550. Sterenborg, J. C. M. H., R. L. P. van Veen, J.-B. Aans, A. Amelink and D. J. Robinson (2013) Light dosimetry for photodynamic therapy: basic concepts. In *Handbook of Photomedicine, Chapter 25* (Edited by M. R. Hamblin and Y.-Y. Huang), pp. 282–291. CRC Press, Boca Raton.
551. Pogue, B. W., J. T. Elliott, S. C. Kanick, S. C. Davis, K. S. Samkoe, E. V. Maytin, S. P. Pereira and T. Hasan (2016) Revisiting photodynamic therapy dosimetry: Reductionist & surrogate approaches to facilitate clinical success. *Phys. Med. Biol.* **61**, R57–R89.
552. Roger, G. S. (2012) Continuous low-irradiance photodynamic therapy: A new therapeutic paradigm. *J. Natl. Compr. Cancer Network* **10**, S14–S17.
553. Kim, A., J. Zhou, S. Samaddar, S. H. Song, B. D. Elzey, D. H. Thompson and B. Ziaie (2019) An implantable ultrasonically-powered micro-light-source (μlight) for photodynamic therapy. *Sci. Rep.* **9**, 1395.
554. Atif, M. (2012) Fluorescence photobleaching dynamics of meso tetrahydroxy phenyl chlorin (mTHPC). *Laser Phys. Lett.* **9**, 387–393.
555. Kareliotis, G., M. Papachristou, D. Priftakis, I. Datseris and M. Makropoulou (2019) Computational study of necrotic areas in rat liver tissue treated with photodynamic therapy. *J. Photochem. Photobiol. B Biol.* **192**, 40–48.
556. Atif, M., M. Zellweger and G. Wagnières (2016) Review of the role played by the photosensitizer's photobleaching during photodynamic therapy. *J. Optoelectron. Adv. Mater.* **18**, 338–350.
557. Atif, M. (2013) In Vitro Studies of Photosensitizer fluorescence changes on singlet oxygen mediated photobleaching. *J. Phys. Conf. Ser.* **414**, 012025.
558. Atif, M. (2013) A study on the effects of photosensitizer concentration on singlet oxygen mediated photobleaching. *Laser Phys.* **23**, 055603.
559. Bonnett, R. and G. Martinez (2002) Photobleaching of compounds of the 5,10,15,20-tetrakis(m-hydroxyphenyl)-porphyrin series (m-THPP, m-THPC, and m-THPBC). *Org. Lett.* **4**, 2013–2016.
560. Bonnett, R., B. D. Djelal, P. A. Hamilton, G. Martinez and F. Wierrani (1999) Photobleaching of 5,10,15,20-tetrakis (m-hydroxyphenyl)porphyrin (m-THPP) and the corresponding chlorin (m-THPC) and bacteriochlorin (m-THPBC). A comparative study. *J. Photochem. Photobiol. B Biol.* **53**, 136–143.
561. Atif, M. (2014) A fluorescence micro-spectroscopy technique for the study of intracellular photobleaching of mTHPC. *J. Optoelectron. Adv. Mater.* **16**, 798–803.
562. Wouters, A., B. Pauwels, F. Lardon and J. B. Vermorken (2007) Review: Implications of in vitro research on the effect of radiotherapy and chemotherapy under hypoxic conditions. *Oncologist* **12**, 690–712.
563. Shen, Z., Q. Ma, X. Zhou, G. Zhang, G. Hao, Y. Sun and J. Cao (2021) Strategies to improve photodynamic therapy efficacy by relieving the tumor hypoxia environment. *NPG Asia Mater.* **13**, 39.
564. Li, B., L. Lin, H. Lin and B. C. Wilson (2016) Photosensitized singlet oxygen generation and detection: Recent advances and future perspectives in cancer photodynamic therapy. *J. Biophotonics* **9**, 1314–1325.
565. Bartusik-Aebisher, D., L. Ozog and D. Aebisher (2021) Alternative methods of photodynamic therapy and oxygen consumption measurements – a review. *Biomed. Pharmacother.* **134**, 111095.

566. Liang, X., K. K.-H. Wang and T. C. Zhu (2012) Singlet oxygen dosimetry modeling for photodynamic therapy. *Proc. SPIE* **8210**, 82100T.
567. Kanofsky, J. R. (2011) Measurement of singlet-oxygen in vivo: Progress and pitfalls. *Photochem. Photobiol.* **87**, 14–17.
568. Ogilby, P. R. (2010) Singlet oxygen: There is indeed something new under the sun. *Chem. Soc. Rev.* **39**, 3181–3209.
569. Vaupel, P., A. B. Flood and H. M. Swartz (2021) Oxygenation status of malignant tumors vs. normal tissues: Critical evaluation and updated data source based on direct measurements with pO2 microsensors. *Appl. Magn. Reson.* **52**, 1451–1479.
570. McKeown, S. R. (2014) Defining normoxia, physoxia and hypoxia in tumours—Implications for treatment response. *Br. J. Radiol.* **87**, 20130676.
571. Looft, A., M. Pfitzner, A. Preuß and B. Röder (2018) *In vivo* singlet molecular oxygen measurements: sensitive to changes in oxygen saturation during PDT. *Photodiagn. Photodyn. Ther.* **23**, 325–330.
572. Essaid, D., P. Chaminade, P. Maillard and A. Kasselouri (2015) Lipophilicity of porphyrins and their retention in IAM, C8–C18 and HILIC chromatographic systems. *J. Pharm. Biomed. Anal.* **114**, 227–240.
573. Bolze, F., S. Jenni, A. Sour and V. Heitz (2017) Molecular photosensitisers for two-photon photodynamic therapy. *Chem. Commun.* **53**, 12857–12877.
574. Xu, J., J. Gao and Q. Wei (2016) Combination of photodynamic therapy with radiotherapy for cancer treatment. *J. Nanomater.* **2016**, 8507924.
575. Vasan, N., J. Baselga and D. M. Hyman (2019) A view on drug resistance in cancer. *Nature* **575**, 299–309.
576. Mansoori, B., A. Mohammadi, S. Davudian, S. Shirjang and B. Baradaran (2017) The different mechanisms of cancer drug resistance: a brief review. *Adv. Pharm. Bull.* **7**, 339–348.
577. Blaudszun, A.-R., G. Moldenhauer, M. Schneider and A. Philippi (2015) A photosensitizer delivered by bispecific antibody redirected T lymphocytes enhances cytotoxicity against EpCAM-expressing carcinoma cells upon light irradiation. *J. Control. Release* **197**, 58–68.
578. Hsu, C.-Y., J. Rao and P.-S. Lai (2010) Bioluminescent quantum dots-induced photodynamic therapy in vitro. In *Nanotech Conference & Expo 2010: An Interdisciplinary Integrative Forum on Nanotechnology, Biotechnology and Microtechnology* (Edited by M. Laudon and B. Romanowicz), pp. 490–493. Nanotech Conference & Expo 2010, Anaheim, CA.
579. Mamone, L., D. Sáenz, P. Vallecorsa, A. Batlle, A. Casas and G. Di Venosa (2014) Photoprotective effect of the plant collaea argentina against adverse effects induced by photodynamic therapy. *Int. J. Photoenergy*, **2014**, 436463.
580. Mohammad, A., S. V. Ballullaya, J. Thumu, S. Maroli and P. Shankarappa (2017) Effect of ultrasonic activation of photosensitizer dye temoporfin (Foscan) on antimicrobial photodynamic therapy: An ex vivo study. *J. Conserv. Dent.* **20**, 419–423.
581. Almeida, A., M. A. F. Faustino and M. G. P. M. S. Neves (2020) Antimicrobial photodynamic therapy in the control of COVID-19. *Antibiotics* **9**, 320.
582. Meunier, T., L. Desmarets, S. Bordage, M. Bamba, K. Hervouet, Y. Rouillé, N. François, M. Decossas, F. H. T. Bi, O. Lambert, J. Dubuisson, S. Belouzard, S. Sahpaz and K. Séron (2022) A photoactivable natural product with broad antiviral activity against enveloped viruses including highly pathogenic coronaviruses. *Antimicrob. Agents Chemother.* **66**, e01581–e01521.
583. Chernyshev, A. (2020) Pharmaceutical targeting the envelope protein of SARS-CoV-2: The screening for inhibitors in approved drugs. *ChemRxiv*. https://doi.org/10.26434/chemrxiv.12286421
584. Absalan, A., D. Doroud, M. Salehi-Vaziri, H. Kaghazian, N. Ahmadi, F. Zali, M. H. Pouriavali's and S. D. Mousavi-Nasab (2020) Computation screening and molecular docking of FDA approved viral protease inhibitors as a potential drug against COVID-19. *Gastroenterol. Hepatol. Bed. Bench.* **13**, 355–360.
585. Fátima-Nunes, D. A., F. R. da Silva Santos, S. T. D. da Fonseca, W. G. de Lima, W. S. da Cruz Nizer, J. M. S. Ferreira and J. C. de Magalhães (2021) NS2B-NS3 protease inhibitors as promising compounds in the development of antivirals against Zika virus: A systematic review. *J. Med. Virol.* **94**, 442–453.
586. Li, Z., M. Brecher, Y.-Q. Deng, J. Zhang, S. Sakamuru, B. Liu, R. Huang, C. A. Koetzner, C. A. Allen, S. A. Jones, H. Chen, N.-N. Zhang, M. Tian, F. Gao, Q. Lin, N. Banavali, J. Zhou, N. Boles, M. Xia, L. D. Kramer, C.-F. Qin and H. Li (2017) Existing drugs as broad-spectrum and potent inhibitors for Zika virus by targeting NS2B-NS3 interaction. *Cell Res.* **27**, 1046–1064.
587. Preuß, A., M. Pfitzner and B. Röder (2019) Mosquito larvae control by photodynamic inactivation of their intestinal flora – a proof of principal study on *Chaoborus* sp. *Photochem. Photobiol. Sci.* **18**, 2374–2380.
588. Norvaiša, K., M. Kielmann and M. O. Senge (2020) Porphyrins as colorimetric and photometric biosensors in modern bioanalytical systems. *Chembiochem* **21**, 1793–1807.
589. Kielmann, M., C. Prior and M. O. Senge (2018) Porphyrins in troubled times: A spotlight on porphyrins and their metal complexes for explosives testing and CBRN defense. *New J. Chem.* **42**, 7529–7550.
590. Rout, B., M. Bigliardi-Qi and P. L. Bigliardi (2017) An expedient multiple information processing pattern-generating chromophore. *Sensors Actuators B* **251**, 164–170.
591. Rout, B. (2016) A miniaturized therapeutic chromophore for multiple metal pollutant sensing, pathological metal diagnosis and logical computing. *Sci. Rep.* **6**, 27115.
592. Liu, Y. and Z. Ma (2021) g-C3N4 modified by meso-tetrahydroxyphenylchlorin for photocatalytic hydrogen evolution under visible/near-infrared light. *Front. Chem.* **8**, 605343.

AUTHOR BIOGRAPHIES

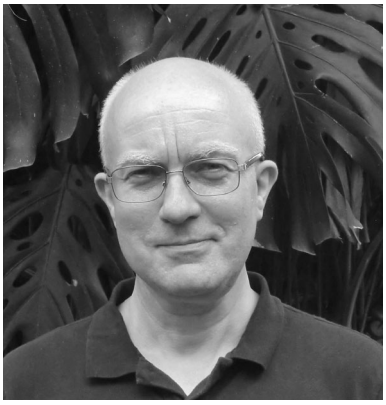

Arno Wiehe studied chemistry, history and educational science at the Freie Universität Berlin. After the state examination in chemistry and history, he focused on chemistry, receiving his Dr rer. nat. in 1997 from the Freie Universität with Prof. H. Kurreck. This was followed by postdoctoral studies with Prof. B. Röder, Humboldt Universität, and Prof. M. O. Senge, Universität Potsdam. In 2001 he joined biolitec as a research scientist. In 2003–2005, during a part-time study at Rheinische Friedrich-Wilhelms-Universität he gained additional qualifications as a master of drug regulatory affairs. His research interests are synthetic organic chemistry, dye applications and drug development.

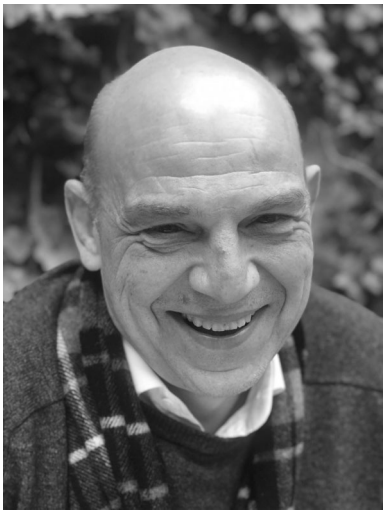

Mathias O. Senge studied chemistry and biochemistry in Freiburg, Amherst, Marburg and Lincoln. After a Ph.D. from the Philipps Universität Marburg (1989) and postdoctoral studies with K. M. Smith at UC Davis, he received his habilitation in Organic Chemistry in 1996 at the Freie Universität Berlin. From 1996 on he was a Heisenberg fellow at the Freie Universität Berlin and UC Davis. In 2002 he was appointed Professor of Organic Chemistry at the Universität Potsdam and since 2005 holds the Chair of Organic Chemistry at Trinity College Dublin. He was the recipient of fellowships from the Studienstiftung des Deutschen Volkes, the Deutsche Forschungsgemeinschaft, and Science Foundation Ireland (Research Professor 2005–2009) and is currently a Hans Fischer Senior Fellow at the Technical University Munich. His interests are synthetic organic chemistry, the (bio)chemistry of tetrapyrroles, photobiology and photomedicine, structural chemistry and history of science.